Université du Québec
à Rimouski

# Optimisation, prédiction et contrôle intelligents de la qualité du soudage au laser des alliages d'aluminium - Une approche inspirée des concepts de l'industrie 4.0.

Mémoire présenté

dans le cadre du programme de maitrise en ingénierie

en vue de l'obtention du grade de maître ès sciences appliquées (M.Sc.A.)

PAR

**© JOYS S. SILVA RIVERA**

**Août 2022**

**Composition du jury :**

**Marc-Denis Rioux, président du jury, Université du Québec à Rimouski.**

**Noureddine Barka, directeur de recherche, Université du Québec à Rimouski.**

**El Ouafi Abderrazak codirecteur de recherche, Université du Québec à Rimouski.**

**Nadia Lehoux, examinateur externe, Université LAVAL**

Dépôt initial le 28 juin 2022 Dépôt final le 12 aout 2022

A Maribel, ma mère, qui est parti, mais qui reste dans mon cœur.

## REMERCIEMENTS

À Maribel Rivera, ma mère, qui m'a donné la vie, les conseils et le soutien pour réussir ce projet. À ma femme Mariani qui marche avec moi et qui est toujours présente pour me soutenir. À ma famille, à mon oncle José Luis, à mes tantes Ledys et Rosa, à mes grands-parents Alcira, José, Carlos et Angela, à mes beaux-parents Marcelo et Eliani.

Au professeur Noureddine Barka pour son soutien, ses conseils et l'opportunité de développer mon projet de recherche. À M. El Ouafi pour la direction du projet. À mes collègues Pedram, Karim, Herinandrianina, Jean, Ahmad, au groupe de recherche FI3 et aux professeurs qui m'ont partagé leurs connaissances et ont amélioré mes compréhensions. Je tiens également à remercier Nadia Lehoux pour son intérêt à apporter son expertise et sa supervision pour les travaux réalisés.

À François, Marc-Olivier et Siyu-Tu, Fatemeh du centre national de recherche du Canada avec qui j'ai travaillé pour développer mon projet de recherche. À l'UQAR et au département d'ingénierie et ses auxiliaires et techniciens : Suzie, Karel, Vianney, Richard, Jean-Charles et Denis qui sont là pour aider les étudiants mais également à Farah et à Jacqueline de l'administration. Au centre d'aide à la réussite plus spécialement à Nancy qui m'a soutenu pour l'écriture de ce mémoire.

## RÉSUMÉ

L'utilisation croissante des alliages d'aluminium dans plusieurs industries a suscité de l'intérêt pour l'étude de différents procédés de transformation tels que le soudage au laser. Ce procédé présente de nombreux avantages, notamment un meilleur rendement énergétique et des vitesses plus élevées. Cependant, le soudage laser peut provoquer différents types de défauts dus à la porosité et aux distorsions thermiques qui doivent être surveillés et contrôlés pour garantir une bonne qualité des soudures. L'effet des distorsions provoque des non-conformités fonctionnelles de nature géométriques et dimensionnelles alors que la porosité entraine des anomalies ayant des conséquences complexes plus sérieuses sur le plan de la sécurité. La porosité est un défaut interne qui peut entraîner une réduction dramatique des performances mécaniques du cordon de soudure et ainsi affecter la qualité du produit fini. Cette recherche vise l'étude et l'analyse du procédé du soudage laser dans le but de proposer une méthodologie de surveillance géométrique pour réduire les distorsions sur les flancs soudés et des modèles d'apprentissage automatique afin de prédire la porosité. Le comportement du procédé de soudage au laser peut être caractérisé par des mesures optiques, thermiques et même acoustiques. Les signaux issus de ces mesures peuvent être utilisées comme base de données pour définir les paramètres de fonctionnement caractéristiques du procédé, les utiliser pour l'optimisation de la qualité et les exploiter pour détecter les défaillances dans le procédé. Cette approche a permis d'identifier les conditions opérationnelles optimales qui réduisent la distorsion à travers la soudure la distorsion le long de la soudure de 57,50 %, 33,47 % pour la distorsion de formation à travers la soudure de 86,52 % pour et la distorsion de formation le long de la soudure 94,32 %. Une amélioration de 127 % du score F1 a été constatée pour la prédiction de la porosité en utilisant un modèle à base de réseaux neuronaux artificiels, et une augmentation de 68 % du paramètre AUC (aire sous la courbe ROC) indique une amélioration des performances du modèle de classification des porosités à l'aide des algorithmes SVM (machine à vecteurs de support). De plus, les résultats ont démontré que le meilleur algorithme d'apprentissage automatique pour faire la prédiction de la porosité pour la configuration utilisée est *Random Forest* avec 0,83 AUC, 75 % de précision, 0,75 en score F1 pour la classe de non-porosité et 0,76 en *score F1* pour la classe avec porosité. Les résultats obtenus montrent que la méthodologie et les modèles proposés pourraient être mis en œuvre dans des applications industrielles variées pour améliorer la qualité pour les plaques soudées au laser et réduire le temps et le coût pour l'analyse de la qualité tout en augmentant la performance opérationnelle du procédé de soudage.



Mots clés : Procédés de fabrication avancés, soudage laser, alliages d'aluminium, surveillance intelligente de la qualité des soudures, fabrication Lean, apprentissage automatique, intelligence artificielle, Industrie 4.0.

## ABSTRACT

The growing implementation of aluminum alloys in different industries has focused the interest in studying different transformation processes such as laser welding. It has many advantages including higher energy efficiency and higher speed rates. But laser welding can get a different kind of defects that might be monitored and controlled to assure the final product quality. The distortion effect is one of the geometrical defects that can be present when using this technique. Porosity is one of the most critical defects in the laser welding process that is an internal defect which is complex to detect. This kind of defects may result in a reduction in mechanical performance and critical failures of the manufactured product, which reduce the product quality and is critical for the final user. This research study and analyse different process and defects monitoring applied to laser welding, propose a geometrical monitoring methodology to reduce the distortion on laser welded blanks and propose a method and workflow to monitor the laser welding process to make porosity prediction with machine learning models. The laser welding method is characterized by optical, thermal, and even acoustic signals. Consequently, the nature of the process can be used to sense and define operation parameters and analyze phenomena to predict and optimize the quality of the final product. As results, the optimal operational conditions that reduce distortion are proposed, with a reduction of 57.50% for distortion across welding, 33.47% for distortion along welding, 86.52% for forming distortion across welding, and 94.32% for forming distortion along welding. For porosity prediction an improvement of 127% in the F1 score for the Artificial Neural Networks algorithm was reported, and an increase of 68% in the AUC parameter that indicates an improvement in the performance of the model to classify porosities for SVM algorithms was achieved. Additionally, it was found that the best Machine Learning Algorithm to make the porosity prediction for the setup is Random Forest with 0.83 AUC, 75% accuracy, 0.75 in F1 score for No Porosity Class, and 0.76 in F1 Score for Porosity Class. The positive results of the proposed model and methodology indicate that it could be implemented in industrial applications for enhancing the final product quality for welded plates and reducing process waste and time for product quality analysis, increasing the operational performance of the process.



Keywords: Advanced manufacturing process, laser welding, aluminum, intelligent welding quality monitoring, Lean manufacturing, machine learning, artificial intelligence, Industry 4.0.

## TABLE DES MATIÈRES

## LISTE DES TABLEAUX

## LISTE DES FIGURES

## LISTE DES ABRÉVIATIONS, DES SIGLES ET DES ACRONYMES

| | |
|---|---|
| **NDT** | Non-destructive methods |
| **CMOS** | Complementary metal oxide semiconductor |
| **ISO** | International Organization for Standardization |
| **SVM** | Support Vector Machine/ Machine à vecteurs de support |
| **PCA** | Principal Component Analysis |
| **N/A** | Non applicable |
| **ACRL** | Actor-Critic Reinforcement Learning |
| **TWBs** | Tailor Welded Blanks |
| **CAD** | Computer Aided Design |
| **ANOVA** | Analysis of Variance |
| **DMAIC** | Design Measure Analyze Improve Control |
| **DOE** | Design of Experiences |
| **YLS** | Yterbium Fiber Lasers |
| **3LS** | 3D Laser Scanning Inspection |
| **CL** | Cloud Mapping |
| **CAM** | Computer Aided Manufacturing |
| **CAI** | Computer Aided Inspection |

| | |
|---|---|
| **QA** | Quality Assurance |
| **SSQ** | Sum of Squared Errors |
| **CORR** | Correlation |
| **W** | Width of the plate |
| **Δy** | Deformation in the y-axis |
| $\boldsymbol{\delta_B}$ | Maximum bending distortion |
| **C** | Curvature |
| **L** | Weld length |
| **P** | Power |
| **V** | Welding Speed |
| **A** | Amplitude |
| **DWD** | Distortion along welding direction |
| **DAWD** | Distortion across welding direction |
| **TDWD** | Total distortion in welding direction |
| **TAWD** | Total distortion across welding direction |
| **FDW** | Forming distortion in welding direction |
| **FAWD** | Forming across welding direction |
| **CNN** | Convolutional Neural Network |
| **RMSE** | Root mean square error |
| $\mathbf{R^2}$ | R squared, coefficient of determination |

| | |
|---|---|
| **ML** | Machine Learning |
| **MW** | Mean window |
| **SW** | Standard deviation window |
| **VW** | Variance window |
| **RF** | Random Forest |
| **AUC** | Area under the curve/ Aire sous la courbe ROC |
| **CPU** | Central processing unit |
| **GPU** | Graphics Processing Units |
| **ROC** | Receiver operating characteristic/ Caractéristique de fonctionnement du récepteur |

## LISTE DES SYMBOLES

| SYMBOLE 1 | Définition du symbole |
|---|---|
| **ms** | Millisecondes |
| **nm** | Nanomètres |
| **Mg** | Magnésium |
| **Zn** | Zinc |
| **Cu** | Cuivre |
| **Al** | Aluminium |
| **kW** | Kilowatts |
| **mm** | Millimètre |
| **mm/s** | Millimètre par second |
| **Ɵ** | Distorsion angle |

# INTRODUCTION GÉNÉRALE

## 1. CONTEXTE ET GENERALITES

L'un des principaux défis auxquels l'industrie est confrontée aujourd'hui consiste à minimiser le gaspillage découlant de la mauvaise conduite des procédés de fabrication et à respecter les réglementations environnementales de plus en plus exigeantes. L'utilisation de matériaux qui aident à la réduction de l'impact sur l'environnement a connu un plus grand intérêt de la part de l'industrie dans plusieurs secteurs productifs [1], [2]. L'aluminium donc est devenu l'une des options parfaites en raison de sa faible densité qui nous permet d'obtenir la légèreté des produits, notamment dans l'industrie du transport. Ce choix a un impact sur les coûts et sur l'efficacité énergétique des produits entraînant une diminution de l'émission de gaz à effet de serre [1]. Il est même admis que l'utilisation de matériaux légers pour la production de composants et de pièces automobiles permettrait de respecter les réglementations toujours plus strictes en matière de pollution atmosphérique et d'améliorer l'efficacité [3], pour cette raison l'aluminium est un matériau largement utilisé dans la fabrication de véhicules électriques [31]. Un autre point d'intérêt de l'utilisation d'aluminium concerne sa recyclabilité, qui représente l'un des principaux avantages du matériau. Quelques alliages de fonderie ont été développés spécifiquement pour la production à partir de déchets refondus [2].

Il existe plus de 500 alliages d'aluminium différents et, pour des raisons de commodité, ils sont séparés en catégories appelées séries d'alliages. L'IADS (système international de désignation des alliages) est un système de classification utilisé dans la plupart des pays pour classer les alliages d'aluminium en fonction de leur composition chimique. Il est employé par l'industrie aérospatiale pour classifier les matériaux utilisés dans les avions. Tous les alliages d'aluminium sont classés dans l'une des huit séries présentées dans le Table 1. Le ou les principaux composants du matériel sont utilisés pour déterminer à laquelle des huit séries un alliage appartient [4]. L'aluminium a plusieurs caractéristiques qui en font un matériau

d’intérêt pour les applications d’ingénierie. Le rapport résistance/poids élevé, la facilité de fabrication, le degré élevé d'ouvrabilité, la ductilité considérable, l’excellente conductivité thermique, la résistance élevée à la corrosion et la bonne finition naturelle sont les caractéristiques qui distinguent les alliages d’aluminium. Leur grande résistance à la corrosion les rend bien adaptés aux applications dans les environnements marins sans protection de surface et avec un faible coût de maintenance. Leur grande durabilité permet de réaliser des structures capables de conserver leurs propriétés intrinsèques même en cas de fortes variations de température. La Table 2 présente les valeurs des propriétés mécaniques et physiques de l'aluminium [4]-[6]. Les matériaux utilisés dans cette étude sont les alliages d'aluminium qui appartiennent à la famille 5000 et 6000, ils sont de bonnes propriétés mécaniques, une résistance à la traction moyenne, une bonne résistance à la corrosion et des performances d'usinage; les deux matériaux sont largement utilisés dans l'industrie automobile, l'industrie aérospatiale et les industries du transport, avec l’implémentation réussie dans les applications navales et en mer profonde [7], [8].

Table 1. Désignation des alliages d’aluminium

| Famille | Composition |
|---|---|
| **1000** | Aluminium pur (99,00 % ou plus) |
| **2000** | Cuivre |
| **3000** | Manganèse |
| **4000** | Silicium |
| **5000** | Magnésium |
| **6000** | Magnésium-silicium |
| **7000** | Zinc |
| **8000** | Aluminium et autres éléments |

Table 2. Propriétés physiques de l'aluminium

| Propriétés | Valeurs | Unités |
|---|---|---|
| **Résistance à la traction** | 10–90 (70–620) | ksi (MPa) |
| **Limite d'élasticité** | 3–84.1 (20–580) | ksi (MPa) |
| **Allongement** | <1–30 | % |
| **Dureté** | 30-150 | HB |
| **Conductivité électrique** | 18–60 | %IACS |
| **Limite de fatigue** | 8–21 (55–145) | ksi (MPa) |
| **Résistance au cisaillement** | 6–46 (42–325) | ksi (MPa) |
| **Module d'élasticité** | 9.5–11.2 (65–80) | $10^6$ psi (GPa) |
| **Gravité spécifique** | 2.57–2.95 | - |

L'utilisation efficace des alliages d'aluminium nécessite le développement et l'optimisation des méthodes de transformation et d'assemblage spécifiques. Parmi les procédés d'assemblage on peut nommer les techniques de soudage, de liaison adhésive et de fixations mécaniques [9]. Ces deux dernières sont des procédés avec une faible consommation d'énergie offrent des solutions avec de bonnes performances mécaniques. Cependant, elles sont limitées par le besoin d'accès aux deux côtés de l'articulation pour les mettre en place. Les joints adhésifs sont intrinsèquement faibles en pelage et la conception des véhicules devrait en tenir compte. Les adhésifs de haute performance actuels sont des systèmes à base d'époxy ou de solvant, ce qui suscite des préoccupations environnementales considérables, notamment en ce qui concerne la résistance aux chocs. La limitation d'accès pour le rivetage à certaines zones du joint, les renflements et les indentations associés aux deux techniques peuvent ne pas être esthétiquement souhaitables. Les rivets auto-poinçonneurs introduisent des éléments consommables supplémentaires, et donc du poids additionnel au produit malgré l'utilisation de revêtements passifs pour prévenir la corrosion, des irrégularités de surface ou des crevasses se produisent à la suite des mécanismes de déformation, ce qui pourrait permettre la production de corrosion [9], [10].

Le procédé de soudage est une technologie largement utilisée en raison de ses nombreux avantages tels que le faible coût, la vitesse élevée, la facilité d'utilisation et l'automatisation et l'aptitude à être utilisé dans la production en grande série malgré les difficultés posées par l'oxyde de surface dans le soudage de l'aluminium et les coûts d'investissement et d'exploitation généralement élevés. La longue expérience de l'industrie

en matière de soudage garantie certainement la poursuite du développement des différentes techniques disponibles. Même les technologies coûteuses telles que les lasers commencent progressivement à trouver des applications dans l'industrie automobile, à mesure que la technologie se développe pour répondre aux besoins de l'industrie [9], [11], [12] . Les techniques de soudage plus implémentées et rapportées dans la littérature sont la soudure par résistance par points (Figure 1), le soudage à l'arc (Figure 2), le soudage par friction-malaxage (Figure 3) et le soudage laser. La difficulté rencontrée lors du soudage par résistance par points de l'aluminium est la décomposition de sa couche d'oxyde superficielle. Le point de fusion nettement plus élevé de cette couche d'oxyde nécessite un chauffage par résistance clairement plus élevé pour la décomposer et permettre ainsi la formation de la soudure[13]. Le soudage par arc de l'aluminium est rendu difficile par la présence d'un film d'oxyde à haut point de fusion qui reste intact même après la fusion du métal. Et en plus des susceptibilités à la fissuration des soudures, la haute distorsion induite par la chaleur et les traitements thermiques nécessaires après soudage sont les limitations rapportées par la littérature [11].

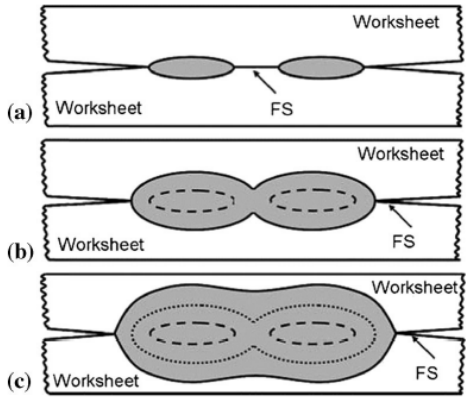


Figure 1. Modèle de formation de noyaux pendant le soudage par points résistifs d'un alliage d'aluminium AA5182. a Début de l'échauffement à la périphérie ; b le chauffage croît plus rapidement vers l'intérieur que vers l'extérieur ; c achèvement de la formation de la pépite. [12]

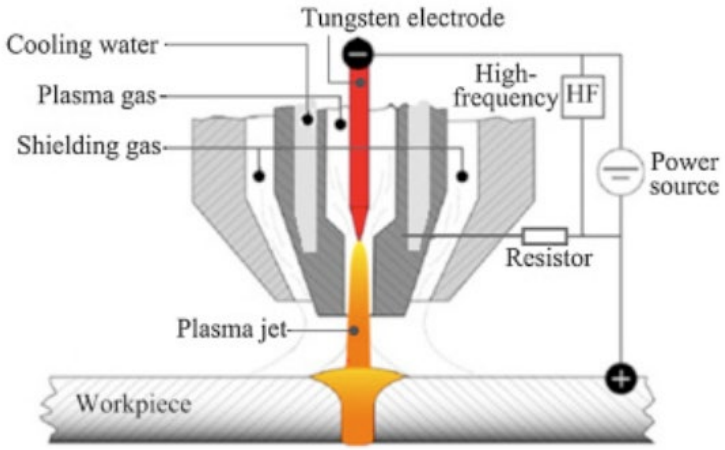


Figure 2. Schéma d'une torche de soudage à l'arc plasma [14].

Le soudage par friction-malaxage donne une intégrité des soudures généralement considérée comme bonne, produisant une structure à grain fin sans défectuosité majeure et capable de faire l'assemblage de matériaux jusqu'à 12 mm d'épaisseur. Ce procédé est relativement lent, avec les valeurs de vitesses rapportées entre 0,3 m/min et 0,6 m/min pour des épaisseurs entre 1,6 mm et 6 mm [11], [15], [16]. Il demande des systèmes de serrage rigides à cause des hautes pressions impliquées pour ce processus. Un trou de sortie d'outil est laissé au point de départ et d'arrêt de la soudure qui doit être rempli après le traitement [11], [15], [17]. Le soudage laser est un procédé qui a gagné beaucoup d'intérêt à cause de sa haute vitesse de traitement et de production, il donne aussi d'autres avantages, le fait qu'il induit très peu de distorsion thermique en raison d'un apport de chaleur global plus faible. Cela est dû au faisceau hautement focalisé et à haute densité d'énergie qui chauffe rapidement une très petite zone et produit un cordon de soudure fin et une étroite zone affectée par la chaleur. Les soudures sont généralement de haute qualité et sont très faciles à former, d'où leur utilisation dans la fabrication de flans sur mesure. Les systèmes laser sont particulièrement propices à l'automatisation, étant programmables et très polyvalents dans les matériaux qui peuvent être traités, entre autres l'aluminium, et les différentes géométries des joints qui sont possibles [18]-[20]. Le soudage à laser est un procédé considéré coûteux à mettre en œuvre. Il est limité pour l'aluminium à des épaisseurs variant entre 2 mm et 6 mm et, en raison de cette petite taille, un apport de chaleur irrégulier tend à causer une

pénétration irrégulière et une instabilité du bain de soudure. Il en résulte des défauts qui doivent être contrôlés pour assurer la bonne qualité et pouvoir profiter de hautes vitesses et des avantages que cette technique de soudure offre [11], [18], [21], [22].

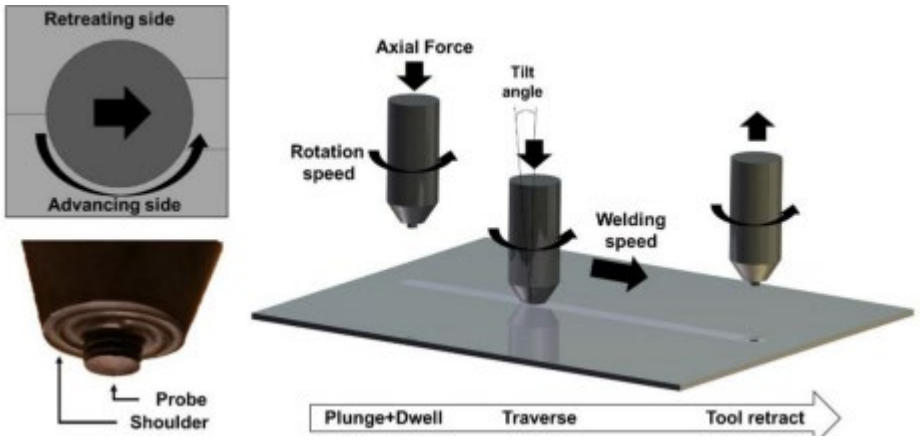


Figure 3. Séquences des opérations en soudage par friction malaxage [23].

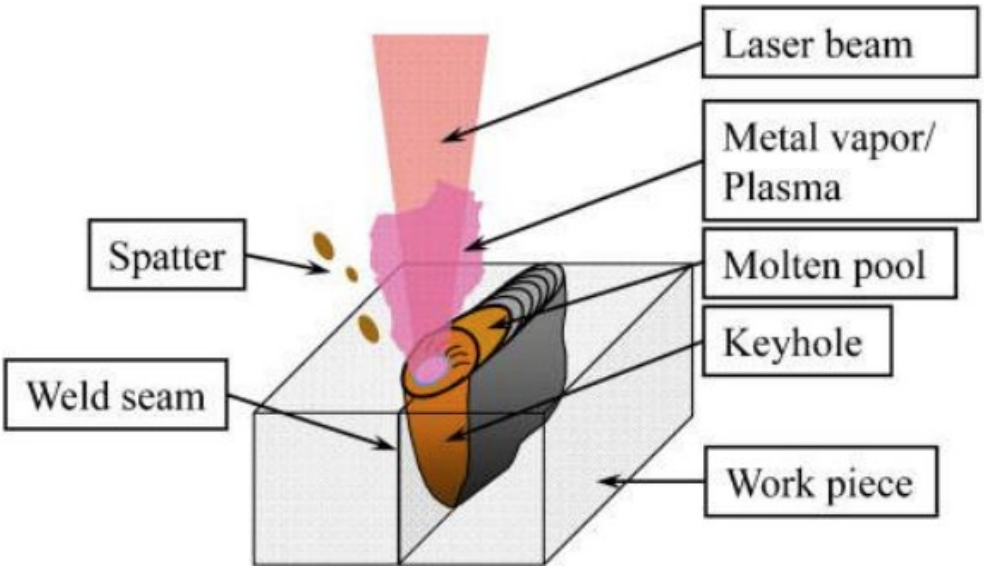


Figure 4. Représentation schématique du soudage laser [20].

## 2. PROBLEMATIQUES

Le soudage au laser est connu comme un procédé d'assemblage de haute qualité, de précision élevée, à faible distorsion, à faible déformation, à haute fréquence, à bonne performance, à grande flexibilité et à haute vitesse [19]. Il facilite également la robotisation, l'automatisation, l'économie de main-d'œuvre et la systématisation des processus [24]. Il est de plus en plus utilisé dans de nombreux secteurs industriels. Néanmoins, indépendamment de l'application, il est important de comprendre comment les phénomènes de soudage laser, qu'ils soient mécaniques, thermiques ou métallurgiques, influencent la qualité finale des produits et comment appliquer les méthodes d'optimisation pour réduire les effets inhérents au procédé qui risquent de dégrader les performances mécaniques des pièces soudées. Les défauts ou les imperfections de soudage peuvent conduire dans certaines conditions à des risques de fractures conduisant à des problèmes de sécurité [25]. Les défauts de soudage au laser sont classés en trois groupes principaux : les défauts géométriques ou d'apparence, les défauts internes ou invisibles (porosité) et les défauts de propriété ou de qualité [24]. Dans le soudage au laser, la porosité se forme facilement dans des soudures profondément pénétrées, caractérisées par un soudage au laser à haute puissance. Les conditions thermiques lors du soudage laser peuvent provoquer des déformations ayant des effets sur les dimensions des pièces soudées. Ces variations dimensionnelles causées par les effets thermiques sont appelées distorsions [26].

Si la distorsion de soudage dépasse la limite tolérable, cela entraine des rejets et cause des retards dans les programmes de production et réduise la productivité en raison des travaux de correction supplémentaires qui peuvent devenir complexes à réaliser [27], [28]. Donc, la surveillance de la conformité géométrique du produit est une opération critique dans les procédés de fabrication. Pour cette raison, le développement de méthodes et de solutions permettant de mesurer et de contrôler la distorsion gagne de plus en plus l'intérêt dans l'industrie [28]. Pour assurer la meilleure qualité dans le produit final, la surveillance du procédé, le contrôle et l'optimisation des paramètres de soudage ainsi que la prédiction des anomalies deviennent vraiment essentiels. La surveillance du procédé de soudage au laser doit se concentrer sur plusieurs caractéristiques parmi lesquelles on peut citer le bain de fusion, le *keyhole*, le panache, les éclaboussures, les signaux de rayonnement et les signaux

acoustiques émis le procédé de soudage, ainsi que les accessoires de fixation et la géométrie des pièces. Qu'elles soient géométriques, thermiques, acoustiques ou optiques, ces caractéristiques peuvent jouer un rôle clé dans la surveillance du procédé [20], [29]. Selon la nature des caractéristiques à évaluer, plusieurs dispositifs de mesure peuvent être considérés. Les données clés pour définir, surveiller, prédire et contrôler, et peuvent provenir selon différentes modalités. Le choix des dispositifs de mesure et la sélection des conditions de mesure sont deux aspects fondamentaux dans le processus de développement du système de surveillance. Il faut s'assurer d'une qualité exemplaire des données pour obtenir les meilleures performances au niveau de l'efficacité et la fiabilité de la surveillance. Les choix à faire représentent des défis importants à cause de la nature dynamique et parfois instable du procédé [30].

## 3. OBJECTIFS

L'objectif de ce projet de recherche consiste à développer une approche permettant d'améliorer la qualité de la soudure au laser des alliages d'aluminium à travers l'identification des conditions opérationnelles optimales permettant de réduire les distorsions thermiques et la porosité dans le cordon de soudure. Pour atteindre cet objectif, trois objectifs spécifiques correspondant aux étapes du projet sont considérés. Plus précisément, il s'agit :

(i) D'identifier les techniques de surveillance du procédé les plus appropriées et de sélectionner les paramètres à contrôler et les méthodes de prédiction et d'optimisation susceptibles de constituer la base d'une approche globale permettant de réduire les problèmes de qualité dans le procédé de soudage au laser.
(ii) De développer une méthode générale pour le contrôle des défauts dimensionnels et géométriques provoqués par les distorsions thermiques. Cette méthode devrait permettre l'identification des conditions optimales des paramètres d'opération tels que la puissance, l'amplitude et la vitesse pour réduire ces défauts.
(iii) De développer une approche de prédictive appliquée à porosité pour une surveillance intelligente en temps réel de la soudure.

## 4. METHODOLOGIE

La première phase du travail consiste à effectuer une recherche détaillée sur l'évolution des technologies applicables pour le procédé de soudage aussi bien au niveau des système de

mesures qui peuvent être mis à contribution pour obtenir les informations nécessaires à la caractérisation du procédé de soudage qu'au niveau des concepts et des méthodes de surveillance continue du procédé qui ont un grand potentiel d'application dans des systèmes industriels à haute cadence de production. Elle liste les principaux défauts et les possibles causes et méthodes pour sa surveillance avec l'objectif de définir les possibles paramètres qui seront mesurés, suivis et contrôlés dans le procédé de soudage laser. Cette phase cherche aussi à trouver des systèmes intelligents qui peuvent être appliqués pour la validation et la prédiction de la qualité finale du produit. Cette revue a aussi l'objectif de rechercher des outils et capteurs qui peuvent être appliqués et qui vont aider à définir une méthodologie qui peut être proposée et adaptée pour différents types d'application tant en industrie qu'en laboratoire. Elle liste des conclusions et la performance des systèmes et méthodes que les recherches précédentes ont faits.

La seconde phase consiste à mesurer la distorsion géométrique des tôles soudées et des tôles embouties dans le but de l'optimiser en fonction de la définition des paramètres d'opération qui ont plus d'impact sur la distorsion géométrique durant les deux phases du procédé pour la fabrication des Tailor Welded Blanks, c'est-à-dire le soudage et l'emboutissage. À cette étape, nous utilisons un algorithme pour l'extraction de données et la mise en œuvre des outils statistiques tels que l'analyse de corrélation avec la méthode de Pearson, l'application ANOVA pour définir l'importance statistique, les équations qui peuvent prédire les valeurs de distorsion géométrique et aussi de faire une analyse pour trouver les valeurs optimales qui vont réduire cette imperfection du produit final causée par la nature thermique du procédé de soudage.

La dernière phase est orientée vers la prédiction de la porosité. Elle utilise l'inspection avec une caméra de haute vitesse en temps réel qui prend les images à 10000 cadres/sec et suit l'évolution et le comportement de la soudure lorsqu'elle est faite. De plus, l'analyse avec la machine à rayons X Yxlon multiplex 5500M dans une section de 1 mm permet de déterminer les porosités de chaque soudure. Ces données sont traitées et extraites avec Image J pour avoir la matrice de paramètres d'entrée et de sortie pour appliquer les techniques de science de données (comme la sélection de paramètres, l'analyse de corrélation, l'application de la méthode Boruta, les techniques pour traiter le problème de déséquilibre) et l'

apprentissage automatique (comme SVM, ANN, Catboost, Random Forest) avec le but d'optimiser les modèles et de définir la méthode la plus performante pour la classification et la prédiction de la porosité par rapport aux conditions géométriques et optiques de la soudure telles que l'épaisseur, le diamètre du *Keyhole,* le rapport d'aspect et l'intensité captés par la caméra. Ces techniques sont évaluées par les paramètres métriques qui sont utilisés pour tester des modèles et des méthodes d'apprentissage automatique et l'intelligence artificielle comme AUC, Accuracy et F1.

## 5. ORGANISATION DU MEMOIRE

Le premier chapitre définit le contexte, présente les principaux éléments et concepts ayant un rapport direct avec l'évaluation et le contrôle de la qualité de la soudure au laser des alliages d'aluminium. Il présente également une brève revue des différentes approches et techniques de caractérisation, de prédiction, d'optimisation et de surveillances continue et intelligente utilisées pour les procédés de soudage. La fin du chapitre présente la problématique à traiter, précise les objectifs à atteindre et clarifie la méthodologie de résolution adoptée.

Le deuxième chapitre présente l'approche proposée pour sur la surveillance géométrique en temps réel avec l'aide des systèmes automatiques de soudage, d'emboutissage et l'inspection 3D par nuage de points avec scanner à laser. Ce chapitre se concentre principalement sur l'étude des effets des paramètres de soudage sur la distorsion géométrique et propose une méthode de surveillance et de contrôle de la qualité dans le cas l'aluminium 5052-H32 et Les résultats relative à la sélection des meilleures combinaisons de paramètres d'opération du procédé pour réduire les distorsions causées par le phénomène thermique sont également présentés et commentés.

Le troisième chapitre présente la méthodologie adoptée pour la prédiction, la classification et la surveillance en temps réel de la porosité. Il décrit la méthode d'extraction de paramètres géométriques et optiques de la soudure à l'aide d'une caméra de haute vitesse

qui a une capacité de 10 000 images par seconde et l'analyse de porosité avec rayons X ainsi que la mise en œuvre des systèmes d'apprentissage automatique. Ce chapitre introduit également les méthodes et les processus les plus compatibles avec les conditions réelles associées aux applications industrielles pour résoudre la problématique, c'est-à-dire un bas taux de défauts qui réduit Les résultats de l'évaluation de la capacité des algorithmes et des modèles intelligents pour la prédiction d'anomalies ainsi que les performances des systèmes de surveillance en temps réel sont également exposées, analysés et commentés.

Finalement, la conclusion générale rappelle la problématique et les objectifs en faisant le lien avec les résultats obtenus et les observations constatées tout en présentant des pistes et des perspectives à donner à ce projet de recherche.

## 6. REFERENCES


[1] A. Giampieri, J. Ling-Chin, Z. Ma, A. Smallbone, and A. P. Roskilly, "A review of the current automotive manufacturing practice from an energy perspective," *Applied Energy*, vol. 261. Elsevier Ltd, Mar. 01, 2020. doi: 10.1016/j.apenergy.2019.114074.

[2] J. G. (John G. Kaufman, E. L. Rooy, and American Foundry Society., *Aluminum alloy castings : properties, processes, and applications*. ASM International, 2004.

[3] D. K. Koli, G. Agnihotri, and R. Purohit, "Advanced Aluminium Matrix Composites: The Critical Need of Automotive and Aerospace Engineering Fields," in *Materials Today: Proceedings*, 2015, vol. 2, no. 4–5, pp. 3032–3041. doi: 10.1016/j.matpr.2015.07.290.

[4] E. A. Starke, "Alloys: Aluminum."

[5] W. Cassada, J. Liu, and J. Staley, "Aluminum alloys for aircraft structures," *Advanced Materials and Processes*, vol. 160, no. 12. ASM International, pp. 27–29, 2002. doi: 10.1533/9780857095152.173.

[6] E. Georgantzia, M. Gkantou, and G. S. Kamaris, “Aluminium alloys as structural material: A review of research,” *Engineering Structures*, vol. 227. Elsevier Ltd, Jan. 15, 2021. doi: 10.1016/j.engstruct.2020.111372.

[7] J. Fathi, P. Ebrahimzadeh, R. Farasati, and R. Teimouri, “Friction stir welding of aluminum 6061-T6 in presence of watercooling: Analyzing mechanical properties and residual stress distribution,” *International Journal of Lightweight Materials and Manufacture*, vol. 2, no. 2, pp. 107–115, 2019, doi: 10.1016/j.ijlmm.2019.04.007.

[8] Z. Huang, W. Wang, Y. Zhang, and J. Lai, “Low speed impact properties of 5052 aluminum alloy plate,” *Procedia Manufacturing*, vol. 50, pp. 668–672, 2020, doi: 10.1016/j.promfg.2020.08.120.

[9] T. A. Barnes and I. R. Pashby, “Joining techniques for aluminium spaceframes used in automobiles Part II Ð adhesive bonding and mechanical fasteners.”

[10] G. Meschut, V. Janzen, and T. Olfermann, “Innovative and highly productive joining technologies for multi-material lightweight car body structures,” in *Journal of Materials Engineering and Performance*, 2014, vol. 23, no. 5, pp. 1515–1523. doi: 10.1007/s11665-014-0962-3.

[11] T. A. Barnes and I. R. Pashby, “Joining techniques for aluminium spaceframes used in automobiles Part I Ð solid and liquid phase welding.”

[12] S. M. Manladan, F. Yusof, S. Ramesh, M. Fadzil, Z. Luo, and S. Ao, “A review on resistance spot welding of aluminum alloys,” *International Journal of Advanced Manufacturing Technology*, vol. 90, no. 1–4. Springer London, pp. 605–634, Apr. 01, 2017. doi: 10.1007/s00170-016-9225-9.

[13] P. Briskham, N. Blundell, L. Han, R. Hewitt, K. Young, and D. Boomer, “Comparison of Self-Pierce Riveting, Resistance Spot Welding and Spot Friction Joining for aluminium automotive sheet,” 2006. doi: 10.4271/2006-01-0774.

[14] Z. M. Liu, S. L. Cui, Z. Luo, C. Z. Zhang, Z. M. Wang, and Y. C. Zhang, “Plasma arc welding: Process variants and its recent developments of sensing, controlling and

modeling," *Journal of Manufacturing Processes*, vol. 23. Elsevier Ltd, pp. 315–327, Aug. 01, 2016. doi: 10.1016/j.jmapro.2016.04.004.

[15] Thomas, W.M., Staines, D.G., Norris, I.M. et al. Friction Stir Welding Tools and Developments. Weld World 47, 10–17 (2003). https://doi.org/10.1007/BF03266403

[16] A. Giampieri, J. Ling-Chin, Z. Ma, A. Smallbone, and A. P. Roskilly, "A review of the current automotive manufacturing practice from an energy perspective," *Applied Energy*, vol. 261. Elsevier Ltd, Mar. 01, 2020. doi: 10.1016/j.apenergy.2019.114074.

[17] J. Stephen Leon, G. Bharathiraja, and V. Jayakumar, "A review on Friction Stir Welding in Aluminium Alloys," in *IOP Conference Series: Materials Science and Engineering*, Oct. 2020, vol. 954, no. 1. doi: 10.1088/1757-899X/954/1/012007.

[18] A. Gorkič, M. Jezeršek, J. Možina, and J. Diaci, "Measurement of weldpiece distortion during pulsed laser welding using rapid laser profilometry," *Science and Technology of Welding and Joining*, vol. 11, no. 1, pp. 48–56, Feb. 2006, doi: 10.1179/174329306X77065.

[19] S. Katayama, *Introduction: Fundamentals of laser welding*, vol. 9, no. 2012. Woodhead Publishing Limited, 2013. doi: 10.1533/9780857098771.1.3.

[20] D. Y. You, X. D. Gao, and S. Katayama, "Review of laser welding monitoring," *Science and Technology of Welding and Joining*, vol. 19, no. 3, pp. 181–201, 2014, doi: 10.1179/1362171813Y.0000000180.

[21] J. Stavridis, A. Papacharalampopoulos, and P. Stavropoulos, "Quality assessment in laser welding: a critical review," *International Journal of Advanced Manufacturing Technology*, vol. 94, no. 5–8, pp. 1825–1847, 2018, doi: 10.1007/s00170-017-0461-4.

[22] K. Hao, G. Li, M. Gao, and X. Zeng, "Weld formation mechanism of fiber laser oscillating welding of austenitic stainless steel," *Journal of Materials Processing Technology*, vol. 225, pp. 77–83, 2015, doi: 10.1016/j.jmatprotec.2015.05.021.

[23] A. Magalhães, J. de Backer, and G. Bolmsjö, “Thermal dissipation effect on temperature-controlled friction stir welding,” *Soldagem e Inspecao*, vol. 24, 2019, doi: 10.1590/0104-9224/SI24.28.

[24] S. Katayama, *Defect formation mechanisms and preventive procedures in laser welding*. 2013. doi: 10.1533/9780857098771.2.332.

[25] Y. Huang, Y. Yuan, L. Yang, D. Wu, and S. Chen, “Real-time monitoring and control of porosity defects during arc welding of aluminum alloys,” *Journal of Materials Processing Technology*, vol. 286, no. July, 2020, doi: 10.1016/j.jmatprotec.2020.116832.

[26] H. M. M. A. Rashed, “Control of Distortion in Aluminium Heat Treatment,” in *Fundamentals of Aluminium Metallurgy*, Elsevier, 2018, pp. 495–524. doi: 10.1016/b978-0-08-102063-0.00013-8.

[27] C. L. Tsai and D. S. Kim, “Understanding residual stress and distortion in welds: An overview,” in *Processes and Mechanisms of Welding Residual Stress and Distortion*, Elsevier Ltd., 2005, pp. 3–31. doi: 10.1533/9781845690939.1.3.

[28] H. Murakawa, “Residual stress and distortion in laser welding,” *Handbook of Laser Welding Technologies*, vol. 2, pp. 374–398, 2013, doi: 10.1533/9780857098771.2.374.

[29] W. Cai, J. Z. Wang, P. Jiang, L. C. Cao, G. Y. Mi, and Q. Zhou, “Application of sensing techniques and artificial intelligence-based methods to laser welding real-time monitoring: A critical review of recent literature,” *Journal of Manufacturing Systems*, vol. 57. Elsevier B.V., pp. 1–18, Oct. 01, 2020. doi: 10.1016/j.jmsy.2020.07.021.

[30] W. Cai, J. Z. Wang, P. Jiang, L. C. Cao, G. Y. Mi, and Q. Zhou, “Application of sensing techniques and artificial intelligence-based methods to laser welding real-time monitoring: A critical review of recent literature,” *Journal of Manufacturing Systems*, vol. 57, no. July, pp. 1–18, 2020, doi: 10.1016/j.jmsy.2020.07.021.

[31] Anonymous "Aluminium in Automotive Conference," Aluminium International Today, vol. 23, (6), pp. 31-32, 2011

# CHAPITRE 1
# SURVEILLANCE DU SOUDAGE LASER UN APPROCHE A L'INDUSTRIE 4.0, MÉTHODES DE SURVEILLANCE ET D'OPTIMISATION

Joys Silva Rivera[1], Ahmad Aminzadeh[1], Pedram Farhadipour[1], Noureddine Barka[1], François Nadeau[2], Abderrazak El Ouafi[1]

[1] Department of Mathematics, Computer Science and Engineering, Université du Québec à Rimouski, Rimouski, Québec, Canada

[2] National Research Council Canada - Aluminium Technology Centre, QC, Canada

*Corresponding author: joys.silvarivera@uqar.ca

*Cet article a été soumis dans The International Journal of Laser Applications portant le numéro de référence JLA22-RV-ALSTA2021-00109*

## 1.1 RÉSUMÉ PREMIER ARTICLE

Dans cet article de synthèse, les techniques de surveillance appliquées au soudage au laser sont présentées et résumées. Un processus de détection en ligne est proposé et décrit dans le but d'introduire un concept de fabrication intelligente pour les applications industrielles. La méthode de soudage au laser est caractérisée par des signaux optiques, thermiques et même acoustiques. Par conséquent, la nature du processus peut être utilisée pour détecter et définir les paramètres de fonctionnement et analyser les phénomènes. Les données obtenues peuvent être analysées et traitées afin d'appliquer des algorithmes d'apprentissage automatique qui prédisent et optimisent la qualité du produit final. Par conséquent, la définition et l'étude de diverses méthodes et techniques de détection est une pratique très importante en ce qui concerne les applications intelligentes et l'évolution des procédés de fabrication de soudage.

## 1.2 CONTRIBUTIONS

Ce premier article, intitulé *« Laser welding monitoring and an approach to industry 4.0, monitoring and optimization methods »* fut essentiellement rédigé par son premier auteur Joys S. Rivera qui a également réalisé toutes les recherches, tableaux, figures et défini la méthodologie pour faire la surveillance en temps-réel proposé par l'article. Ahmad

Aminzadeh est le second auteur de cet article et il a prodigué des conseils pour améliorer le travail, Pedram Farhadipour a participé dans la révision de l'article avec Noureddine Barka, Abderrazak El Ouafi et François Nadeau. Ces derniers ont agi comme superviseurs du projet. Ils ont également contribué à l'amélioration de la rédaction pour la version finale.

## 1.3 TITRE DU PREMIER ARTICLE

Laser welding monitoring and an approach to industry 4.0, monitoring and optimization methods

## 1.4 ABSTRACT

In this review paper, the monitoring techniques applied to laser welding are presented and summarized. An on-line sensing process is proposed and described with the aim of introducing an intelligent manufacturing concept for industrial applications. The laser welding method is characterized by optical, thermal, and even acoustic signals. Consequently, the nature of the process can be used to sense and define operation parameters and analyze phenomena. The obtained data can be analyzed and treated in order to apply machine learning algorithms that predict and optimize the quality of the final product. Therefore, defining and studying diverse sensing methods and techniques is a very important practice with regards to intelligent applications and the evolution of welding manufacturing processes.

***Keywords*****:** *Laser welding, intelligent monitoring, Industry 4.0, smart manufacturing, on-line monitoring, machine learning.*

## 1.5 NOMENCLATURE

| | |
|---|---|
| **NDT** | Non-destructive methods |
| **CMOS** | Complementary metal oxide semiconductor |
| **ISO** | International Organization for Standardization |
| **SVM** | Support Vector Machine |
| **PCA** | Principal Component Analysis |
| **N/A** | Non applicable |

**ACRL** Actor-Critic Reinforcement Learning

**ms** Millisecondes

**nm** Nanomètres

**Mg** Magnésium

**Zn** Zinc

**Cu** Cupper

**Al** Aluminum

**kW** Kilowatts

## 1.6 INTRODUCTION

Laser welding's benefits include higher productivity, deep penetration welding, high welding speeds, adaptability and high-power density. These characteristics are of utmost interest when compared with other welding processes [1]. Thanks to its automation potential, it is possible to implement controlled systems integrating artificial intelligence, data science and machine learning that help to optimize each step of the process and predict and control the parameters needed to operate the equipment in a way that ensures the best balance between quality, cost, and delay for the product. For these reasons, laser welding's applications in automotive, aerospace, shipbuilding, railcar and electronic manufacturing have increased on a large scale [2]–[5]. This article presents a review of the monitoring and optimization systems and methods used in laser welding, with the objective defining the relationship between welding parameters, weld properties and weld quality.

The evolution of welding processes has occurred in four main phases, which are represented in Figure 5. In the first phase, welding was done by hand, which had limitations in efficacy and process consistency. In phase two, automation and robotics were applied, leading to model and control difficulties. The third phase used "teach and playback" robots

in off-line conditions with limits associated with operational changes and disruptions. In the fourth phase, intelligent systems are applied to the welding process for monitoring and controlling welding parameters, dynamics and quality. This phase is characterized by the evolution from manual (human-physical) to intelligent systems (human-cyber-physical)[1], [6], [7].

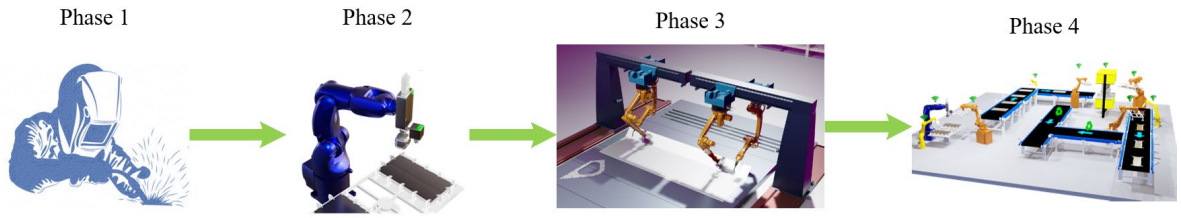


Figure 5. Representation of welding evolution phases.

In Figure 6 a schematic representation of the 4.0 laser welding is shown, characterized by online monitoring and control of the welding process, and composed of monitoring devices that register different kinds of signals emitted by the process, such as acoustic, optical and thermal signals. These signals can be treated in order to ensure the best accuracy in parameter control and quality predictions according to the learned data and experience of the system. This process is continuous, and a response time below 2 ms should be respected to provide accurate conditions for real-time monitoring [8]. This paper is structured as follows: section 1 discusses on-line monitoring, section 2 is about the inspection of laser welding with nondestructive methods (NDT), and section 3 considers optimization and metaheuristic approaches for modeling and optimization. These sections mention methods and techniques that can be applied for aluminum laser welding monitoring and optimization.

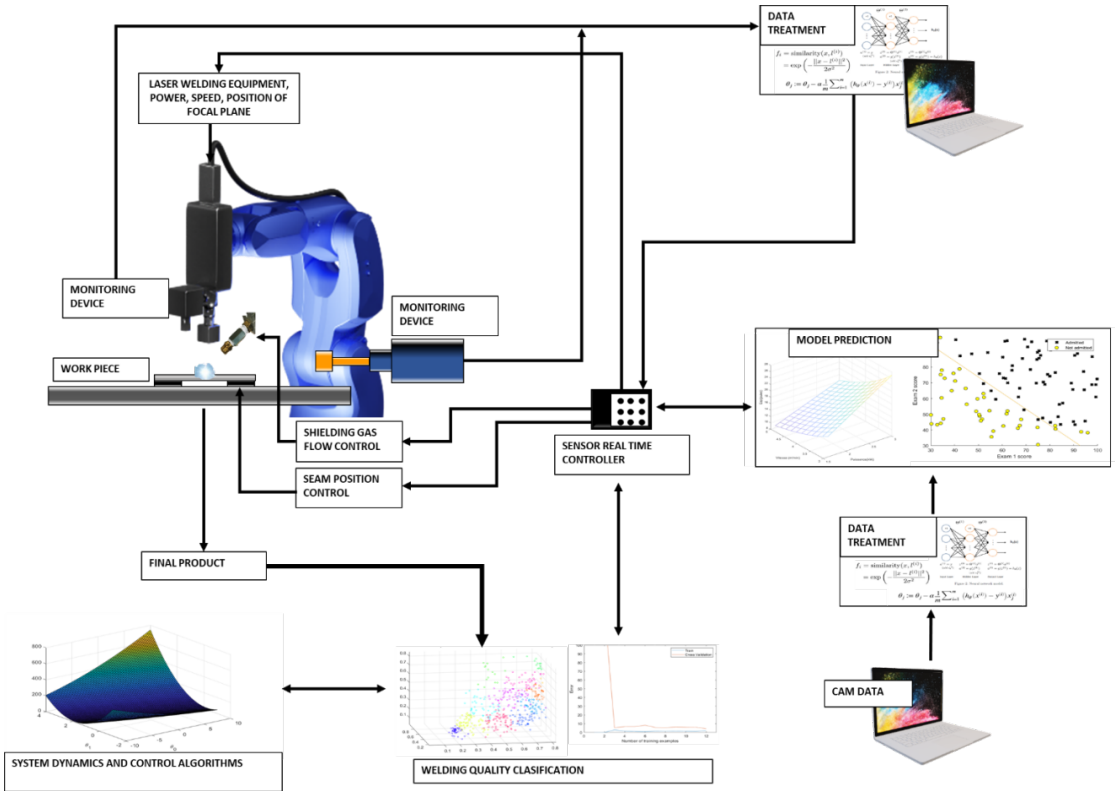


Figure 6. Schematic representation of the 4.0 laser welding process

## 1.7 METHODS AND RESULTS

### 1.7.1 Real-time monitoring of laser welding

Off-line monitoring and testing of welding is an inefficient and costly process in terms of time, material losses and limitations in productivity. Real-time monitoring systems have been proposed and developed in order to effectively control welding parameters, equipment response and the expected process quality. Therefore, several real-time welding quality monitoring solutions have been proposed to provide real-time information to control the welding process. Figure 7 d describes the different stages of process monitoring according to the operational stage and the common monitoring objective in the industry [9]. These stages help to define the proper parameters related to the laser welding process itself. Plasma, metal plume, spatters, seam geometry, keyhole, molten pool, laser back reflection and penetration hole give information from which it is possible to obtain optical, thermal or acoustic signals. Table 3 shows each process stage's control and monitoring devices and the signals associated to the monitoring objectives. The referred articles describe how a successful monitoring process with high potential to be scaled in industrial applications was

reached. This table describes literature-reported methods based on the different phenomena and variables of the laser welding process, taking benefit from the signals that are present.

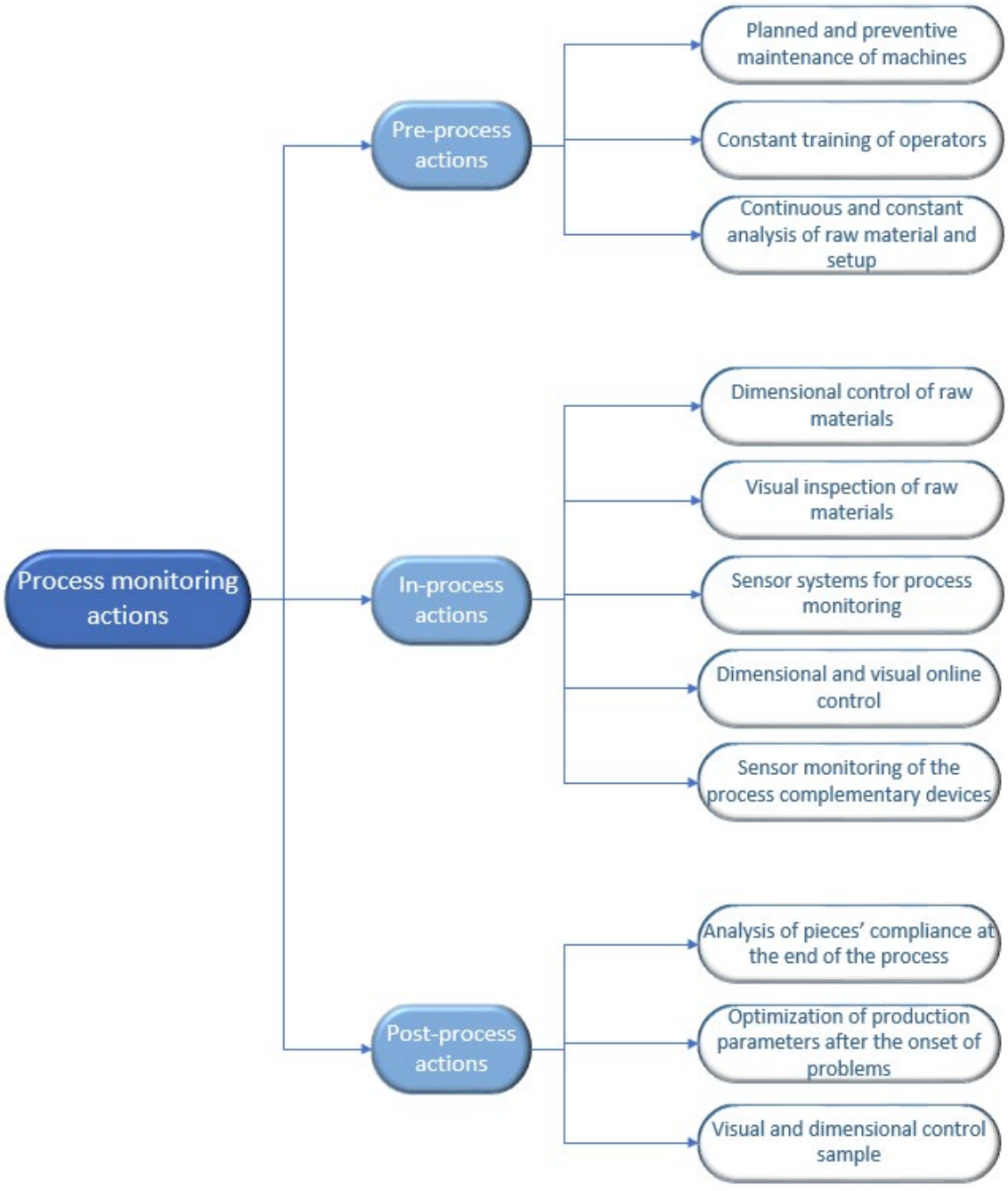


Figure 7. Actions to be implemented for pre-, in- and post-process monitoring.

Table 3. Monitoring devices and signals associated to monitoring and process stage objectives.

| Stage | Monitoring objective | Monitoring signal | Monitoring equipment |
|---|---|---|---|
| Pre-process | Seam tracking | Optical signal | CMOS camera, 640 x 300 pixels. [39] |
| | Gap measuring | | Camera-based, max. rate 1500 Hz, resolution 144 x 176 pixels. [40] |
| In-process (on-line) | Welding stability | Acoustic signal | High-definition microphone and audible range of 20 Hz to 20 kHz. [41] |
| | Defects monitoring | Optical signal | High-speed camera system (Memrecam fx RX6, 200 frames/s, resolution 512 x 512 pixels[42] |
| | Molten pool | Optical signal | A Photron SA4 high-speed camera.[37] |
| | Keyhole geometry | Optical signal | A Photron SA4 high-speed camera. [37] |
| | Keyhole depth | Optical signal | Phantom V611 high-speed camera + CAVITAR CAVILUX™ Smart [43] |
| | Penetration hole | Optical signal | A Photron SA4 high-speed camera. [37] |
| | Metal plume | Optical signal Thermal signal | Photodiode, optical parametric oscillator, uncoated planoconvex lens, Czerny-Turner spectrometer[44] |
| | Feedback control | Thermal signal | Si-Photodiode for temperature observation (wavelength 200 - 1100 nm)[45] |
| Post-process | Defects monitoring | Optical signal | PbSn- basedc amera (resolution 32x 32 pixels, framerate 500Hz). [40] |
| | Weld geometry classification | Acoustic emission | Microphone. [46] Inspection, metallographic test [47], [48] |

### 1.7.2 Real-time monitoring configurations

To obtain the signals that make it possible to get key data to monitor, control, define and predict the quality results of laser welding, it is important to choose and implement the correct devices according to the nature of expected signals, thus ensuring optimal configuration to get the best performance for monitoring processes [20], [21]. The traditional configuration used for these devices and sensors are coaxial or paraxial, where the coaxial can get information directly above the welding zone and where paraxial monitoring allows to adjust the distance and angle of the device with reference to the welding zone [20] . Thermal and optical signals can be monitored at the same time with the use of coaxial and paraxial configuration for the sensors and monitoring devices [22]. Figure 8 illustrates the paraxial and coaxial monitoring devices' configuration. X. Xiao et al. implemented a coaxial monitoring configuration with a pyrometer sensor to collect and measure the temperature profile of the laser welding process and the impact of focal length in the temperature sensing results, where a relationship between the temperature and geometrical parameters such as penetration and width was found [23]. Z. Zhang et al. implemented a coaxial configuration with a high-speed camera to monitor the welding geometry and measure and estimate the keyhole and the welding pool behavior, which helps to predict and diagnose the penetration condition. Four main penetration conditions were defined and predicted (partial penetration, moderate penetration, full penetration, and excessive penetration, with a classification accuracy of 94.6%) [8]. D. You et al. implemented the combination of paraxial and coaxial configuration to monitor the laser welding process, where light emission intensity was sensed with a photodiode in coaxial position and a high-speed camera was employed in order to monitor the metallic plasma on the top and bottom of the welded plate, where a relationship between the instability of the vapor plume and the change in the intensity value was found [24].

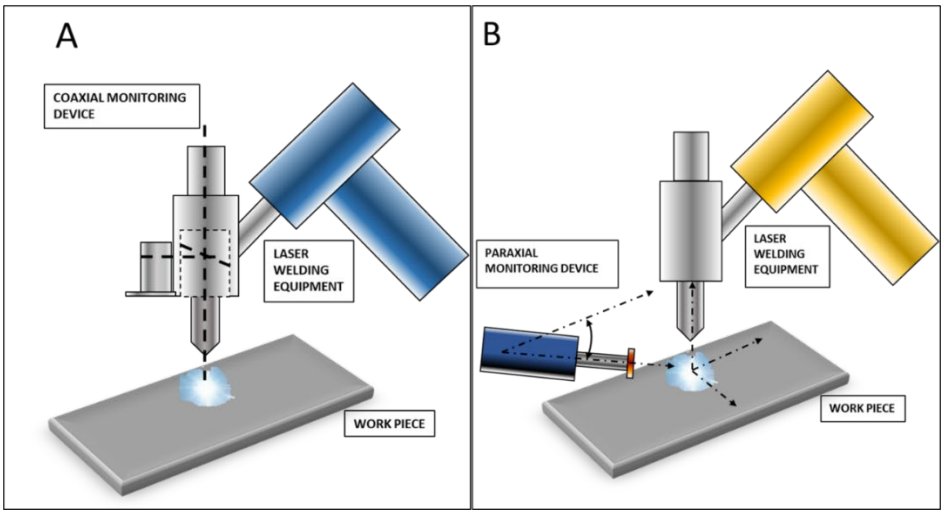


Figure 8. Illustration of monitoring configuration devices. A. Coaxial monitoring configuration. B. Paraxial monitoring configuration.

### 1.7.3 Optical signals and thermal signals

In laser welding, thermal signals are significant as they are related to the characteristics of the process with which the laser beam increases the temperature of the material plate above the melting temperature. Therefore, the laser welding process could be classified as a thermal fabrication process. In the keyhole, where the energy of the laser beam is concentrated, thermal radiation signals are considerable and allow to capture important information to characterize the process[1]. The molten pool composed of melted metal and metallic vapor emits an enormous quantity of radiation as well, thus these zones are interesting to monitor.

For optical signals, photodiodes, optical parametric oscillators and plano-convex lenses registered material emissions from the metal plume as well as atom emissions, which are related to laser power and pulse duration. [25] To obtain images of the keyhole, molten pool, penetration hole, and metal plume, high-speed cameras supported by filters and image sensors were implemented, providing excellent results and high accuracy in determining each mentioned feature of the welded zone on real-time monitoring [26] [8]. To capture different optical spectrum ranges, such as visible, infrared, and ultraviolet light, photodiodes and spectrometers can be implemented [11][25]. Figure 9 presents the usual configuration for optical signals acquisition. The illustrated setup shows how the optical signal is collected,

transmitted and processed by spectrometer (collimator) and amplifier (photodiode) to a monitoring computer, where the inspection process continues with the data analysis and implementation of machine learning algorithms that will define the operational conditions for laser welding machines based on welding quality prediction and analysis [20], [27].

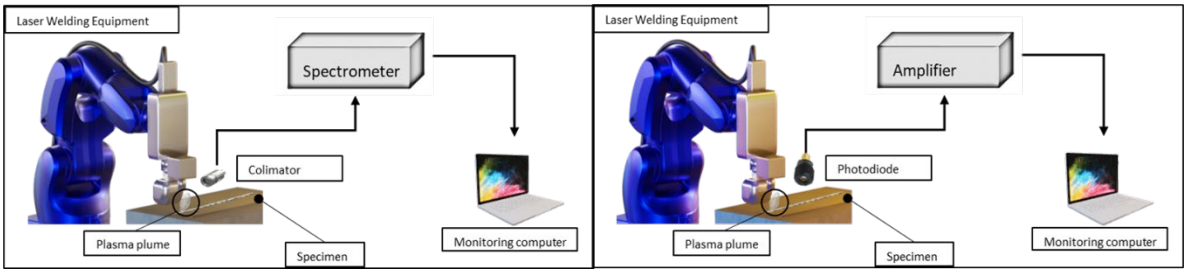


Figure 9. Monitoring setup for optical signals acquisition. Left: Collimator-Spectrometer, Right: Photodiode-Amplifier.

Optical devices and specific temperature sensors could be implemented in order to capture the radiation and temperature signals in the welding process. Pyrometers and infrared cameras are commonly used sensors for obtaining thermal signals[28]. Pyrometer sensors are a cheap and efficient monitoring solution that can be used in severe conditions, but which are normally limited by the testing frequency[29]. The infrared camera widely reflects the temperature distribution of the welding zone, and this benefit allows to collect surface temperature information[28]. For temperature observation, photodiodes were used to examine the temperature in keyhole and plasma radiation, monitor the welding process and obtain information to train a support vector machine classification algorithm [11]. Table 4 presents the monitoring phenomena of the laser welding process that can be sensed by different instruments for data acquisition from optical and thermal signals and the reported limitations in implementing them.

Table 4. Sensor and method attributes for welding monitoring based on optical and thermal signals [20].

| Sensor or Method | Monitoring Phenomena | Limitations and Comments |
|---|---|---|
| **Pyrometer** | Temperature of plasma<br>Temperature of molten pool | Low sampling and no defect information |
| **Infrared or Near Infrared Camera** | Thermal field | Low sampling and high cost |
| **Vision Camera** | Plasma plume<br>Molten pool<br>Keyhole<br>Spatters<br>Welding gap | Additional equipment required and images processing needed |
| **Spectrometer** | Spectrum of plasma | Monitoring reduced to plasma behaviour |
| **Photodiode** | Plasma<br>Reflective laser beam<br>Thermal radiation | Low efficiency in identifying microdefects |
| **Novel Monitoring Technology** | X-ray<br>Inline image collector<br>Magneto-optical imaging | High cost and limited use environment |

### 1.7.4 Acoustic signals

Acoustic emissions concern a sensor that takes the process sounds and converts them into an electrical output to a quantitative variable. Condenser microphones that are composed of a capacitor, which measure sound and the change in its capacitance, are commonly used as measurement microphones [17]. Y. Luo et al. reported that acoustic signals in the laser welding process are produced by the recoil force caused by the evaporation of metal vapor and plasma. In Figure 10, a schematic representation of acoustic emission phenomena in laser welding is represented [30]. Acoustic signals on laser welding provide information and data regarding material phase changes and have been used to determine the quality of the welding. Consequently, acoustic monitoring could be applied on inspection methods related to melting, vaporization, keyhole formation and plasma emission [31]. This monitoring technique is an affordable and simple operational solution for laser welding inspection, but a common disadvantage of acoustical monitoring is that for non-contact acoustic sensors, the environmental noise could make it harder to detect signals and use them in on-line monitoring

applications [12], [20]. For this reason, and with the objective to take advantage of these signals in the online monitoring process, the current study focuses on how to improve signal identification accuracy and implement intelligent algorithms to correlate signals with welding parameters and quality [32].

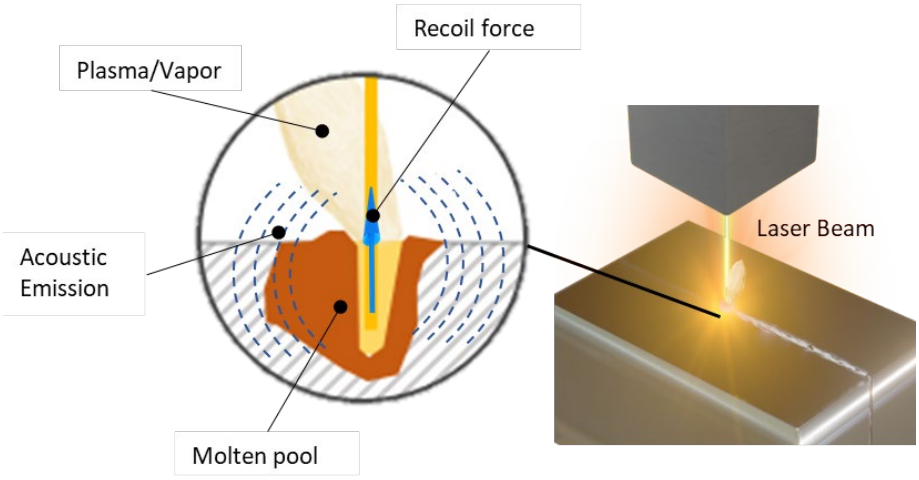


Figure 10. Schematic diagram of acoustic emission signal in the laser welding process.

Figure 11 presents the monitoring array for aluminum laser welding proposed by L. Schmidt et al. This paper reported that is possible to monitor the process with a structure-borne acoustic emission system that uses microphones. Due to treating the obtained signals with machine learning methods, a high prediction rate of over 95% in welding speed identification can be achieved [33]. Zhen L. et al. implemented an array of eight microphones and a signal treatment algorithm to conduct laser welding monitoring by source localization and tracking processing. In this study, a relationship was found between acoustic pressure levels changes and welding defects, and the most important challenge mentioned in this article is the surrounding acoustic signal, which affects the quality of the acquired data in the monitoring process. In Figure 12 the reported result of this study is presented [34]. Y-L. Mao et al. found a link between acoustic emission energy fluctuation and process parameters such as welding speed, power and focusing. In this study, the acoustic signals were analyzed using a real-time monitoring process [31].

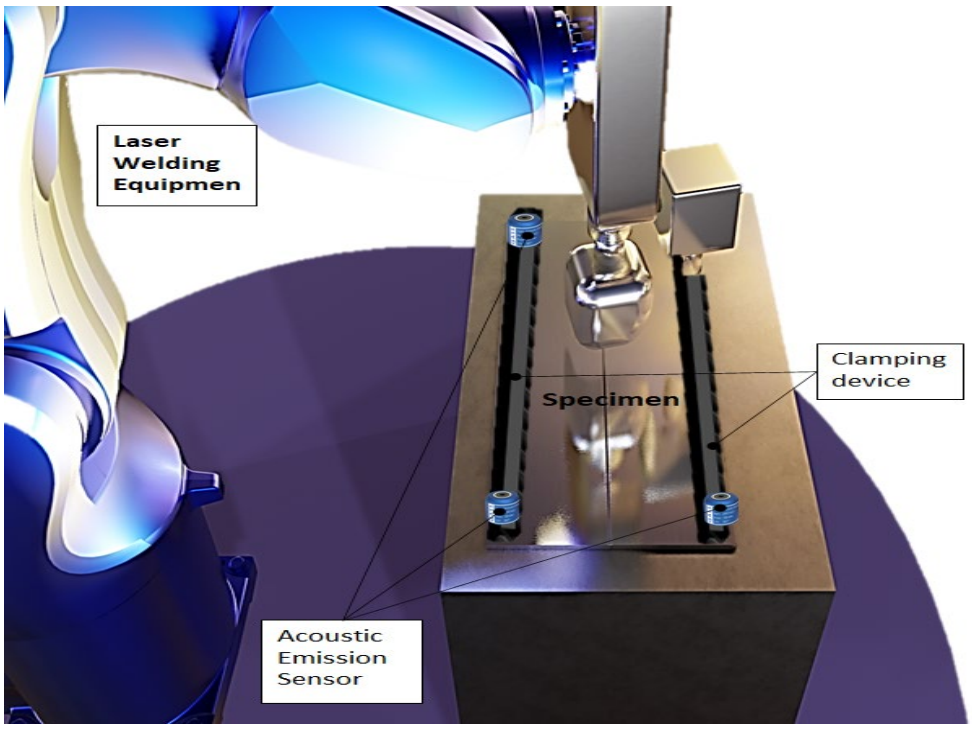


Figure 11. Acoustic signal monitoring setup for laser welding.

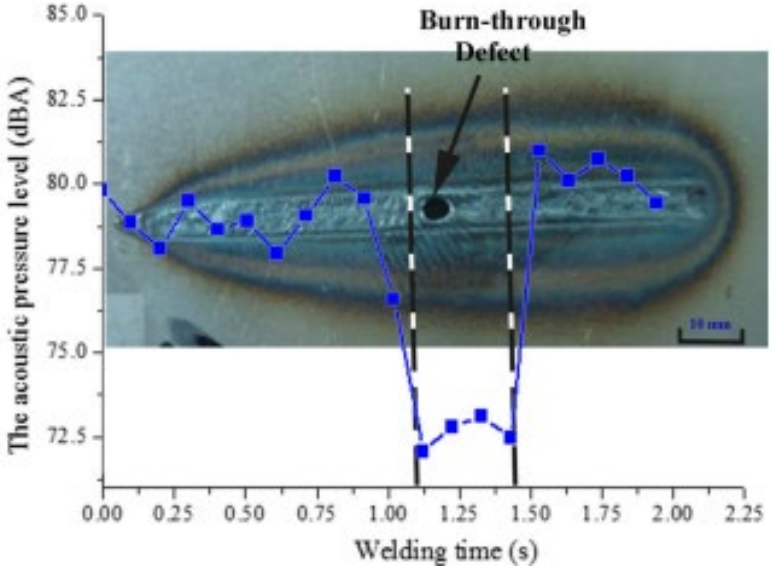


Figure 12. Acoustic pressure level deviation and laser welding defects [34].

### 1.7.5 Loop systems in real-time monitoring

Loop systems refer to the data processing and objective of the collected information. The literature refers to two categories of loop systems, open-loop and closed-loop systems.

Both open- and closed-loop control is used in welding [35]. The open-loop system is characterized by not implementing signals to control main welding process parameters These systems do not prevent defects and are implemented in order to create the signals and data and to associate the process conditions with the noticed defects. The closed-loop system is used to evaluate the quality of the product and ensure the accuracy of the process.

In the laser welding process, the closed-loop system typically implements the optical signals emitted by the plasma plume and reflected laser radiation. A study of laser welding of aluminum alloys reported a correlation between back laser radiation and welding quality, and this signal has enormous potential for closed-loop systems [17]. Another study reported a closed-loop system that can control the seam position with images captured by a CMOS camera [36]. A third study used photodiodes and cameras to monitor and control the process, getting prediction results of 21 μs to implement the welding parameters auto-correction [11]. This study shows promising results that can help to implement on-line control in industrial applications.

## 1.8 INSPECTION OF LASER WELDING AND- NON-DESTRUCTIVE METHODS

In laser welding, the defects are related to the nature of the process and its environmental and material conditions. For aluminum laser welding, the most common defects are lack of penetration (due to the material's poor absorption properties), weld oxidation (associated with gas protection), porosities (due to gas entrapment during welding solidification) and cracks (due to the coefficient of thermal expansion)[37]. The ideal situation for laser welding is to be implemented in materials with high absorption values and a low thermal conductivity, which are not the characteristics of aluminum. At high temperatures, this material's absorptivity increases faster, and the welding process becomes unstable. As a result, a lot of spatters appear. At high welding speeds, the humping phenomenon affects the surface quality, thus affecting the aspect of the surface plaque and of the welding[38]. Therefore, it is very important to control the mentioned welding defects in order to ensure the best conditions in the welding results. The quality evaluation techniques for each stage of the process are mentioned in the literature. Table 5 resumes quality criteria and techniques that can be applied in aluminum laser welding.

Table 5. Quality evaluation stages and criteria with the most common implemented techniques.

| **Quality evaluation stage** | **Quality criteria** | **Implemented techniques and technology** |
|---|---|---|
| Pre-process | Part geometry, gap seam tracking, fixtures. | Machine vision, ultrasound [35] [36] |
| In-process | Weld defects, melt pool dimension, penetration hole, metal plume, penetration state. | Machine vision, dimensional reduction techniques, discrete Fourier, neural network, support vector machine, convulsionary neural network, X-ray monitoring [8][32][35] [39] |
| Post-process | Weld geometry, visible defects (size, types and orientations). | Machine vision, visual inspection, liquid penetrant, magnetic particle, ultrasonic and radiographic testing, acoustic emission, multi-element eddy-current sensors. [32][35] |

The first quality test for seam quality can be done in the pre-process stage with the implementation of fixtures that can ensure the correct position and allow to fix the workpiece with the smallest gap possible. A fixture maintains the workpiece in place during the process. These fixtures are designed according to the configuration, the joint position of the piece and the welding process type[35]. In Figure 13, the quality of the welding process with and offset bigger than 1 mm is shown. This shows that it is evident that welding could not be made for both pieces.

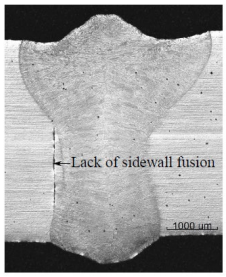


Figure 13. Cross section of welding with 1 mm offset from the joint.[64]

In real-time seam quality inspection, the method used is the seam tracking process. This is conducted with optical devices and machine learning algorithms that analyze the path of the

welding and that can predict the next points of the welding paths on the seam. A study reported the use of a monitoring system to control the joint and seam position based on image treatment and filtering (Canny edge detection algorithm, Kalman-based filter), with high potential to be used in industrial applications [36]. Another study presented a method for on-line weld seam tracking and welding quality analysis with a robust design of the image-blending tracking method [40]. This method can lower working time and costs by reducing the handling of material associated with manual weld seam inspection.

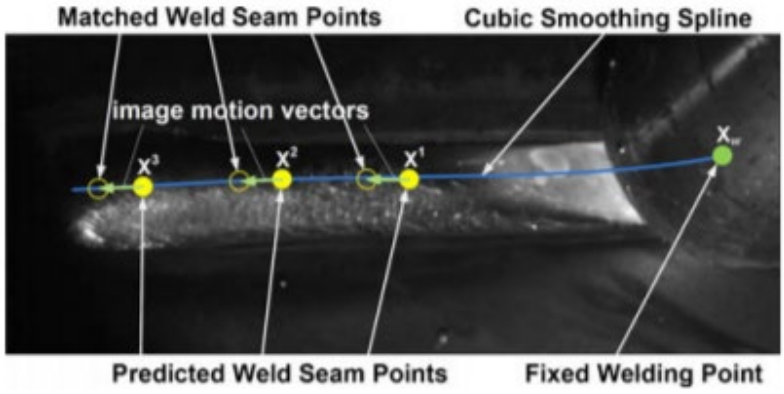


Figure 14. Seam tracking with image analysis [40].

Ultrasonic signals of the laser welding process have interesting potential for non-destructive inspection of the internal defects of the weld. A study researched ultrasonic inspection technology as a way to detect welding defects in thin aluminum sheets, finding that was possible to identify the presence of pores in the welding [28]. For laser welding of aluminum, the literature classifies two types of porosities that may occur. One is known as metallurgical porosity, related to the evaporation of the components of the aluminum alloy, such as hydrogen, Mg, Zn, etc. The other is caused by the collapse of unstable and shrinking keyholes [41]. The pores decrease the cross-section area of the welding, causing a reduction in strength, elongation, tensile properties, and fatigue [41][37]. Therefore, porosities have a big impact on the quality of the welding. For this reason, these types of defects have been widely studied and methods to detect and predict them have been developed. The most common method to test porosities is the X-ray analysis. Porosities are related to welding parameters such as power, speed and shielding gas flux, which are used to predict the density

of the porosities in the welding [41]. A study found a new technique for porosity tests that can be used to verify laser weld quality. An ultrasonic technique was used to determine if the inspected weld contained porosities or not [42].

To obtain the best performance results and reduce the economic and productivity impact related to quality defects and destructive tests, non-destructive tests are applied for the laser welding process. These non-destructive tests tend to be in real-time thanks to the automated characteristics of laser welding and sensing methods and to the development of machine learning and artificial intelligence tools. Table 6 mentions the monitoring method for the most common defects on laser welding and relates these defects to the monitoring method and the kind of signals that capture them.

Table 6. Defects monitoring methods and signals.

| Monitoring technique | Signal | Defects | Reference |
|---|---|---|---|
| **Image processing technique** | Thermal | Humping | [43], [44] |
| | | Blowouts | |
| | | Cracks | |
| | | Porosity | |
| | | Penetration | |
| | Vision | Penetration | [45]–[47] |
| | | Width | |
| | | Undercut | |
| | | Spatters | |
| | Combined | Molten pool geometry | [32][20] |
| | | Undercut | |
| | | Crack porosity | |
| | | Blowouts | |
| | | Penetration | |
| **Acoustic emission technique** | Acoustic | Penetration | [31], [32] |
| **Optical signal techniques** | Photodiode sensor | Penetration | [20], [48], [49] |
| | | Undercut | |
| | Spectrometer sensor | Undercut | |
| | | Blowouts | |
| | | Cracks | |
| | Pyrometer sensor | Penetration | |
| | Fused techniques | Molten pool geometry | [32], [49] |
| | | Crack porosity | |

| Monitoring technique | Signal | Defects | Reference |
|---|---|---|---|
| | | Undercut | |
| | | Spatters | |
| | X-ray radiography | Porosity | [32], [50] |
| | | Cracks | |
| | | Penetration | |
| | | Slags | |

## 1.9 Intelligent laser welding monitoring

Intelligent manufacturing is a novel manufacturing concept where production machines are interconnected through a network, monitored by sensors and controlled by advanced computational systems [51]. The application of sensing methods and machine learning algorithms is a novel monitoring technique applied on laser welding, where the performance of the process and the final product quality are improved [52]. In addition, life-cycle analysis (LCA) studies are growing, which is an important criterion for manufacturing companies to reduce scrap rate and thus further embrace an intelligent laser welding cell concept.

Brian J. et al. discovered that with the application of laser-induced fluorescence, it is possible to conduct in situ monitoring for Cu/Al laser welding based on the signals of atoms emitted by the plume during the welding process and even to define the quality of the welding [15]. J. Gunther et al. proposed a system that has the capacity to improve its own performance on the laser welding process using on deep learning algorithms, online monitoring and process correction, and that is based on welding quality classifications according to standard ISO 13919-:1996 [11]. Knaak C. et al. developed a monitoring system to control the joint and seam position based on image treatment and filtering, with high potential to be used in industrial applications [53]. Chen J. et al. reported that plume and spatters images contain information that help to predict the welding quality and used an SVM (support vector machine) algorithm to provide quality classification. They proved that this method provides high accuracy results in defect classification and that it is a practical real-time monitoring method for the laser welding process [26]. Zhang Z. et al. defined a relationship between the welding penetration and penetration hole geometry and presented a laser welding monitoring

system based on a convolutional neural network, which could diagnose the penetration results using a coaxial monitoring platform with the objective of obtaining output results in less than 2ms [8]. Table 7 presents a summary of pioneer studies for intelligent laser welding monitoring systems and setups, where the control equipment and machine learning methods are described.

Table 7. Intelligent inspection methodology and main studies of algorithms.

| Materials | Input Parameters | Output | Control Equipment | Algorithm or Machine Learning Method | Reference |
|---|---|---|---|---|---|
| - Aluminum/ copper, 0.2 mm thickness, shielding gas N2. | - Continuous wave fiber laser of 1070 nm wavelength, beam diameter 0.6 mm.<br>- Power 2.0 – 8.0 kW, Pulse duration 2 - 5 ms.<br>- Reflected wavelength.<br>- Wavelength Intensity.<br>- Backscattered weld laser light. | -Material emission in pulsed welding process.<br>- Atoms' CU intensity and laser power relationship.<br>- Pulse duration dependence on plume material emission concentration. | Photodiode, optical parametric oscillator, uncoated-planoconvex lens, Czerny-Turner spectrometer. | N/A | [15] |
| Zinc-coated laser welding process in an overlap position. | - Keyhole.<br>- Temperature.<br>- Plasma radiation.<br>- Laser back reflection. | - Quality classification of the seam according to EN ISO 13919-1: 1996.<br>- Online monitoring and process control.<br>- Computing predictions in 21 µs for real-time operations. | -Camera-based max. rate 1500 Hz, resolution 144 x 176 pixels.<br>-Photodiode for temperature observation (wavelength 1100 - 1800 nm).<br>- Photodiode for plasma radiation observation (wavelength 400 - 600 nm)<br>- Photodiode for laser back reflection (wavelength 1050 - 1080 nm). | - Actor–critic reinforcement learning (ACRL) algorithm.<br>- Support vector machine (SVM).<br>- Principal component analysis (PCA). | [11] |
| - Stainless steel 316.<br>- Argon shielding gas. | - Laser power of 6 kW.<br>- Laser spot diameter of 1.12 mm.<br>- Seam position pictures. | The joint position and welding nominal path. | - CMOS camera, 640 x 300 pixels.<br>- LED lamps, wavelength 450 nm. | - Canny edge detection algorithm.<br>- Kalman-based filter. | [10] |
| Low carbon steel. | - Weld pool images.<br>- Keyhole area images.<br>- Example with welding defects to train the algorithm. | - The accuracy of feature selection.<br>- The accuracy of welding defect prediction.<br>- The prediction of welding quality. Good weld, weld width exceeds, lack of fusion and undercut. | - Si-based camera to observe the process zone (resolution 1312 x 1080 pixels, frame rate 100 Hz).<br>- PbSn-based camera to compare the significance of different welding defects (resolution 32x 32 pixels, frame rate 500 Hz). | - Principal component analysis (PCA).<br>- Classification algorithm. | [53] |
| - 304 stainless steel.<br>- Argon shielding gas, nozzle angle 45°. | - Spatter images.<br>- Plume images. | - Defects classification accuracy associated to feature quantity.<br>- Selection and definition of most important features for welding quality prediction.<br>- Classifiers for real-time monitoring based on plume and spatters images. | - Memrecam fx RX6 high-speed camera system (200 frames/s, resolution 512 x 512 pixels).<br>- Metal oxide semiconductor image sensors. | - Support vector machine (SVM). | [26] |
| - Aluminum.<br>- Argon shielding gas. | - Pictures with welding pool, keyhole and penetration hole.<br>- Laser power 0.8 - 1.7 kW. | - Classification of penetration condition of the welding process related to the thickness and laser power. The welding is classified as partial penetration, moderate penetration, full penetration and excessive penetration. | -A Photron SA4high-speed camera.<br>- Neutral density filter and an 808 nm band pass filter in the camera lens. | - Convolutional neural network.<br>- Backpropagation algorithm. | [8] |

## 1.10 Metaheuristic approaches for modeling and optimization of laser welding

Nowadays, industrial processes seek to optimize their process parameters as this is one of the most important issues for companies [54]. Figure 15 illustrates the factors that compose an industrial process, where to produce an expected output as a result of the defined inputs and their interactions with control and noise, factors necessary to ensure the optimal conditions for process productivity [55]. The definition of the process parameters and the correct identification of noise and input parameters have an important role on the optimization of the responses, and these steps are defined as the starting point for process modelling [56].

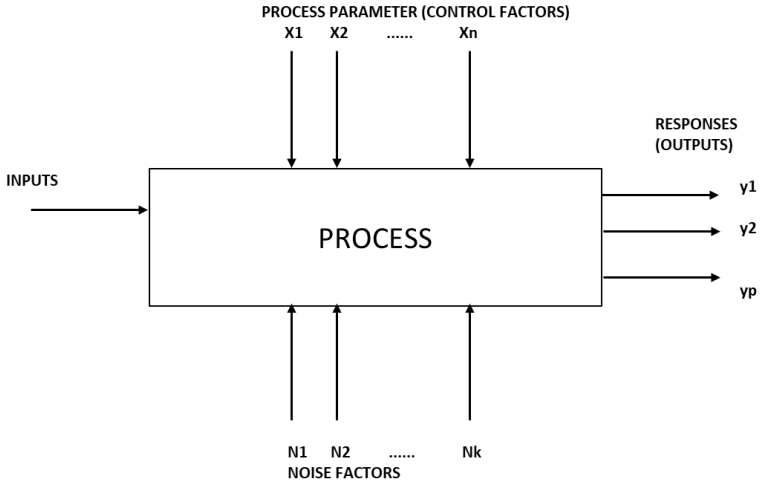


Figure 15. General model of an industrial process. [78]

The application of machine learning and artificial intelligence in the optimization parameters of the emerging process, where the correlations between factors are unknown and non-linear, receives much interest and development [57]. The most common artificial intelligence techniques used for parameter optimization include the radial basis function neural networks, support vector regression, back propagation neural networks, deep learning and genetic algorithms [16].

### 1.10.1 Metaheuristic algorithms

Metaheuristic algorithms offer higher-level procedures to provide a satisfactory solution to an optimization problem. This is formally defined as an iterative generation process guiding a subordinate heuristic, which is an aid to learning, discovery or problem-solving by experimental and trial-and-error methods and combining intelligently different concepts for exploring and exploiting the search space. Learning strategies are used to structure information and find near-optimal solutions. The principal metaheuristic algorithms are:

- Genetic algorithm: commonly used for parameter process optimization (see Figure 16).
- Simulated annealing: this algorithm imitates the metal annealing process.
- Particle swarm optimization: it imitates the movement of a set of particles in a multidimensional space.

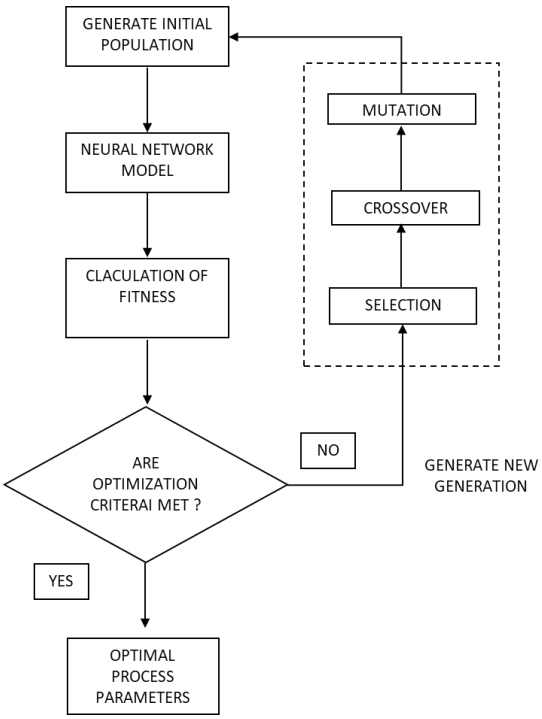


Figure 16. Flow chart for the optimization parameters using genetic algorithms [58].

A study reported results to improve the lap joint quality using the Taguchi and neural-genetic approach methods [59]. These methods were used to find the optimal values for pulse conditions and focus distance, and with the use of the neural-genetic approach the defective rate improved by 6.79% with respect to the optimal values found by the Taguchi method. Another study applied the radial basis function neural network and genetic algorithms to optimize the laser power, welding speed, focal position, and the gap of the plaques in order to find the optimal values for the welding dimensions [60]. As a result, it was possible to get better results in welding geometry, microstructure, and tensile strength with the optimal welding geometry. As shown in Figure 17, the optimization process considerably improves the quality results of the welding with respect to the random values used for the process.

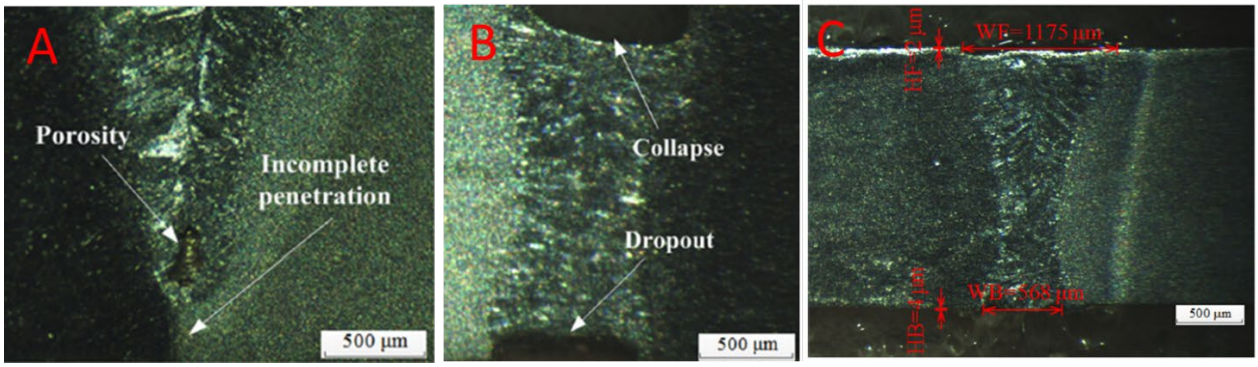


Figure 17. Results of different conditions and parameters for the welding process. A and B show random welding parameter values, C shows optimal welding parameter values.[83]

## 1.11 CONCLUSION

Laser welding process application is a growing field in industries and monitoring systems are a challenge when it comes to implementation, process parameters optimization and quality inspection on the final product. The laser welding process offers important advantages for industries, including a small heat-affected zone which reduces geometrical distortion, high energy efficiency, and higher welding speed compared to conventional welding methods, but it is nevertheless a

complex process due to the involved physical phenomena and the difficulties in monitoring and controlling. For this reason, studying and defining monitoring methods and technologies is a very important subject for the development and application of this solution. The recent technological evolution of Industry 4.0 brings an important tool in resolving the problems of monitoring and controlling the process parameters. Implementing machine learning algorithms and artificial intelligence solutions can ensure the best product quality and more efficient use of the raw materials and resources in real life applications. In this paper, a literature review of sensing configurations, monitoring techniques and technologies, intelligent monitoring and algorithms applied to the laser welding process is studied and presented for an approach to Industry 4.0. This article gives the orientation of the technologies that can be employed in the industrial process and introduce the most effective methods for online monitoring in laser welding applications. Additionally, a monitoring workflow is described and presented, which can be applied as a practical guide to the real applications for research and industrial developments.

## 1.12 REFERENCES


[1] S. Katayama, *Introduction: Fundamentals of laser welding*, vol. 9, no. 2012. Woodhead Publishing Limited, 2013. doi: 10.1533/9780857098771.1.3.

[2] X. Wang, X. Zhou, Z. Xia, and X. Gu, "A survey of welding robot intelligent path optimization," *Journal of Manufacturing Processes*, no. December 2019, pp. 0–1, 2020, doi: 10.1016/j.jmapro.2020.04.085.

[3] J. Klæstrup Kristensen, "Applications of laser welding in the shipbuilding industry," *Handbook of Laser Welding Technologies*, pp. 596–612, 2013, doi: 10.1533/9780857098771.4.596.

[4] M. Graudenz and M. Baur, "Applications of laser welding in the automotive industry," *Handbook of Laser Welding Technologies*, pp. 555–574, 2013, doi: 10.1533/9780857098771.4.555.

[5] H. Wang, "Applications of laser welding in the railway industry," *Handbook of Laser Welding Technologies*, pp. 575–595, 2013, doi: 10.1533/9780857098771.4.575.

[6] J. Zhou, Y. Zhou, B. Wang, and J. Zang, “Human–Cyber–Physical Systems (HCPSs) in the Context of New-Generation Intelligent Manufacturing,” *Engineering*, vol. 5, no. 4, pp. 624–636, 2019, doi: 10.1016/j.eng.2019.07.015.

[7] M. de Graaf and R. Aarts, “Applications of robotics in laser welding,” *Handbook of Laser Welding Technologies*, pp. 401–421, 2013, doi: 10.1533/9780857098771.3.401.

[8] Z. Zhang, B. Li, W. Zhang, R. Lu, S. Wada, and Y. Zhang, “Real-time penetration state monitoring using convolutional neural network for laser welding of tailor rolled blanks,” *Journal of Manufacturing Systems*, vol. 54, no. January, pp. 348–360, 2020, doi: 10.1016/j.jmsy.2020.01.006.

[9] S. Ferretti, D. Caputo, M. Penza, and D. M. D’Addona, “Monitoring systems for zero defect manufacturing,” in *Procedia CIRP*, 2013, vol. 12, pp. 258–263. doi: 10.1016/j.procir.2013.09.045.

[10] M. Nilsen, F. Sikström, A. K. Christiansson, and A. Ancona, “In-process Monitoring and Control of Robotized Laser Beam Welding of Closed Square Butt Joints,” *Procedia Manufacturing*, vol. 25, pp. 511–516, 2018, doi: 10.1016/j.promfg.2018.06.123.

[11] J. Günther, P. M. Pilarski, G. Helfrich, H. Shen, and K. Diepold, “Intelligent laser welding through representation, prediction, and control learning: An architecture with deep neural networks and reinforcement learning,” *Mechatronics*, vol. 34, pp. 1–11, 2016, doi: 10.1016/j.mechatronics.2015.09.004.

[12] L. Zhang, A. C. Basantes-Defaz, D. Ozevin, and E. Indacochea, “Real-time monitoring of welding process using air-coupled ultrasonics and acoustic emission,” *International Journal of Advanced Manufacturing Technology*, vol. 101, no. 5–8, pp. 1623–1634, 2019, doi: 10.1007/s00170-018-3042-2.

[13] J. Chen, T. Wang, X. Gao, and L. Wei, “Real-time monitoring of high-power disk laser welding based on support vector machine,” *Computers in Industry*, vol. 94, pp. 75–81, 2018, doi: 10.1016/j.compind.2017.10.003.

[14] J. Xu, Y. Rong, Y. Huang, P. Wang, and C. Wang, “Keyhole-induced porosity formation during laser welding,” *Journal of Materials Processing Technology*, vol. 252, pp. 720–727, Feb. 2018, doi: 10.1016/j.jmatprotec.2017.10.038.

[15] B. J. Simonds, B. Tran, and P. A. Williams, “In situ monitoring of Cu/Al laser welding using Laser Induced Fluorescence,” *Procedia CIRP*, vol. 94, pp. 605–609, 2020, doi: 10.1016/j.procir.2020.09.088.

[16] D. Colombo, B. M. Colosimo, and B. Previtali, “Comparison of methods for data analysis in the remote monitoring of remote laser welding,” *Optics and Lasers in Engineering*, vol. 51, no. 1, pp. 34–46, Jan. 2013, doi: 10.1016/j.optlaseng.2012.07.022.

[17] T. Purtonen, A. Kalliosaari, and A. Salminen, “Monitoring and adaptive control of laser processes,” *Physics Procedia*, vol. 56, no. C, pp. 1218–1231, 2014, doi: 10.1016/j.phpro.2014.08.038.

[18] M. Rossini, P. R. Spena, L. Cortese, P. Matteis, and D. Firrao, “Investigation on dissimilar laser welding of advanced high strength steel sheets for the automotive industry,” *Materials Science and Engineering A*, vol. 628, pp. 288–296, Mar. 2015, doi: 10.1016/j.msea.2015.01.037.

[19] A. Lisiecki, “Diode laser welding of high yield steel,” in *Laser Technology 2012: Applications of Lasers*, Jan. 2013, vol. 8703, p. 87030S. doi: 10.1117/12.2013429.

[20] W. Cai, J. Z. Wang, P. Jiang, L. C. Cao, G. Y. Mi, and Q. Zhou, “Application of sensing techniques and artificial intelligence-based methods to laser welding real-time monitoring: A critical review of recent literature,” *Journal of Manufacturing Systems*, vol. 57. Elsevier B.V., pp. 1–18, Oct. 01, 2020. doi: 10.1016/j.jmsy.2020.07.021.

[21] Z. jue Tang, W. wei Liu, N. Zhang, Y. wen Wang, and H. chao Zhang, “Real–time prediction of penetration depths of laser surface melting based on coaxial visual monitoring,” *Optics and Lasers in Engineering*, vol. 128, May 2020, doi: 10.1016/j.optlaseng.2020.106034.

[22] D. Chen *et al.*, “Research on in situ monitoring of selective laser melting: a state of the art review”, doi: 10.1007/s00170-020-06432-1/Published.

[23] X. Xiao, X. Liu, M. Cheng, and L. Song, “Towards monitoring laser welding process via a coaxial pyrometer,” *Journal of Materials Processing Technology*, vol. 277, no. August 2019, p. 116409, 2020, doi: 10.1016/j.jmatprotec.2019.116409.

[24] D. You, X. Gao, and S. Katayama, “Multiple-optics sensing of high-brightness disk laser welding process,” *NDT and E International*, vol. 60, pp. 32–39, 2013, doi: 10.1016/j.ndteint.2013.07.005.

[25] B. J. Simonds, B. Tran, and P. A. Williams, “In situ monitoring of Cu/Al laser welding using Laser Induced Fluorescence,” *Procedia CIRP*, vol. 94, pp. 605–609, 2020, doi: 10.1016/j.procir.2020.09.088.

[26] J. Chen, T. Wang, X. Gao, and L. Wei, “Real-time monitoring of high-power disk laser welding based on support vector machine,” *Computers in Industry*, vol. 94, pp. 75–81, 2018, doi: 10.1016/j.compind.2017.10.003.

[27] O. O. Oladimeji and E. Taban, “Trend and innovations in laser beam welding of wrought aluminum alloys,” *Welding in the World*, vol. 60, no. 3, pp. 415–457, 2016, doi: 10.1007/s40194-016-0317-9.

[28] W. Cai, J. Z. Wang, P. Jiang, L. C. Cao, G. Y. Mi, and Q. Zhou, “Application of sensing techniques and artificial intelligence-based methods to laser welding real-time monitoring: A critical review of recent literature,” *Journal of Manufacturing Systems*, vol. 57, no. July, pp. 1–18, 2020, doi: 10.1016/j.jmsy.2020.07.021.

[29] M. Doubenskaia, Ph. Bertrand, H. Pinon, and I.Smurov, “On-line optical monitoring of Nd: YAG laser lap welding of Zn-coated steel sheets ,” *IV International WLT-Conference on Lasers in Manufacturing*, no. January 2015, pp. 543–547, 2007.

[30] Y. Luo, L. Zhu, J. Han, X. Xie, R. Wan, and Y. Zhu, “Study on the acoustic emission effect of plasma plume in pulsed laser welding,” *Mechanical Systems and Signal Processing*, vol. 124, pp. 715–723, Jun. 2019, doi: 10.1016/j.ymssp.2019.01.045.

[31] Y. Mao, G. Kinsman, and W. W. Duley, " Real-Time Fast Fourier Transform Analysis of Acoustic Emission during CO 2 Laser Welding of Materials ," *Journal of Laser Applications*, vol. 5, no. 2, pp. 17–22, Oct. 1993, doi: 10.2351/1.4745326.

[32] J. Stavridis, A. Papacharalampopoulos, and P. Stavropoulos, "Quality assessment in laser welding: a critical review," *International Journal of Advanced Manufacturing Technology*, vol. 94, no. 5–8, pp. 1825–1847, 2018, doi: 10.1007/s00170-017-0461-4.

[33] L. Schmidt *et al.*, "Acoustic process monitoring in laser beam welding," *Procedia CIRP*, vol. 94, pp. 763–768, 2020, doi: 10.1016/j.procir.2020.09.139.

[34] Z. Luo, W. Liu, Z. Wang, and S. Ao, "Monitoring of laser welding using source localization and tracking processing by microphone array," *International Journal of Advanced Manufacturing Technology*, vol. 86, no. 1–4, pp. 21–28, Sep. 2016, doi: 10.1007/s00170-015-8095-x.

[35] B. Wang, S. J. Hu, L. Sun, and T. Freiheit, "Intelligent welding system technologies: State-of-the-art review and perspectives," *Journal of Manufacturing Systems*, vol. 56, no. July, pp. 373–391, 2020, doi: 10.1016/j.jmsy.2020.06.020.

[36] M. Nilsen, F. Sikström, A. K. Christiansson, and A. Ancona, "In-process Monitoring and Control of Robotized Laser Beam Welding of Closed Square Butt Joints," *Procedia Manufacturing*, vol. 25, pp. 511–516, 2018, doi: 10.1016/j.promfg.2018.06.123.

[37] J. M. Sánchez Amaya, M. R. Amaya-Vázquez, and F. J. Botana, *Laser welding of light metal alloys: Aluminium and titanium alloys*. 2013. doi: 10.1533/9780857098771.2.215.

[38] M. R. Maina, Y. Okamoto, A. Okada, M. Närhi, J. Kangastupa, and J. Vihinen, "High surface quality welding of aluminum using adjustable ring-mode fiber laser," *Journal of Materials Processing Technology*, vol. 258, no. April, pp. 180–188, 2018, doi: 10.1016/j.jmatprotec.2018.03.030.

[39] S. Katayama, *Defect formation mechanisms and preventive procedures in laser welding*. 2013. doi: 10.1533/9780857098771.2.332.

[40] M. Heber, M. Lenz, M. Rüther, H. Bischof, H. Fronthaler, and G. Croonen, "Weld seam tracking and panorama image generation for on-line quality assurance," *International Journal of Advanced Manufacturing Technology*, vol. 65, no. 9–12, pp. 1371–1382, 2013, doi: 10.1007/s00170-012-4263-4.

[41] K. Li, F. G. Lu, S. T. Guo, H. C. Cui, and X. H. Tang, "Porosity sensitivity of A356 Al alloy during fiber laser welding," *Transactions of Nonferrous Metals Society of China (English Edition)*, vol. 25, no. 8, pp. 2516–2523, 2015, doi: 10.1016/S1003-6326(15)63870-5.

[42] G. Diot, A. Koudri-David, H. Walaszek, S. Guégan, and J. Flifla, "Non-destructive testing of porosity in laser welded aluminium alloy plates: Laser ultrasound and frequency-bandwidth analysis," *Journal of Nondestructive Evaluation*, vol. 32, no. 4, pp. 354–361, 2013, doi: 10.1007/s10921-013-0189-5.

[43] E. Rodriguez *et al.*, "Integration of a thermal imaging feedback control system in electron beam melting," *WM Keck Center for 3D Innovation, University of Texas at El Paso*, pp. 945–961, 2012.

[44] Y. Zhang, D. You, X. Gao, N. Zhang, and P. P. Gao, "Welding defects detection based on deep learning with multiple optical sensors during disk laser welding of thick plates," *Journal of Manufacturing Systems*, vol. 51, pp. 87–94, Apr. 2019, doi: 10.1016/j.jmsy.2019.02.004.

[45] Z. Chen, Y. Song, J. Zhang, W. Zhang, L. Jiang, and X. Xia, "Laser vision sensing based on adaptive welding for aluminum alloy," *Frontiers of Mechanical Engineering in China*, vol. 2, no. 2, pp. 218–223, 2007, doi: 10.1007/s11465-007-0038-2.

[46] S. Hua, B. Li, L. Shu, P. Jiang, and S. Cheng, "Defect detection method using laser vision with model-based segmentation for laser brazing welds on car body surface," *Measurement: Journal of the International Measurement Confederation*, vol. 178, Jun. 2021, doi: 10.1016/j.measurement.2021.109370.

[47] A. C. Popescu, C. Delval, and M. Leparoux, "Control of porosity and spatter in laser welding of thick AlMg5 parts using high-speed imaging and optical microscopy," *Metals (Basel)*, vol. 7, no. 11, Nov. 2017, doi: 10.3390/met7110452.

[48] T. Sibillano, A. Ancona, V. Berardi, and P. M. Lugarà, "A real-time spectroscopic sensor for monitoring laser welding processes," *Sensors*, vol. 9, no. 5. pp. 3376–3385, Apr. 27, 2009. doi: 10.3390/s90503376.

[49] P. de Bono, C. Allen, G. D'Angelo, and A. Cisi, "Investigation of optical sensor approaches for real-time monitoring during fibre laser welding," *Journal of Laser Applications*, vol. 29, no. 2, p. 022417, May 2017, doi: 10.2351/1.4983253.

[50] S. Shevchik *et al.*, "Supervised deep learning for real-time quality monitoring of laser welding with X-ray radiographic guidance," *Sci Rep*, vol. 10, no. 1, pp. 1–12, 2020.

[51] J. Wang, P. Fu, and R. X. Gao, "Machine vision intelligence for product defect inspection based on deep learning and Hough transform," *Journal of Manufacturing Systems*, vol. 51, pp. 52–60, Apr. 2019, doi: 10.1016/j.jmsy.2019.03.002.

[52] D. F. Farson, K. S. Fang, and J. Kern, "Intelligent laser welding control," in *LIA (Laser Institute of America)*, 1992, vol. 74, pp. 104–112. doi: 10.2351/1.5058430.

[53] C. Knaak, U. Thombansen, P. Abels, and M. Kröger, "Machine learning as a comparative tool to determine the relevance of signal features in laser welding," *Procedia CIRP*, vol. 74, pp. 623–627, 2018, doi: 10.1016/j.procir.2018.08.073.

[54] T. Sibalija, *Metaheuristic Algorithms in Industrial Process Optimisation: Performance, Comparison and Recommendations*, vol. 1198. Springer Singapore, 2020. doi: 10.1007/978-981-15-5232-8_24.

[55] L. Zhang, L. Zhou, L. Ren, and Y. Laili, "Modeling and simulation in intelligent manufacturing," *Computers in Industry*, vol. 112. Elsevier B.V., Nov. 01, 2019. doi: 10.1016/j.compind.2019.08.004.

[56] J. Ryan and C. Heavey, "Process modeling for simulation," *Computers in Industry*, vol. 57, no. 5, pp. 437–450, Jun. 2006, doi: 10.1016/j.compind.2006.02.002.

[57] A. N. Bakhtiyari, Z. Wang, L. Wang, and H. Zheng, "A review on applications of artificial intelligence in modeling and optimization of laser beam machining," *Optics and Laser Technology*, vol. 135. Elsevier Ltd, Mar. 01, 2021. doi: 10.1016/j.optlastec.2020.106721.

[58] G. Casalino, “Computational intelligence for smart laser materials processing,” *Optics and Laser Technology*, vol. 100, pp. 165–175, 2018, doi: 10.1016/j.optlastec.2017.10.011.

[59] H. L. Lin, “The Use of the Taguchi Method and a Neural-Genetic Approach to Optimize the Quality of a Pulsed Nd:YAG Laser Welding Process,” *Experimental Techniques*, vol. 39, no. 4, pp. 21–29, 2015, doi: 10.1111/j.1747-1567.2012.00849.x.

[60] Y. Ai, X. Shao, P. Jiang, P. Li, Y. Liu, and C. Yue, “Process modeling and parameter optimization using radial basis function neural network and genetic algorithm for laser welding of dissimilar materials,” *Applied Physics A: Materials Science and Processing*, vol. 121, no. 2, pp. 555–569, 2015, doi: 10.1007/s00339-015-9408-5.

# CHAPITRE 2

# INSPECTION LASER 3D BASÉE SUR LA CARTOGRAPHIE DES NUAGES DE POINTS, ANALYSE DE L'EFFET DES PARAMÈTRES ET OPTIMISATION AVEC ANOVA POUR LA DISTORSION GÉOMÉTRIQUE DES FLANS DE TAILLEUR SOUDÉS EN ALUMINIUM 5052-H32

Joys S. Rivera, Ahmad Aminzadeh, Ilyasse Houban, Pedram Farhadipour, Sasan S. Karganroudi, Noureddine Barka, Abderrazak El Ouafi.

Department of Mathematics, Computer Science and Engineering, Université du Québec à Rimouski,
Rimouski, Québec, Canada

*Corresponding author: joys.silvarivera@uqar.ca

*Cet article a été soumis dans The International Journal of Laser Applications portant le numéro de référence JLA22-AR-ALSTA2021-00116*

## 2.1 RÉSUMÉ

Les flans soudés sur mesure offrent des applications intéressantes pour plusieurs secteurs industriels en raison de leurs avantages en termes de qualité et de coût. Un effet de déformation peut être présent lors de l'utilisation de cette technique. Une distorsion excessive est un défaut indésirable qui réduit la formabilité de la pièce et affecte les performances mécaniques du produit final. Dans cette étude, une méthode d'inspection géométrique laser 3D automatique basée sur les principes de la fabrication en nuage est proposée afin d'analyser l'effet des paramètres de soudage de la puissance, de la vitesse et de l'amplitude dans la distorsion et, en fin de compte, réduire son effet sur le produit final. Les résultats ont révélé une signification statistique entre la distorsion et les paramètres du procédé de soudage. En outre, les conditions opérationnelles optimales qui réduisent la distorsion sont proposées, avec une réduction de la distorsion de 57,50 % pour la

distorsion totale dans la direction de soudage, de 33,47 % pour la distorsion totale dans la direction de soudage, de 86,52 % pour la distorsion totale de formage dans la direction de soudage et de 94,32 % pour la distorsion totale de formage dans la direction de soudage. Les résultats prometteurs du modèle proposé suggèrent qu'il peut être étendu différentes applications industrielles pour améliorer la qualité du produit final, ce qui entraîne une réduction des déchets.

## 2.2 CONTRIBUTIONS

Ce deuxième article ayant pour titre *« 3D laser inspection based on point cloud mapping, parameter effect analysis and optimization with ANOVA for geometrical distortion of welded tailor blanks of aluminum 5052-H32 »* fut essentiellement rédigé par son premier auteur Joys S. Rivera qui a également réalisé l'optimisation de la méthodologie de mesure de la distorsion géométrique, les travaux requis pour l'acquisition des données, l'algorithme pour faire l'extraction de données et toutes les analyses graphiques et statistiques présentés. Il a pu être développé aussi grâce à la collaboration de l'équipe de recherche du Professeur Noureddine Barka, c'est-à-dire, Ahmad Aminzadeh, Ilyasse Houban, Pedram Farhadipour, et Sasan S. Karganroudi qui ont soutenu la réalisation des essais de soudage et des mesures avec le scan 3D et qui ont guidé dans le développement de la méthodologie. La totalité des travaux de rédaction a été faite par le premier auteur sous la supervision de Noureddine Barka et Abderrazak El Ouafi qui sont également les mentors du projet de recherche.

## 2.3 TITRE DU DEUXIÈME ARTICLE

3D laser inspection based on point cloud mapping, parameter effect analysis and optimization with ANOVA for geometrical distortion of welded tailor blanks of aluminum 5052-H32

## 2.4 ABSTRACT

Tailor-welded blanks offer interesting applications for industries due to process, quality and cost advantages. A distortion effect can be present when using this technique. Excessive distortion is an undesirable defect that reduces the formability of the part and affects the mechanical

performance of the final product. In this study, an automatic 3D laser geometrical inspection method based on cloud manufacturing principles is proposed in order to analyze the effect of the welding parameters of power, speed and amplitude in distortion and ultimately reduce its effect on the final product. From the results, a statistical significance was found between distortion and welding process parameters. Additionally, the optimal operational conditions that reduce distortion are proposed, with a reduction in distortion of 57.50% for total distortion across welding direction, 33.47% for total distortion along welding direction, 86.52% for total forming distortion across welding direction and 94.32% for total forming distortion along welding direction. The promising results of the proposed model suggest that it can be escalated to industrial applications for improving the final product quality, which results in process waste reduction.

***Keywords****: Automatic inspection, 3D laser scanning, distortion inspection, laser-welded blanks, lean manufacturing, Industry 4.0, cloud manufacturing.*

## 2.5 NOMENCLATURE

| | |
|---|---|
| **TWBs** | Tailor Welded Blanks |
| **CAD** | Computer Aided Design |
| **ANOVA** | Analysis of Variance |
| **DMAIC** | Design Measure Analyze Improve Control |
| **DOE** | Design of Experiences |
| **YLS** | Yterbium Fiber Lasers |
| **3LS** | 3D Laser Scanning Inspection |
| **CL** | Cloud Maping |

| | |
|---|---|
| **CAM** | Computer Aided Manufacturing |
| **CAI** | Computer Aided Inspection |
| **QA** | Quality Assurance |
| **SSQ** | Sum of Squared Errors |
| **CORR** | Correlation |
| **W** | Width of the plate |
| **Δy** | Deformation in the y-axis |
| $\boldsymbol{\delta_B}$ | Maximum bending distortion |
| **C** | Curvature |
| **L** | Weld length |
| **P** | Power |
| **V** | Welding Speed |
| **A** | Amplitude |
| **DWD** | Distortion along welding direction |
| **DAWD** | Distortion across welding direction |
| **TDWD** | Total distortion in welding direction |
| **TAWD** | Total distortion across welding direction |
| **FDW** | Forming distortion in welding direction |
| **FAWD** | Forming across welding direction |
| **Mg** | Magnésium |

| | |
|---|---|
| **Zn** | Zinc |
| **Cu** | Cuivre |
| **Al** | Aluminium |
| **kW** | Kilowatts |
| **mm** | Millimeters |
| **mm/s** | Millimeters per second |
| **Ɵ** | Distorsion angle |

## 2.6 INTRODUCTION

Welded blanks implementation in process and production optimization offers advantages such as being lightweight, improving resistance properties, economical savings, and profit for scrap part consolidation [1]. The laser welding process is used to join aluminum alloy plates. It offers higher energy efficiency and higher speeds compared to the spot and arc welding process, and it can also be bounded with gases to increase the efficiency of the process and minimize the oxidation of surfaces [2] [3]. The laser welding process is widely used in industry due to the deep penetration, narrow bead, lower heat input and the relatively smaller induced welding distortion and residual stress caused by the laser welding process compared to conventional arc welding [4]. However, even with the lower amount of deformation induced by the laser welding process, if the in-process control techniques are not employed accurately, excessive distortion and deformations could occur [3]. Tailor-welded blanks (TWBs) are defined as the plates that are welded prior to the forming process. This solution has generated an important interest in industries due to weight reductions, scrap saving, and improved crash results in the automotive industry caused by the increased stiffness of laser-welded plates compared with the traditionally spot-welded process [5] [6]. However, the residual stress and material hardening caused by the welding process and the heat-affected zone has an impact on the formability of the material and can produce undesired distortion and defects on TWBs [7]. For this reason, finding and controlling

the parameters that have the most impact in welding deformation of the welded plate and the final formed part is a very important subject to consider in order to reach the best possible quality results for the final product.

L. H. Shah et al. studied wobbling laser welding in the aluminum alloy 6XXX series based on the energy flux irradiated on the material and its impact on the mechanical performance of the welded plate [8]. K. Hao et al. discovered the geometrical impact of the amplitude and the speed on the weld in wobbling laser welding [9]. To verify the geometrical effect of the laser welding process in materials, some inspection methods have been proposed. N. Jia et al. suggested a 3D reconstruction method based on surface and fusion analysis using grid laser illumination. This technique determined the weld geometry and did not verify the geometry of the plate after welding [10]. S. Hua et al. analyzed the defects in laser brazing on the surface of a car body with a laser vision, model-based method using 2D profiles. This method revealed defects such as overlaps, spatters, and pores [11]. However, this approach was limited to studying the joint area.

A. Weckenmann et al. proposed a geometrical inspection process for formed parts using virtual distortion compensation, an optical measurement process and a finite elements deduction for surface pattern recognition. This method reduced the inspection time and gave the estimated profile for the part, but the surface could not be totally measured and inspected because the method did not complete all the surface and part geometry, reducing the method performance caused by the uncertainty of the measured coordinates [12]. Matthias S. et al. developed an adapted inspection method to examine the formed surface. This method was based on three sensors that captured the real surface of formed parts and compared the results with a CAD model, finding a maximal deviation of 0.08 mm. This method obtained good results in inspection, but it is restricted to small geometries and analyzes specific zones of the part [13]. A. Ghafar et al. proposed a computer vision-based inspection method that measures the misalignment of the part according to the centroid punch position. This method developed an automatic process and could only recognize the part with the addition of red paint on the monitoring surface. Additionally, it was restricted to just one inspection parameter [14]. In this study, a novelty automatic inspection method with 3D laser scanning inspection (3LS) by cloud mapping (CM) for geometrical

distortion measurements was developed for the analysis of aluminum alloy welded blanks and aluminum alloy TWBs made with automatic welding and automatic forming processes, applying the correlation and ANOVA (analysis of variance) methods. This method aims to find the parameters that should be controlled in the online monitoring of the process line for welding and tailor-welded blanks based on distortion results, optimize the distortion by minimizing it, and give an approach for the 3D industrial inspection process based on cloud manufacturing principles and the DMAIC Lean method. This inspection method is developed in 4 main steps: 1. setup validation, 2. automatic material transforming process, 3. geometrical distortion measurement, 4. parameter validation and operational setup optimization.

## 2.7 MATERIAL AND METHODS

The material implemented in this study is the 5052 H32 aluminum alloy. It has good mechanical properties, medium strength, excellent corrosion resistance and good machining performance. It is widely implemented in the aerospace, automotive and transportation industries [15] [16]. Tables 8 and 9 show the nominal chemical composition and tensile strength properties of the base material. To complete the welding process, the defined sheet dimensions were of 150 mm x 125 mm, 14 imperial gauge thickness (2.03 mm). The material was prepared to clean contaminates and oxides besides the seam zone and get the best results in the laser welding process.

Table 8. Nominal chemical composition of 5052 H32 Al alloys.

| Material | Al (%) | Cr (%) | Cu (%) | Fe (%) | Mg (%) | Mn (%) | Si (%) | Ti (%) | Zn (%) | Others (%) |
|---|---|---|---|---|---|---|---|---|---|---|
| 5052 H32 | 95.7 - 97.7 | 0.15 - 0.35 | <=0.1 | <= 0.4 | 2.2 - 2.8 | <= 0.1 | <= 0.25 | - | <=0.10 | <= 0.15 |

Table 9. Mechanical properties of 5052 H32 Al alloys.

| Material | Tensile Strength, Ult (Mpa) | Tensile Strength, Yield (Mpa) | Elongation (%) |
|---|---|---|---|
| 5052 H32 | 230 | 195 | 12 |

### 2.7.1 Design of Experiments

Design of experiments (DOE) is an important step in process response studies and in final product quality analysis. With DOE, the optimal combinations of values for the parameters in the process can be defined, which will help to obtain the best possible results according to the real conditions [17]. In this study, the defined input factors are power, welding speed and amplitude, and the process responses are distortion along and across welding and forming distortion. Three factors of analysis are defined at two levels for the experimental procedure. Table 10 shows factors and levels, and Table 11 shows the experimental design by Taguchi method in Minitab™ for the experiments. The operational parameters' range of values were selected according to the best welding performance in the preliminary test results [18].

Table 10, Factors and levels for experiment.

| Factors | Levels | |
|---|---|---|
| | 1 | 2 |
| Laser Power (kW) | 2.0 | 2.2 |
| Welding Speed (mm/s) | 30 | 40 |
| Amplitude (mm) | 0.75 | 1 |

Table 11. Experimental design.

| Experiment Number | Input parameters | | |
|---|---|---|---|
| | Laser Power (kW) | Speed (mm/s) | Amplitude (mm) |
| 1 | 2.0 | 30 | 0.75 |
| 2 | 2.0 | 40 | 0.75 |
| 3 | 2.0 | 30 | 1.00 |
| 4 | 2.0 | 40 | 1.00 |
| 5 | 2.2 | 30 | 0.75 |
| 6 | 2.2 | 40 | 1.00 |
| 7 | 2.2 | 30 | 1.00 |
| 8 | 2.2 | 40 | 0.75 |

### 2.7.2 Expérimental Setup

Figure 18 presents the entire experimental process schema and monitoring method implemented in this study, which is based on six-sigma DMAIC (Define, Measure, Analyze, Improve, Control), a Lean method applied to improve existing process problems with unknown causes [19], and the cloud manufacturing concept that allows on-line monitoring systems for automatic manufacturing processes [20]. In this experimental setup, the Al 5052-H32 sheets were fixed with mechanical clamps. A robotized fiber laser welding (six-axis robotic system FANUC M-710ic), using IPG Photonics YLS-3000 ( ytterbium fiber lasers) with a wavelength of 1070 nm and a focal diameter of 0.45 mm for LWBs, was used to weld two plates, obtaining a consolidated plate of 300 mm x 300 mm. Following this, consolidated sheet AA 5052-H32 was carried to the automatic forming process with constant setup parameters, namely speed (1.5 mm/sec), blank holder force (20 pounds) and dry lubrication condition. Forming process force was monitored with a load cell. A 3LS method and 3D seam extraction algorithm by CM was used to obtain the geometrical information of fixture positions, welded composed sheets, and formed parts.

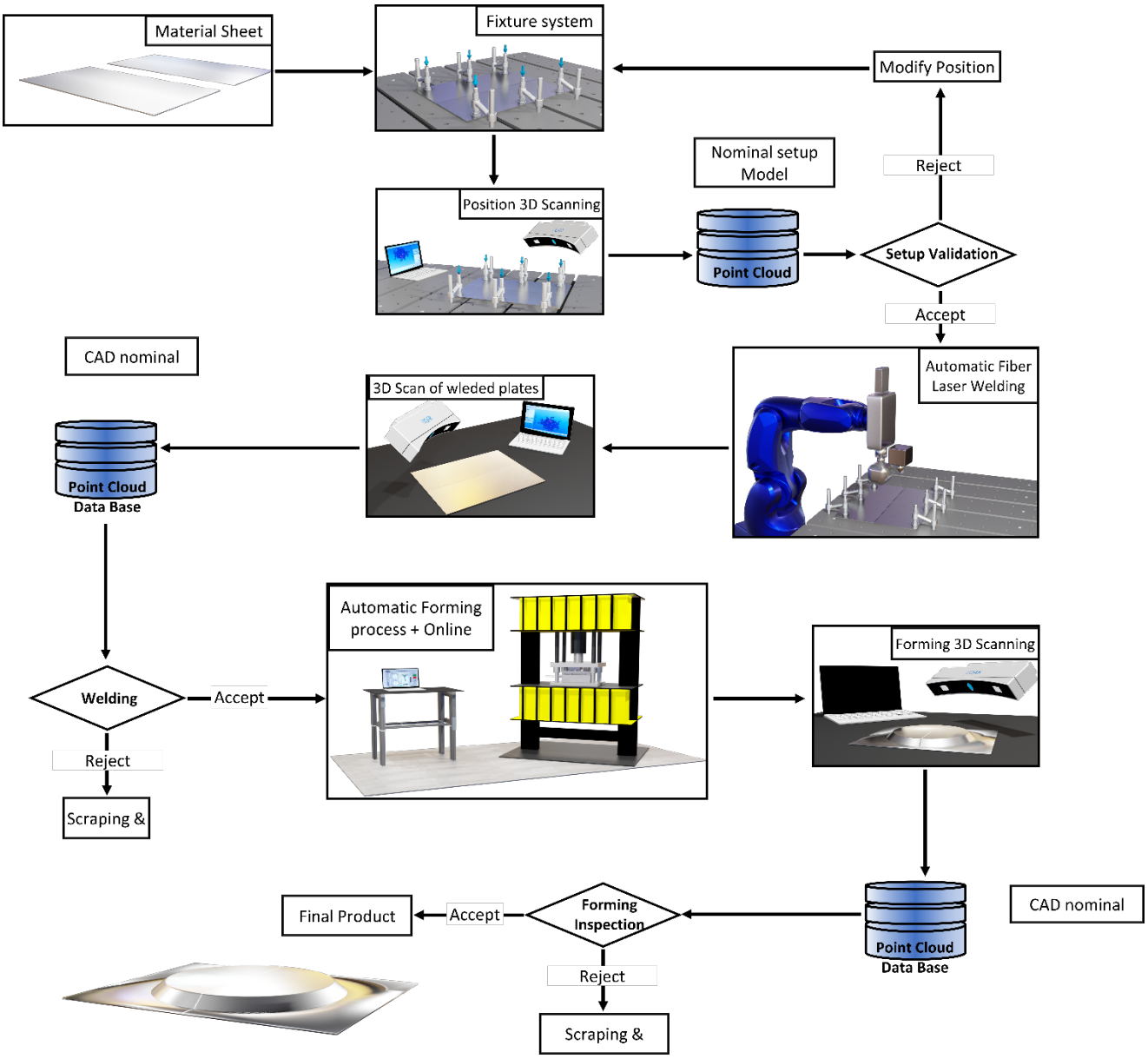


Figure 18. Experimental setup for 3D laser cloud mapping distortion with computer-aided inspection metho on automatic laser welding and automatic forming process.

### 2.7.3 Distortion measurements

For position monitoring, welding distortion and forming distortion measurement, a 3D laser scanner was employed. Reference points were implemented with a distance of 10 cm in between them. With this, the laser inspection is calibrated based on CAM model information and the in-process inspection process. Distortion analysis was investigated based on computer-aided inspection (CAI) using point cloud reconstruction in GOMTM software. Figure 19 shows the in-time 3D laser scanning setup. The 3D scanning obtains the form of a physical object using two lines of laser light and three cameras. The implementation of 3D laser scanning gives us very precise results for the geometrical analysis and setup verification in the pre-processing and post-processing control stages of quality assurance (QA) of the final product [21]. These control stages give the quality condition of the process and are very important for laser welding control systems. Quality assurance is normally done using camera-based systems, but it requires the aforementioned stages in order to filter and treat data to get more precise results [22] [23], and this is normally limited to 2D analysis.

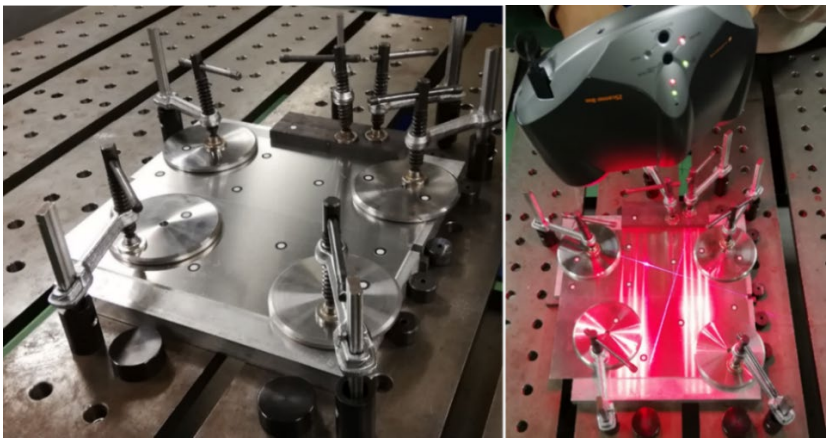

Figure 19. 3D laser scanning setup, reference points and equipment.

Figure 20. Automatic fiber laser system, six-axis robotic system FANUC M-710ic with IPG Photonics YLS-3000 ( ytterbium fiber lasers).

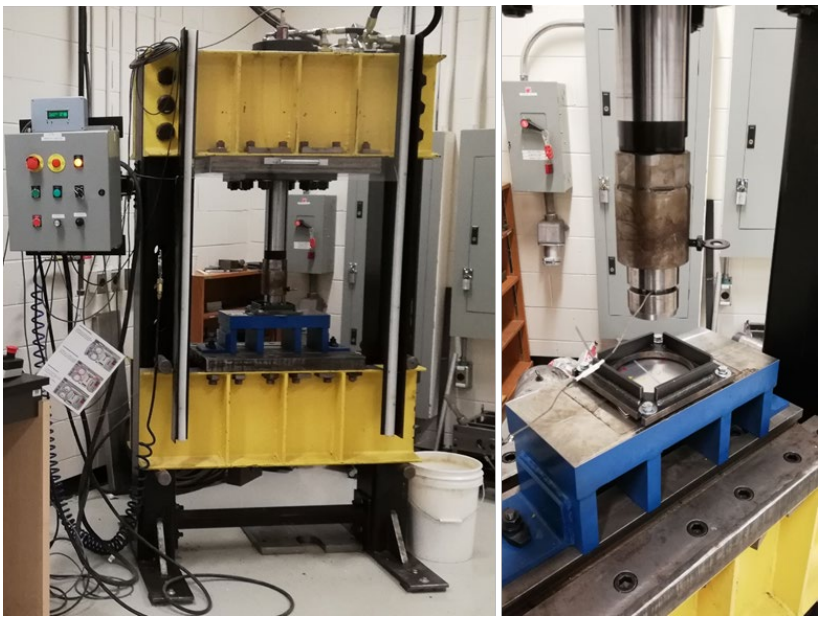

Figure 21. Automatic forming machine.

### 2.7.4 Analysis of Variance (ANOVA)

ANOVA (Analysis of Variance) is a powerful statistical method that is probably the most used for hypothesis testing. It has a rich application field and the flexibility to cover a larger number of experimental designs and procedures. Studying and interpreting an ANOVA table for a given analysis helps to determine which of the parameters need control and which do not in order to get the optimal expected output [24]. In this research, some terms such as sum of squared differences (SSQ), P-value, R-squared (R2) and correlation (CORR) values for comparing models are key in defining interactions and influences of process parameters in responses. The MINITAB$^{TM}$ software tool is used to get an ANOVA table and to define regression equations. In the following sections, the influence of process parameters and their contribution percentage along with factors' interactions with respect to responses, welding distortion and forming distortion are discussed. A linear regression model is then developed based on main process parameters and their interaction to predict welding and forming geometrical distortion.

### 2.7.5 Welding Distortion

Welding distortion is one of the common problems in manufacturing welded materials, resulting in quality degradation and process performance reduction. Impacting dimensional tolerance, product appearance and geometrical stability, it can lead to costly reworks and production delays. Therefore, control of weld distortion is a vital task in welding manufacturing [25]. According to previous studies and results, it is accepted that the main cause of distortion by welding process is the shrinkage that is associated to the heating and cooling cycle of base and weld metal.[26] Equation 1 gives the theorical plate distortion in welded plates [25], where Θ is the distortion angle and W is the width of the plate. A negative angle means that the edges are higher than the plate. As is shown in Figure 22, the y-axis is the direction upwards of the plate, so Δy is the deformation in the y-axis [105][25].

$$\Delta y = -\frac{W \sin(\theta)}{2} \quad (1)$$


Figure 22. Plate schema and axes representation for theorical deformation in plates (Equation 1).

The maximum bending distortion in the welding process ($\delta_B$) is theoretically estimated by Equation 2 [26], which calculates it integrating the curvature (C) of all cross-sections along the weld length (L) and can be written as:

$$\delta_B = \frac{CL}{8} \quad (2)$$

Even with these mathematical estimations, some physical phenomena that occur during welding and cause the distortion may not be described by theoretical equations, and the effects of these phenomena can only be analyzed by numerical simulations and experimental results [26] [25]. An engineering approach to estimating welding distortion establishes the relationships between material behavior and variables associated with the welding process, namely power (P), welding speed (V) and amplitude (A). The welding amplitude is determined by the oscillating pattern or path implemented in the welding Wobbling welding has very good results in mechanical properties on laser-welded plates and helps with the material flow and the reduction of the energy concentration [8]. For this test, wobbling welding was implemented with a sinusoidal pattern, increasing the amplitude value to study the impact of this parameter in distortion results. Figure 23 represents the defined pattern for the experiment. To analyse the distortion, two geometrical parameters were defined based on welding direction, distortion along welding direction (DWD) and distortion across welding direction (DAWD). Figure 24 represents the geometrical conditions for them.

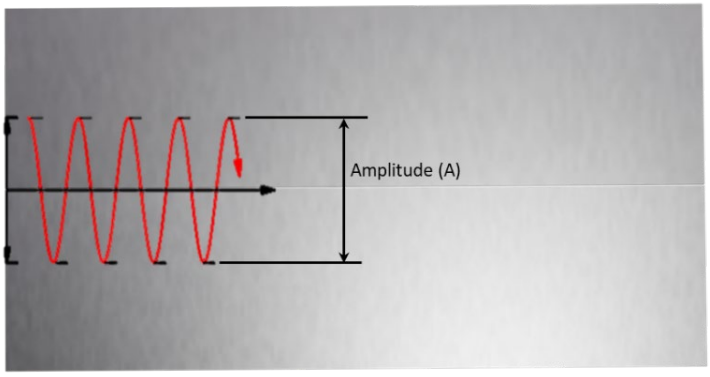


Figure 23. Wobbling welding and amplitude.

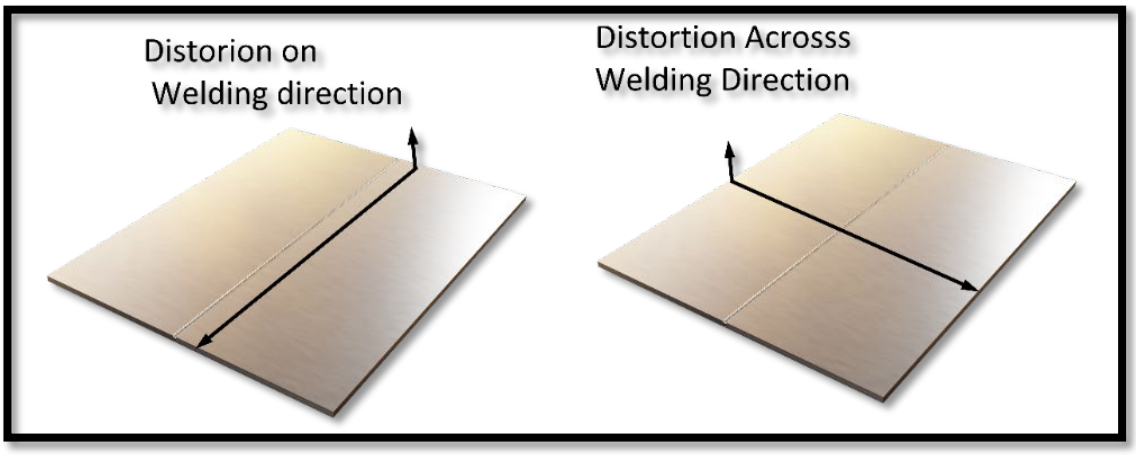


Figure 24. Representation of geometrical parameters to analyze distortion, left DWD and right DAWD.

## 2.8 RESULTS AND DISCUSSION

### 2.8.1 Geometrical Distortion

#### 2.8.1.1 Welded Plate Distortion

In this section, the 3D measurement results, distortion profiles and total distortion values are represented. Figure 25 shows the GOM software results for 3D geometrical analysis according

to laser scanning data. Based on the GOM distortion analysis, the information values across and along welding direction were extracted in a .CSV file. Figures 26, 27, 28 and 29 represent the deformation profile across and along welding based on power and welding speed values for all experiment conditions. To calculate the total distortion, Equations 3 and 4 were defined in order to calculate it based on the maximal and minimal value obtained in the 3D measurements and .CSV file with reference to X and Z axes (see Figure 5). An algorithm was coded using MATLAB R2020b software in order to get the results from the .CSV file of each test and automatically calculate the total distortion value for each experiment. Table 13 shows the total distortion values that were obtained for each test of the experiment.

$$Total\ DAWD\ (TAWD) = [Max\ \Upsilon\ ] + [Min\ \Upsilon], along\ X\ axis \quad (3)$$

$$Total\ DWD\ (TDWD) = [Max\ \Upsilon\ ] + [Min\ \Upsilon], along\ Z\ axis \quad (4)$$

Where $\Upsilon$ is defined as the value in Y axis.

Table 12. Distortion length across and along welding.

| Experiment Number | Power (W) | Speed (mm/s) | Amplitude (mm) | Total distortion on welding direction (mm) | Total distortion across welding direction (mm) |
|---|---|---|---|---|---|
| 1 | 2000 | 30 | 0.75 | 3.02 | 2.21 |
| 2 | 2000 | 40 | 0.75 | 3.04 | 2.83 |
| 3 | 2000 | 30 | 1.00 | 4.03 | 3.01 |
| 4 | 2000 | 40 | 1.00 | 3.79 | 4.57 |
| 5 | 2200 | 30 | 0.75 | 3.57 | 4.47 |
| 6 | 2200 | 40 | 1.00 | 3.89 | 5.20 |
| 7 | 2200 | 30 | 1.00 | 4.78 | 3.32 |
| 8 | 2200 | 40 | 0.75 | 3.30 | 3.25 |

| Experiment 1 | Experiment 2 |
| --- | --- |
| 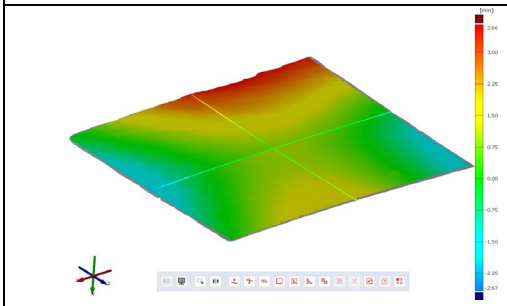 | 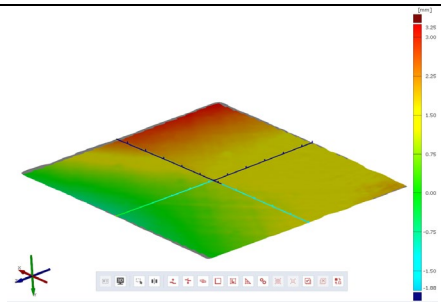 |
| **Experiment 3** | **Experiment 4** |
| 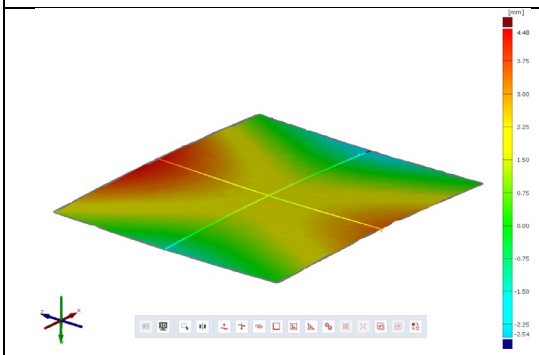 | 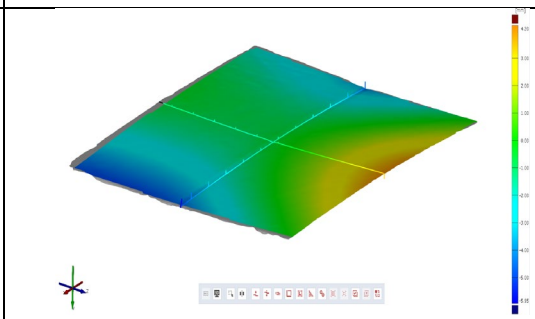 |
| **Experiment 5** | **Experiment 6** |
| 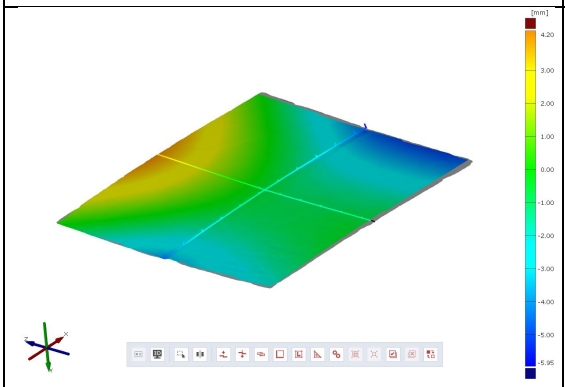 | 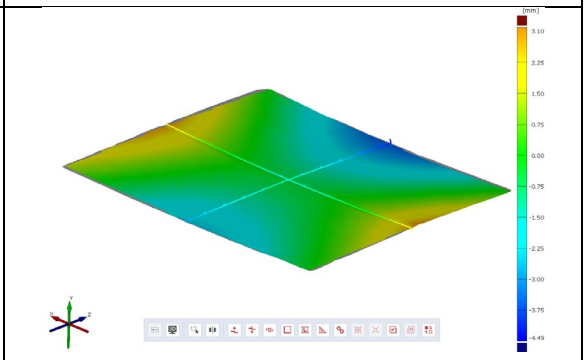 |
| **Experiment 7** | **Experiment 8** |

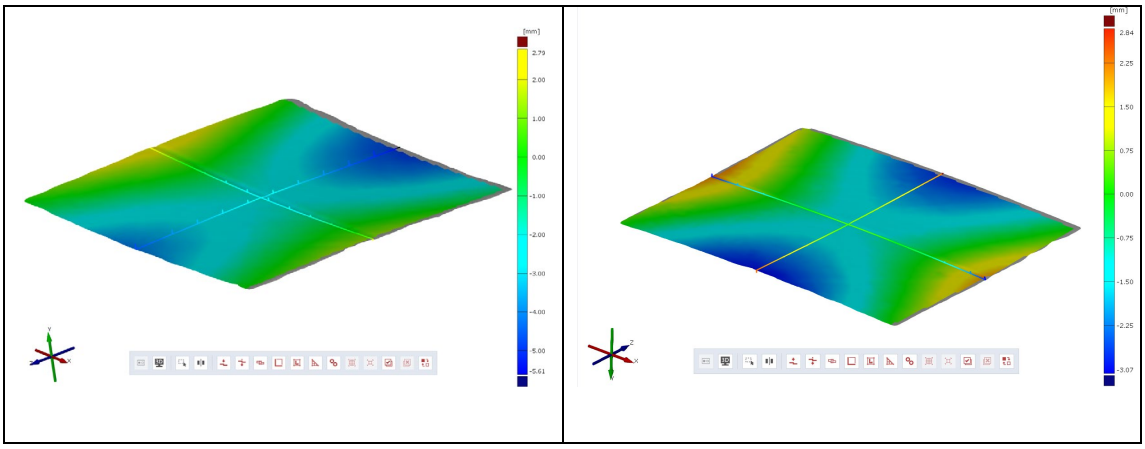

Figure 25. GOM 3D laser scanning measurements results for welded blanks.

The results of GOM measurements give the surface profile for all of the experiment conditions and are represented in Figure 25. These profiles and shapes are based on the theoretical model and simulation results presented by several articles [27] [28] [29] as well as the experimental results reported in other articles [3] [28]. The maximal (red) and minimal (blue) plane deformation is well characterized in the outcomes. Welding heat input is considered as the most critical parameter for estimating the distortion in welding. The heat input induces expansions and contractions in the material structure and causes distortion in welded plates [28] [29] [30]. Figures 26 and 27 show that maximal distortion values are reached at 2.2 kW, and at the same power conditions, the maximal distortion profile is reached at high amplitude values, which can be explained as being due to the high energy input that is associated to the increase of amplitude and weld size in laser welding [31] [29]. It is reduced with higher speed values, as high welding speed is related to low welding energy input [3], resulting in the reduction of compressive stress on the plate [29] and explaining the reduction of the distortion at low-speed values. Figures 28 and 29 show the angular distortion generally caused by transversal welding direction shrinking and plastic deformation [29][28], which changes the angle of the parts. The plate shape is influenced by the groove geometry, energy input, and plate thickness [32]. The profile results do not give a clear behaviour related to welding parameters.

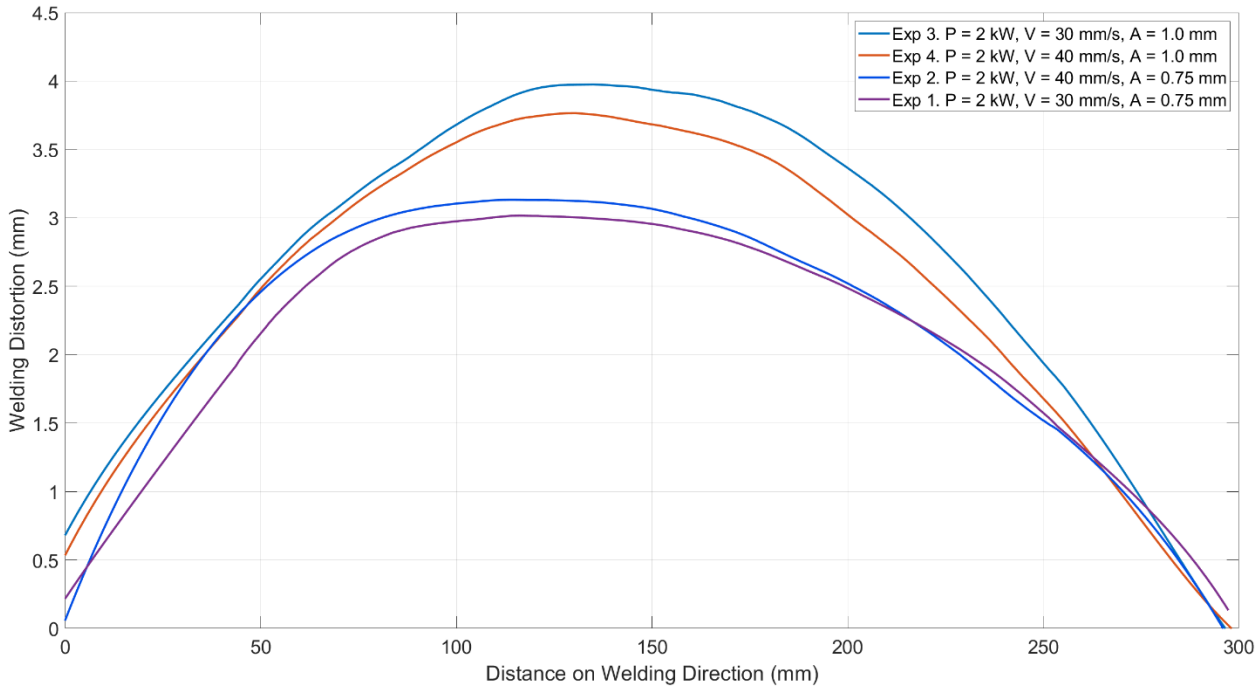


Figure 26. Distortion on welded plate along welding direction at 2.0 kW.

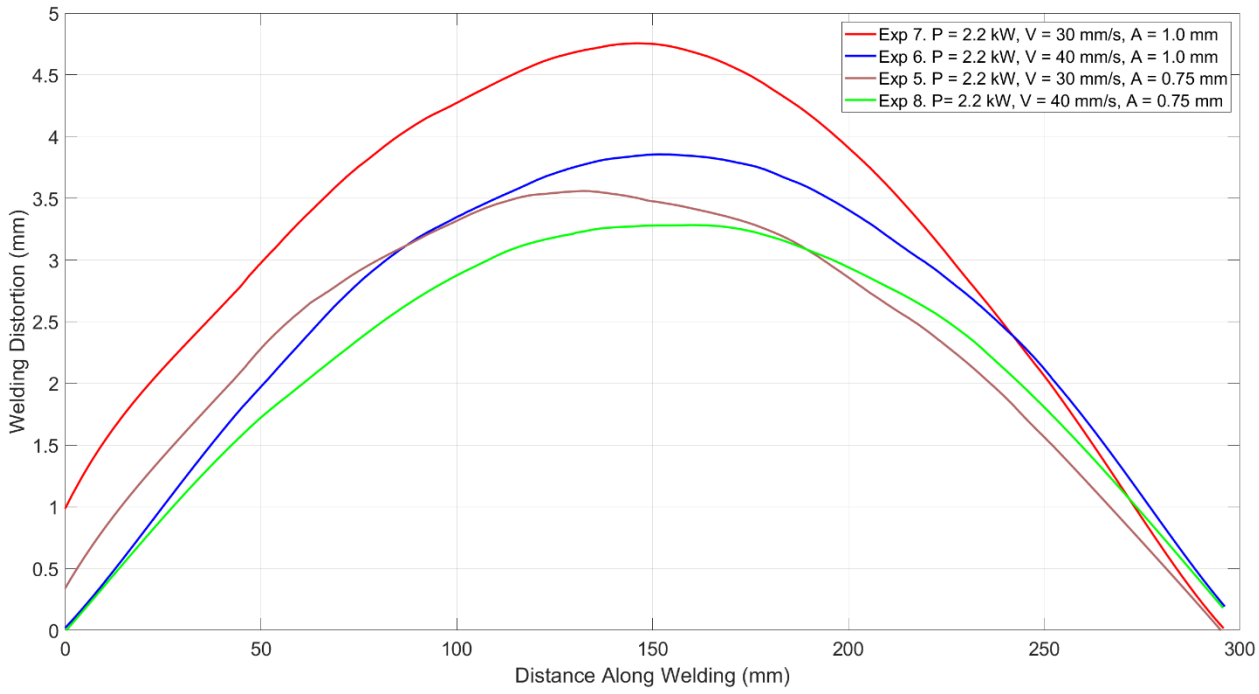


Figure 27. Distortion on welded plate along welding at 2.2 kW.

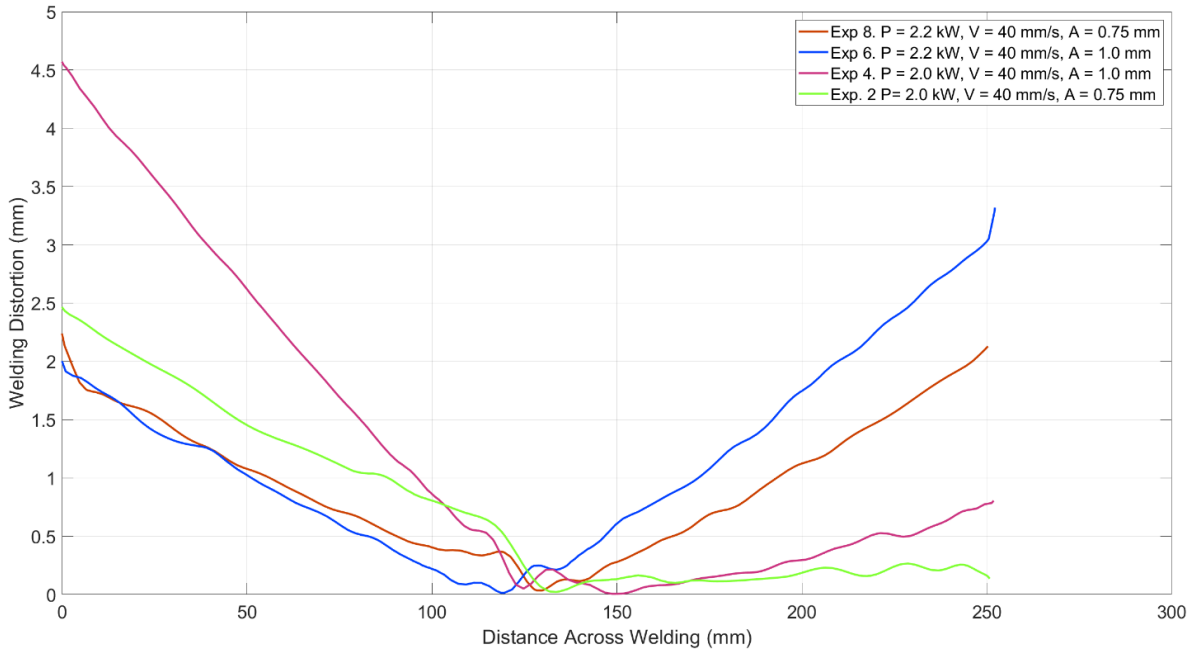


Figure 28. Distortion on welded plate across welding direction at 40mm/s.

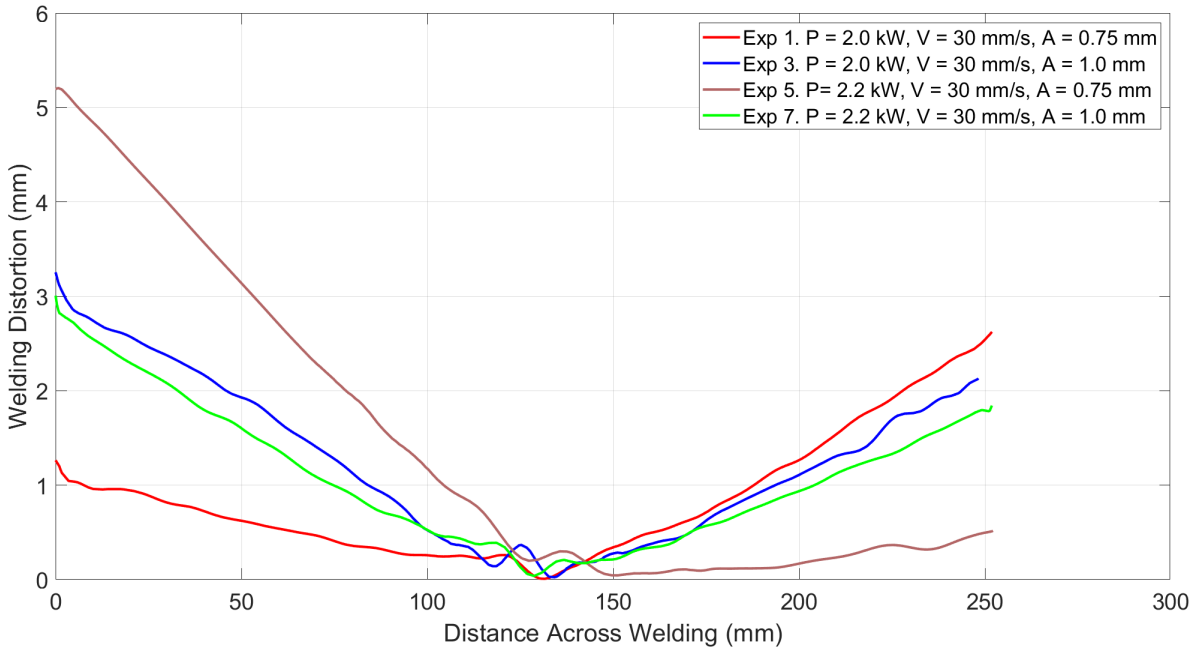


Figure 29. Distortion on welded plate across welding direction at 30 mm/s.

#### 2.8.1.2 Formed Welded Blank Distortion

Figure 33 shows the GOM software results for 3D measurement and geometrical evaluation based on laser scanning data. A .CSV file of the geometrical distortion after the forming process is extracted from the GOM software. To get the data from the .CSV file, a MATLAB R2020b coded algorithm is used for the automatic data extraction and distortion calculation process. Figures 34, 35, 36 and 37 show the formed welded blank profile and distortion after forming along and across welding direction according to the amplitude value. The distortion value is calculated based on the nominal CAD model depth, which is the expected geometry on the formed plate (see Figure 32), and the maximal point in Y direction is obtained from the profile information and .CSV file values calculated in MATLAB R2020b (see Figure 30). Equations 4 and 5 show how the distortion is calculated for all experiment results. Table 13 presents the total displacement values that were obtained by the algorithm. The total forming distortion in welding direction (FDW) and the total forming distortion across welding direction (FAWD) is defined below (Equations 4 and 5).

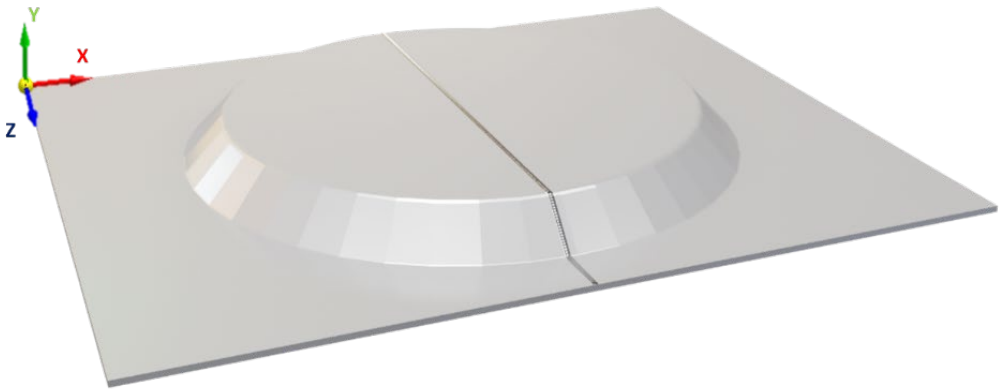


Figure 30. Formed welded blank representation for forming distortion.

$$FAWD = [Max\ \Upsilon\ in\ Formed\ Cup] - Nominal\ Depth, along\ X\ axis \quad (4)$$

$$FDW = [Max\ \Upsilon\ in\ Formed\ Cup] - Nominal\ Depth\ , along\ Z\ axis \quad (5)$$

Where $\Upsilon$ is defined as the value in Y axis.

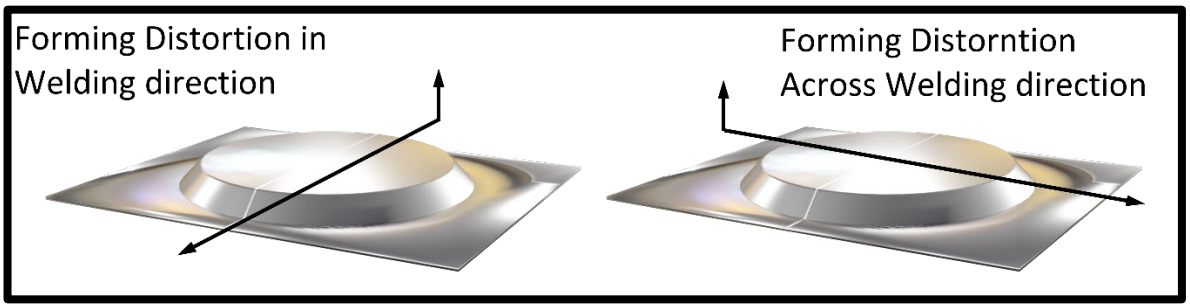


Figure 31. Representation of geometrical parameters to analyze forming distortion and displacement, left DWD and right DAWD.

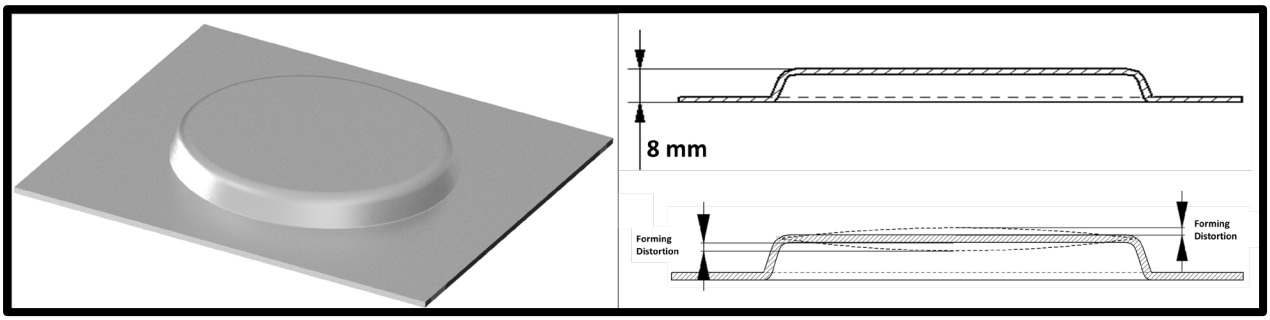


Figure 32. CAD model for formed plate. Left shows the 3D model and right the nominal depth.

Table 13. Forming distortion results across and along welding direction.

| Experiment Number | Power (KW) | Speed (mm/s) | Amplitude (mm) | Forming distortion across welding direction (mm) | Forming distortion on welding direction (mm) |
|---|---|---|---|---|---|
| 1 | 2000 | 30 | 0.75 | 0.10 | 0.45 |
| 2 | 2000 | 40 | 0.75 | 2.30 | 1.41 |
| 3 | 2000 | 30 | 1.00 | 0.12 | 0.20 |
| 4 | 2000 | 40 | 1.00 | 1.45 | 1.13 |
| 5 | 2200 | 30 | 0.75 | 0.44 | 0.66 |
| 6 | 2200 | 40 | 1.00 | 0.20 | 0.74 |
| 7 | 2200 | 30 | 1.00 | 0.03 | 0.78 |
| 8 | 2200 | 40 | 0.75 | 0.52 | 0.49 |

| Experiment 1 | Experiment 2 |
| --- | --- |
| 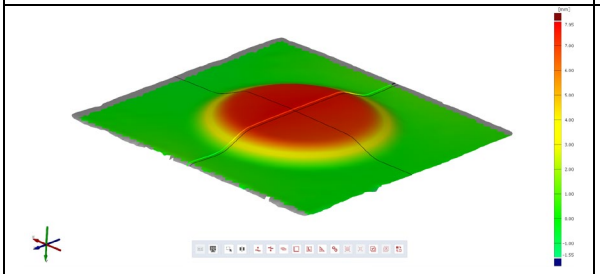 | 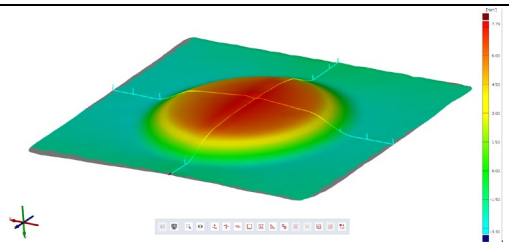 |
| **Experiment 3** | **Experiment 4** |
| 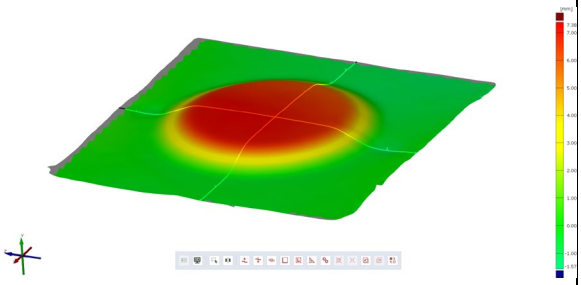 | 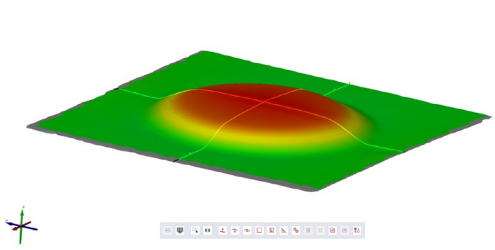 |
| **Experiment 5** | **Experiment 6** |
| 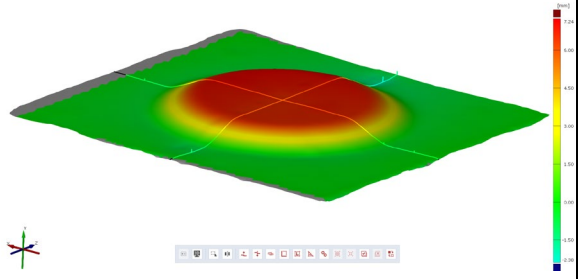 | 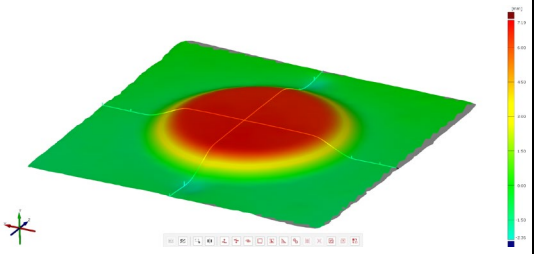 |
| **Experiment 7** | **Experiment 8** |

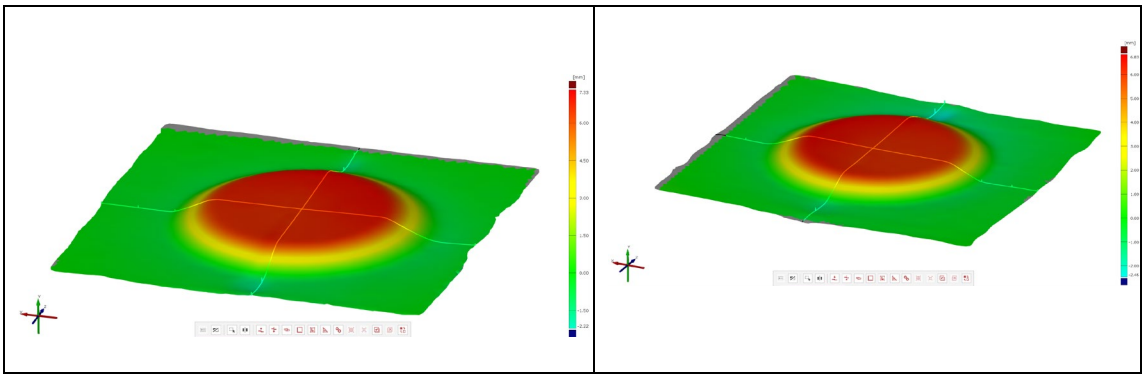

Figure 33. GOM 3D laser scanning measurement results for laser-welded formed blanks.

Figure 33 presents the surface profiles for the formed welded plates that were obtained by the GOM software, the .CSV file and the algorithm coded in MATLAB R2020b. The profiles follow the expected theoretical geometry (see Figure 32). Figures 34, 35, 36 and 37 show that there is a possible rupture in the weld after forming the welded blank in Experiments 2 and 4. This was confirmed by visual inspection of the parts (see Figure 38) and happened at the lowest power condition (2.0 kW) and highest speed setup (40 mm/s). This can be explained by the low depth penetration obtained in the welding process and the higher formability at lower energy input conditions [7] [33]. The forming profiles and the results reported on Table 14 show that at the lowest power value, highest speed rate and lowest amplitude condition, higher forming distortion values were obtained. This behaviour is replicated for both forming distortion along welding direction and across welding direction results. Katayama S. et al. reported that there is a direct relationship between penetration and power and speed values [34][35][33], which demonstrated that the welding depth penetration is reduced at higher speed values, and that with the increase of power there is a growth of the depth of penetration. This can be caused by the power density and heat input [35][36][33]. Whang Z. et al. reported that low input energy and low depth penetration in laser welding are related to low mechanical performance in aluminum alloys [37], which can explain the fact that higher distortion values across and along welding direction were reached with higher speed conditions at lower power values in the results.

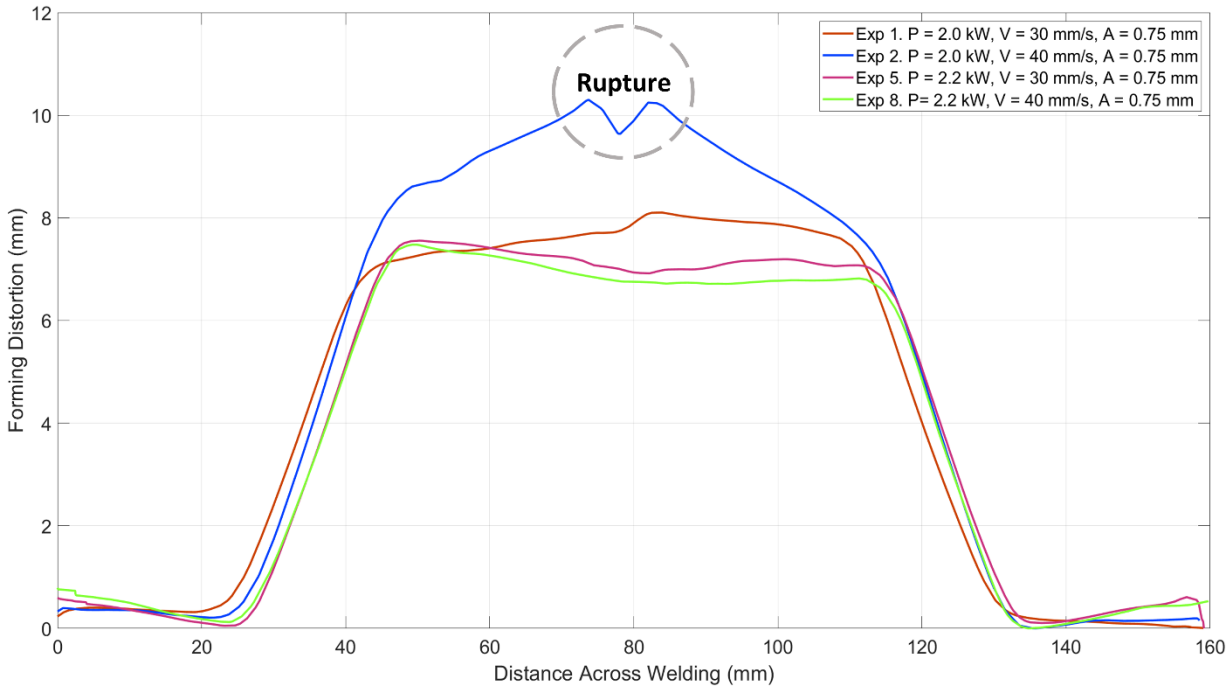


Figure 34. Distortion after the forming process across welding direction at A= 0.75 mm.

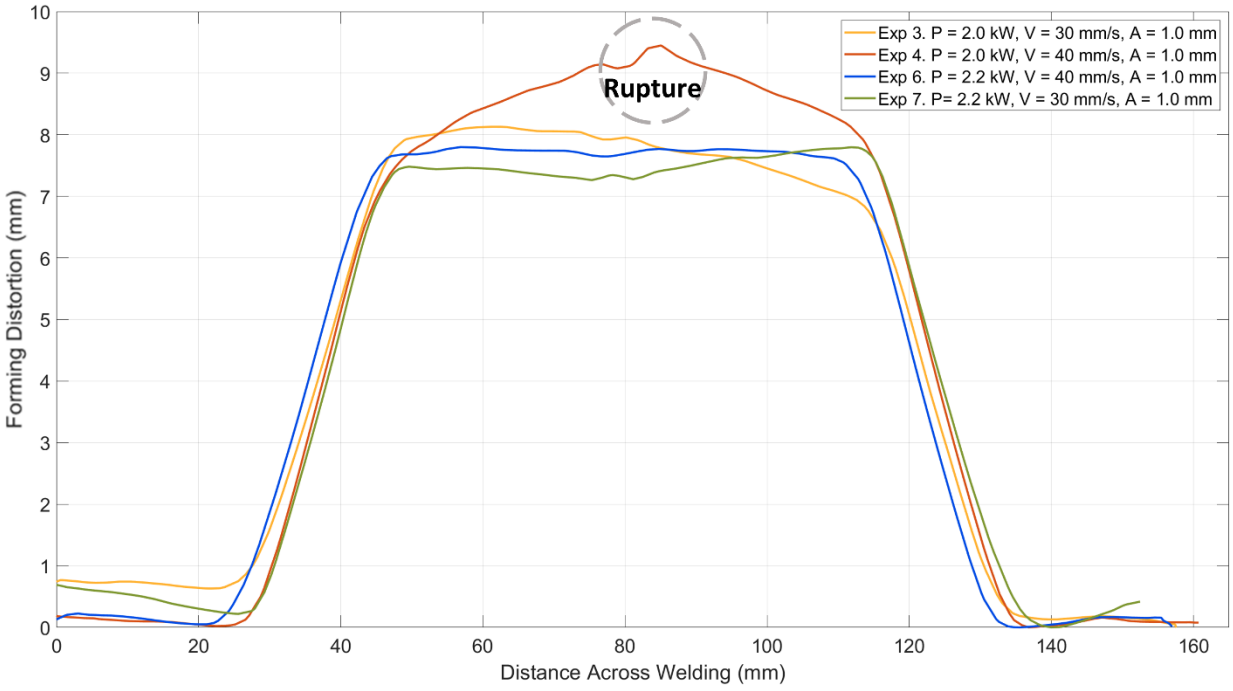


Figure 35. Distortion after the forming process across welding direction at A= 1.00 mm.

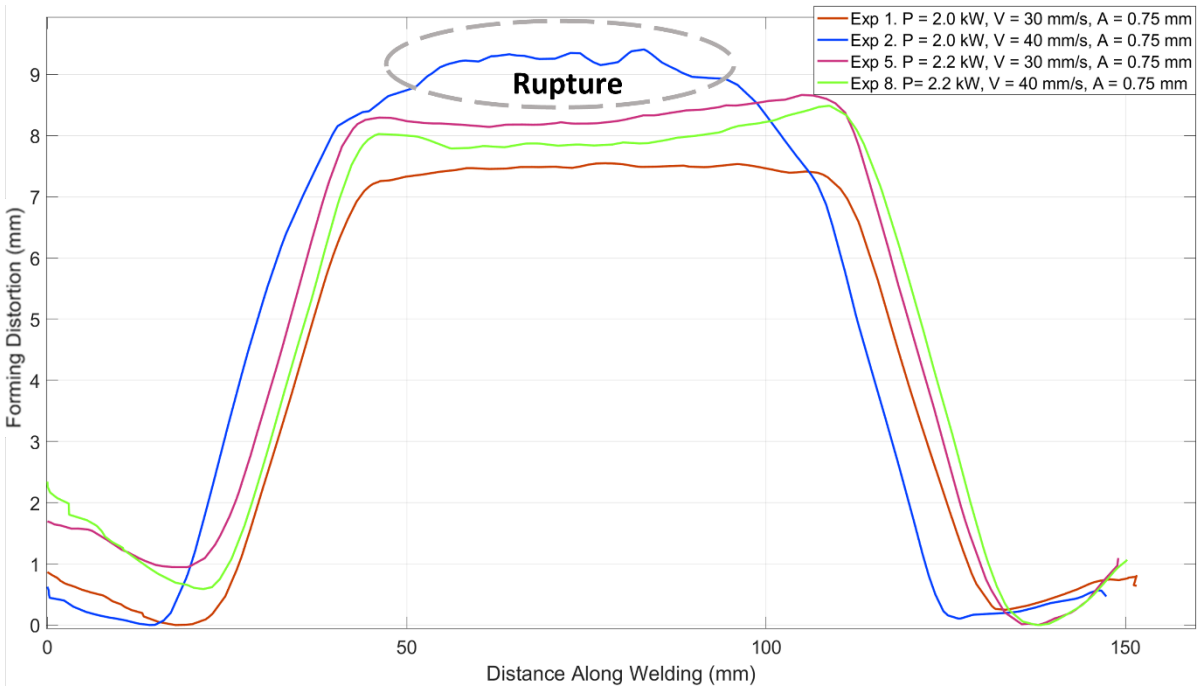


Figure 36. Distortion after forming process along welding direction at A= 0.75 mm.

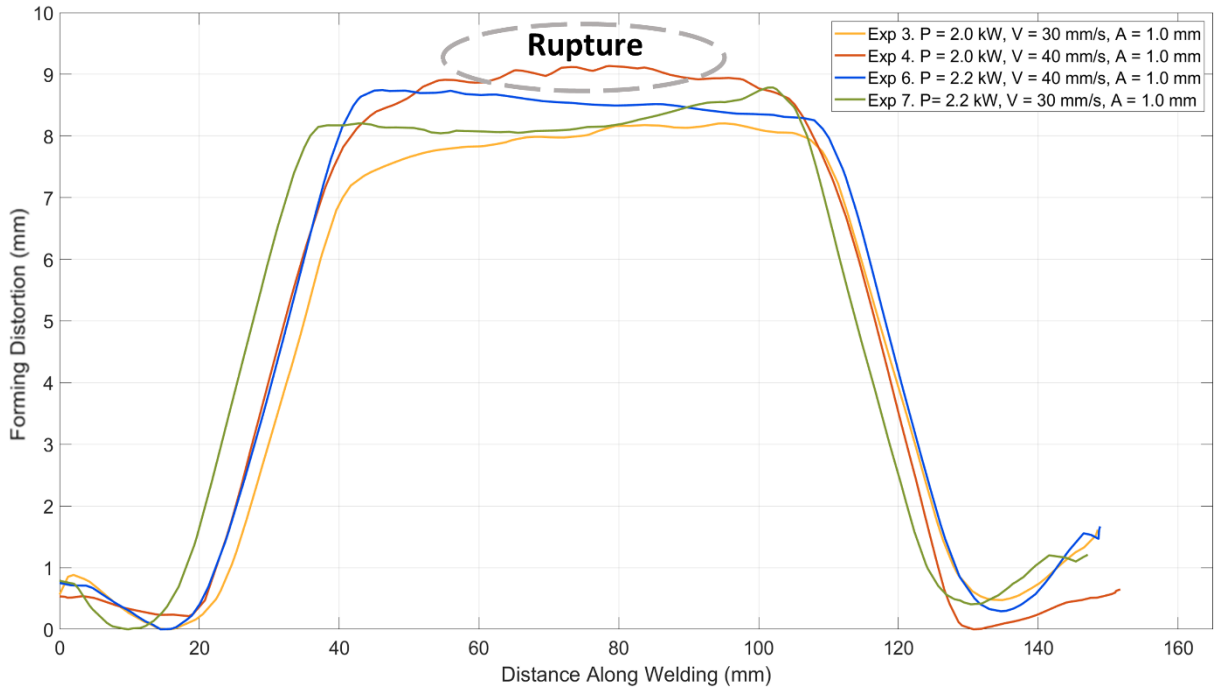


Figure 37. Distortion after forming process along welding direction at A= 1.00 mm.

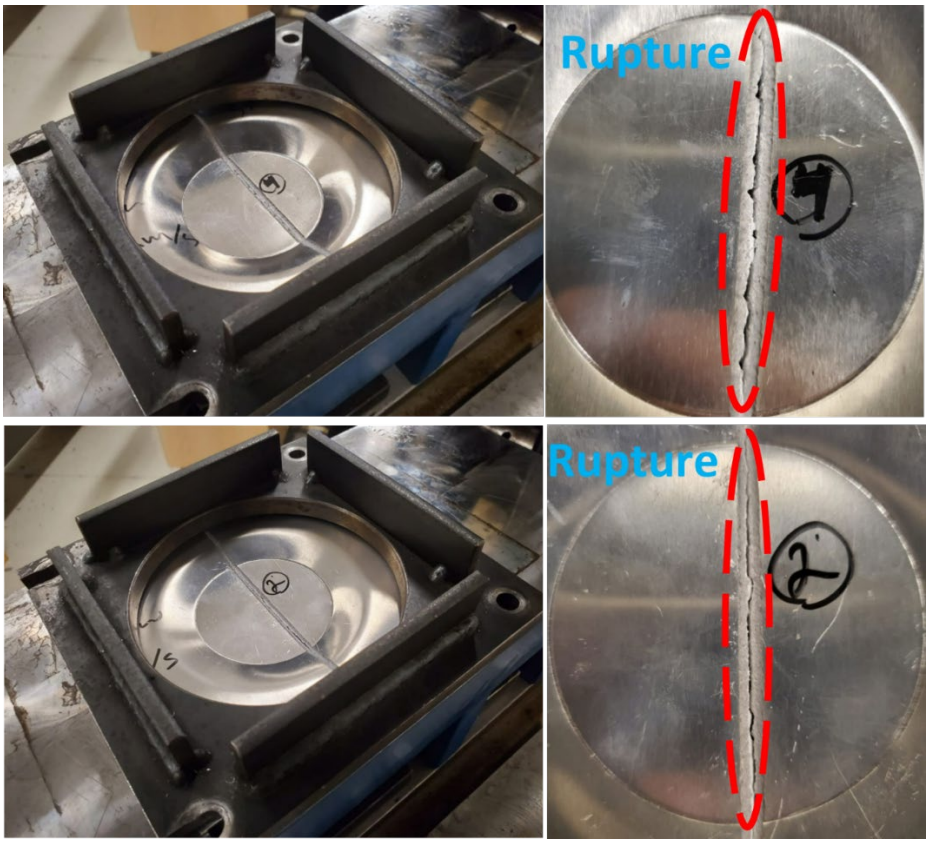


Figure 38. Rupture in formed welded blanks. Up Experiment 4, Down Experiment 2.

### 2.8.2 Correlation Analysis Results

#### 2.8.2.1 Correlation Analysis for Geometrical Distortion on Welded Plates

Based on the results presented in Table 13 and to define the parameters that will be used in the ANOVA analysis, the correlation analysis method was implemented as a first step of statistical parameters analysis. Correlation analysis is a statistical method whose purpose is to measure and interpret the strength of a linear or nonlinear relationship between two continuous variables [38][39], and is widely used as a filter method in the statistical analysis of data [40]. In this study, the Pearson correlation method was applied on MATLAB R2020b software, and the results are presented in Figure 39. To analyze the correlation (Corr), one standard and statistical range of values and thresholds is defined and used to determine if the relation between parameters and

response is a strong (|Corr| > 0.7), moderate (0.4 < |Corr| < 0.7) or weak correlation (|Corr| < 0.4) in a range of values from -1 to 1 [40][30][31]. According to the correlation results, it was found that the distortion along welding is strongly impacted by amplitude (Corr = 0.81), with a directly proportional relationship. Thus, when the amplitude increases, the distortion value increases as well. The results also suggest that there is a possible correlation with welding power (P) and welding speed (V). For the ANOVA analysis, the three input parameters will be analyzed to confirm how strong the impact on distortion results is when A, P, and V are defined as control parameters in real-time distortion monitoring and controls for process analysis and product quality checks. For the distance across welding, A, P and V seems to have a similar impact on the response, therefore the three parameters will be analyzed as well.

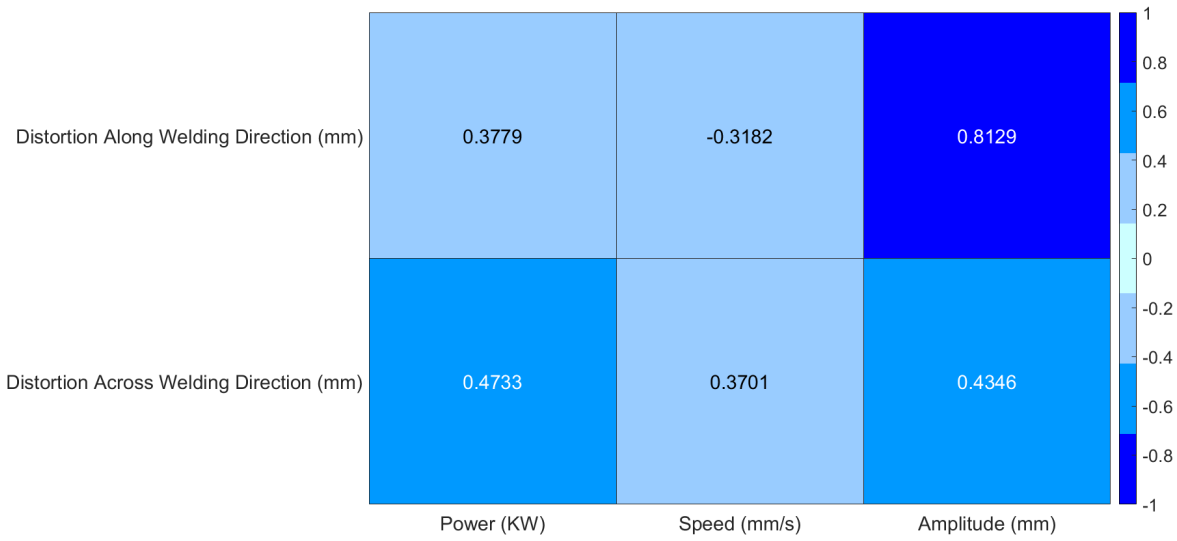


Figure 39. Pearson correlation heat map for welding distortion along and across welding.

### 2.8.2.2 Correlation Analysis for Geometrical Distortion on Formed Plates

Figure 40 presents the results of the correlation analysis performed on MATLAB R2020b software. The correlation analysis is done as a first step of statistical parameter analysis for FDW and FAWD based on the results of Table 6. For the correlation (Corr) analysis, the standard and

statistical range of values and thresholds defined to determine the relation between parameters and responses are presented as follows: strong correlation (|Corr| > 0.7), moderate correlation (0.4 < |Corr| < 0.7) and weak correlation (|Corr| < 0.4) in a range of values from -1 to 1 [32][30][31]. The results suggest that for FAWD, the parameter that has the strongest correlation (Corr = 0.62) is speed, and there is a possible correlation with power (Corr = -0.46). Amplitude has the weakest correlation with the response. For FWD, speed has the highest correlation with the response (Corr = 0.58), and power and amplitude have no correlation with the response. These results will be confirmed by the ANOVA analysis in the next section.

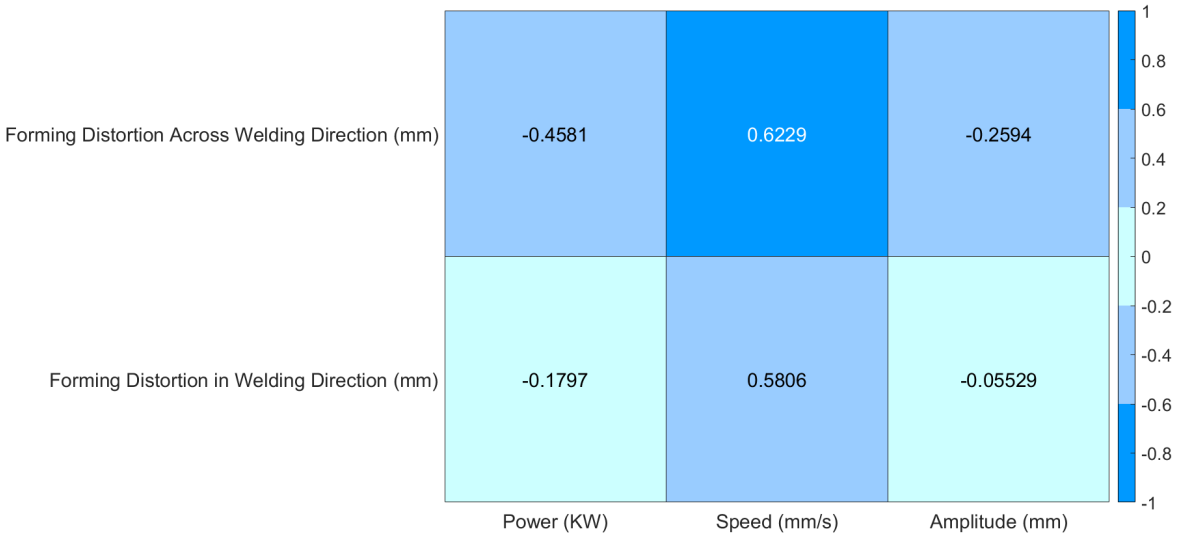


Figure 40. Pearson correlation heat map for forming distortion along and across welding direction.

### 2.8.3 ANOVA Analysis

#### 2.8.3.1 *ANOVA Analysis for Geometrical Distortion on Welded Plates*

For the total distortion on welding direction (TDWD), Table 14 and Figure 41 show that the most significant parameter for distortion along welding direction on laser welding is amplitude, with an effect contribution of 66.08% in the response and with a P-value of 0.006, lower than the α= 0.05. This value is suggested as the threshold that defines the probability of

rejecting the null hypothesis when it is true [21]. Therefore, this result confirms the effect obtained in the correlation analysis (Figure 39) and in the profile results (Figures 26 and 27), which show a strong relationship between TDWD and amplitude parameters, with the highest TDWD mean value at 1.0 mm amplitude. The power effect is the next most important parameter to be controlled on the process, with a contribution of 14%. The P-value of 0.07 suggests that it did not contribute in a statistically significant way to the TDWD. For the speed contribution, Figure 41 suggests that speed at 30 mm/s is associated with the highest mean strength. However, the Table 14 results indicate that the main effect is not statistically significant: speed has the lowest contribution on response with 10.13%, and a P-value of 0.108 confirms the null hypothesis of its impact on the TDWD.

Table 14. ANOVA table for distortion along welding direction.

| Source | DF | Seq. SS | Contribution | Adj. SS | Adj. MS | F-Value | P-Value |
|---|---|---|---|---|---|---|---|
| Power (kW) | 1 | 0.3406 | 14.28% | 0.3406 | 0.34062 | 6.00 | 0.070 |
| Speed (mm/s) | 1 | 0.2416 | 10.13% | 0.2416 | 0.24161 | 4.26 | 0.108 |
| Amplitude (mm) | 1 | 1.5764 | 66.08% | 1.5764 | 1.5764 | 27.78 | 0.006 |
| Error | 4 | 0.227 | 9.51% | 0.2270 | 0.05675 | | |
| Total | 7 | 2.3856 | 100.00% | | | | |

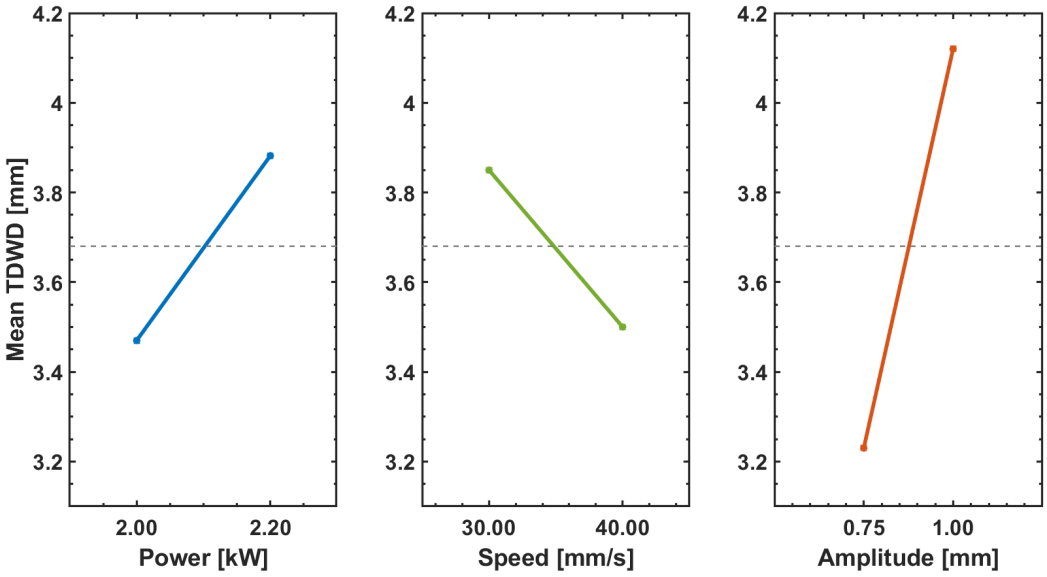

Figure 41. Main effects plot of parameters on means of total welding distortion along welding direction.

Table 15 presents the ANOVA table for the total distortion across welding direction (TAWD). The ANOVA table and Figure 42 show that the most significant parameter for distortion across welding direction on laser welding is power. The main effects plot suggests it and the results of Table 8 confirm it, with a 22.4% effect contribution in the response and a P-value of 0.016, lower than the $\alpha = 0.05$ and supported by the correlation analysis (Figure 39). Speed has the lowest effect according to statistical results with 0.53%, and a P-value of 0.02 rejects the null hypothesis of its effect on TAWD. The main effects plot suggests a high impact of amplitude on TAWD. However, the ANOVA table results indicate that it is not statistically significant for the response with a contribution of 15.07%, and a P-value of 0.095. A significant interaction of 54.18% and a P-value of 0.02 indicate that the relationship between power and TAWD depends on speed, which is confirmed by Figure 42 based on the non-parallel direction of the main effects plot for power and speed.

Table 15. ANOVA table for distortion across welding direction.

| Source | DF | Seq. SS | Contribution | Adj. SS | Adj. MS | F-Value | P-Value |
|---|---|---|---|---|---|---|---|
| Power (kW) | 1 | 1.647 | 22.40% | 4.6526 | 4.6526 | 24.39 | 0.016 |
| Speed (mm/s) | 1 | 0.041 | 0.56% | 3.9350 | 3.9350 | 20.63 | 0.020 |
| Amplitude (mm) | 1 | 1.108 | 15.07% | 1.1077 | 1.1077 | 5.81 | 0.095 |
| Power*Speed | 1 | 3.982 | 54.18% | 3.9822 | 3.9822 | 20.88 | 0.020 |
| Error | 3 | 0.572 | 7.79% | 0.5722 | 0.1907 | | |
| Total | 7 | 7.35 | 100.00% | | | | |

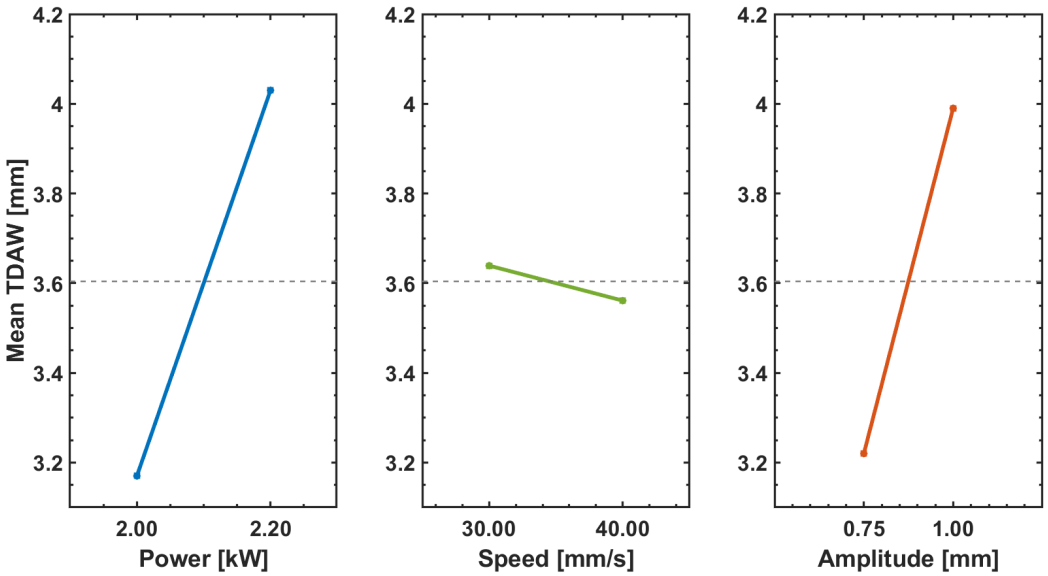


Figure 42. Main effects plot of parameters on means of total welding distortion across welding direction.

Table 16 and Figure 43 show the ANOVA analysis results for forming distortion across welding direction (FAWD). According to the results, speed is the parameter with the highest contribution for FAWD with 38.79%, and the P-value obtained is 0.017, lower than the $\alpha = 0.05$, which rejects the null hypothesis and means that speed is statistically significant for the response. Figure 43 shows that the highest mean FAWD is obtained at 40mm/s and the lowest mean FAWD value is reached at 30 mm/s. Based on the results and findings in Figure 40, it is possible to confirm that speed has the most statistical impact on the response for the experiment. For power,

it is concluded that it has an effect contribution of 20.98% on the response, with a P-value of 0.028 which confirms that all population means are not equal. It is thus possible to reject the null hypothesis. Amplitude has the lowest contribution with 6.73%, but the P-value does not show statistical significance for the FAWD. An additional interaction was proposed between speed and power. This interaction has a 29.31% contribution on the response with a P-value of 0.019, consequently the statistical significance of this combination is confirmed.

Table 16. ANOVA table of forming distortion across welding direction.

| Source | DF | Seq. SS | Contribution | Adj. SS | Adj. MS | F-Value | P-Value |
|---|---|---|---|---|---|---|---|
| Power (W) | 1 | 0.9611 | 20.98% | 1.0167 | 1.0168 | 15.92 | 0.028 |
| Amplitude (mm) | 1 | 0.3082 | 6.73% | 0.3082 | 0.3083 | 4.83 | 0.115 |
| Speed (mm/s) | 1 | 1.7769 | 38.79% | 1.4902 | 1.4902 | 23.34 | 0.017 |
| Power*Speed | 1 | 1.3424 | 29.31% | 1.3424 | 1.3424 | 21.02 | 0.019 |
| Error | 3 | 0.1915 | 4.18% | 0.1915 | 0.06385 | | |
| Total | 7 | 4.5082 | 100.00% | | | | |

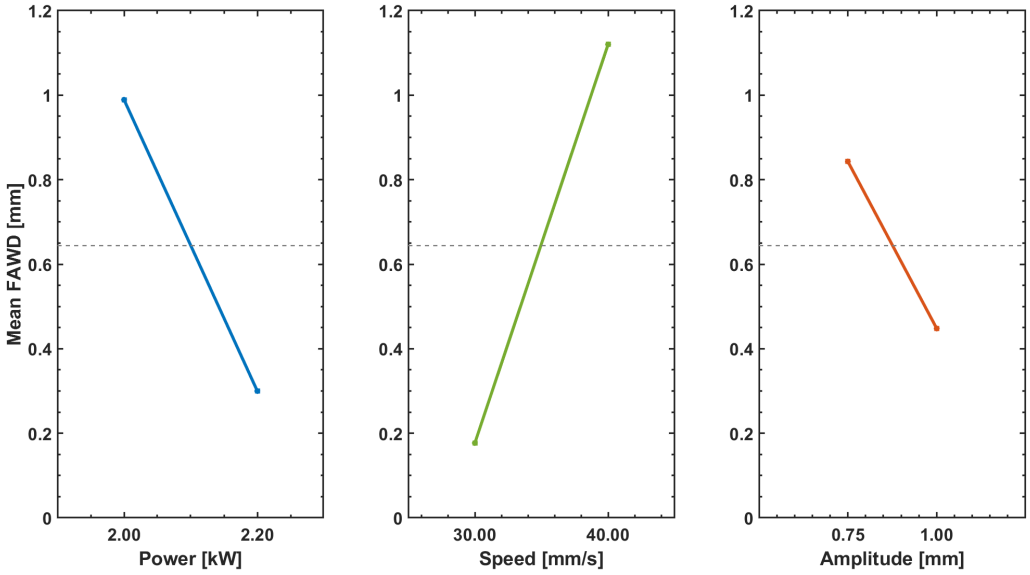


Figure 43. Main effects plot of parameters on means of forming distortion across welding direction.

ANOVA analysis results for forming distortion along welded direction (FDW) is shown in Table 18, where speed is the parameter that has the most contribution in FDW with 33.7% and a P-value of 0.033, which reject the null hypothesis and confirms the statistical significance on the response. This result is supported by the correlation analysis and the main effects plot (see Figure 44), where the highest mean FDW value is obtained at the highest speed condition and the lowest one at the lowest speed setup. Amplitude has the lowest contribution with 0.31% and no statistical significance with a P-value of 0.783. Power has a contribution of 3.23% and a confirmed statistical significance proved by the 0.033 P-value and the slope in the main effects plot. An additional parameter is proposed with the interaction between power and speed. It has the highest contribution on FDW with 52.66%, with a confirmed statistical significance supported by the 0.029 P-value.

Table 17. ANOVA table for forming distortion in welding direction.

| Source | DF | Seq. SS | Contribution | Adj. SS | Adj. MS | F-Value | P-Value |
|---|---|---|---|---|---|---|---|
| Power (W) | 1 | 0.03380 | 3.23% | 0.50268 | 0.50268 | 14.27 | 0.033 |
| Amplitude (mm) | 1 | 0.00320 | 0.31% | 0.00320 | 0.00320 | 0.09 | 0.783 |
| Speed (mm/s) | 1 | 0.35280 | 33.70% | 0.59271 | 0.59271 | 16.82 | 0.026 |
| Power *Speed | 1 | 0.55125 | 52.66% | 0.55125 | 0.55125 | 15.65 | 0.029 |
| Error | 3 | 0.10570 | 10.10% | 0.21986 | 0.03523 | | |
| Total | 7 | 1.04675 | 100.00% | | | | |

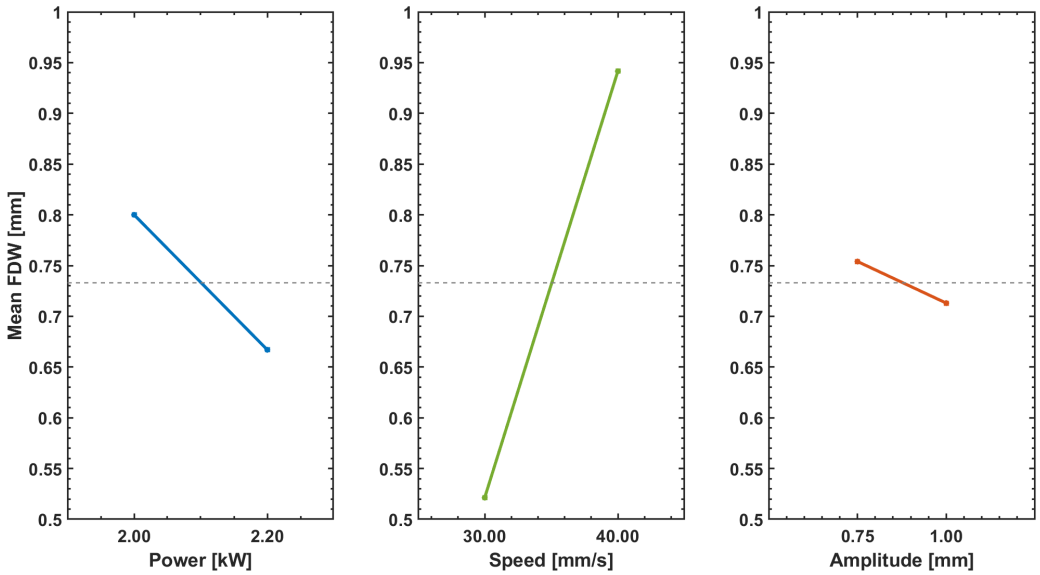


Figure 44. Main effects plot of parameters on means of forming distortion along welding direction.

### 2.8.4 Surface Plot Results

#### 2.8.4.1 Surface Plots for Geometrical Distortion on Welded Plates

Figure 45 presents a contour plot to show the relationship between the amplitude and power settings used for laser-welded blanks and the total welding distortion along welding direction. The yellow region indicates higher distortion values and blue regions indicates the lowest ones. It shows that lower TWDW values range from 0.75-0.79 mm and 2.0-2.05 kW. At this range of values, it is possible to reduce the TDWD in welded blanks. In Equation 5, the linear regression model is presented, leading a predictive model for TDWD.

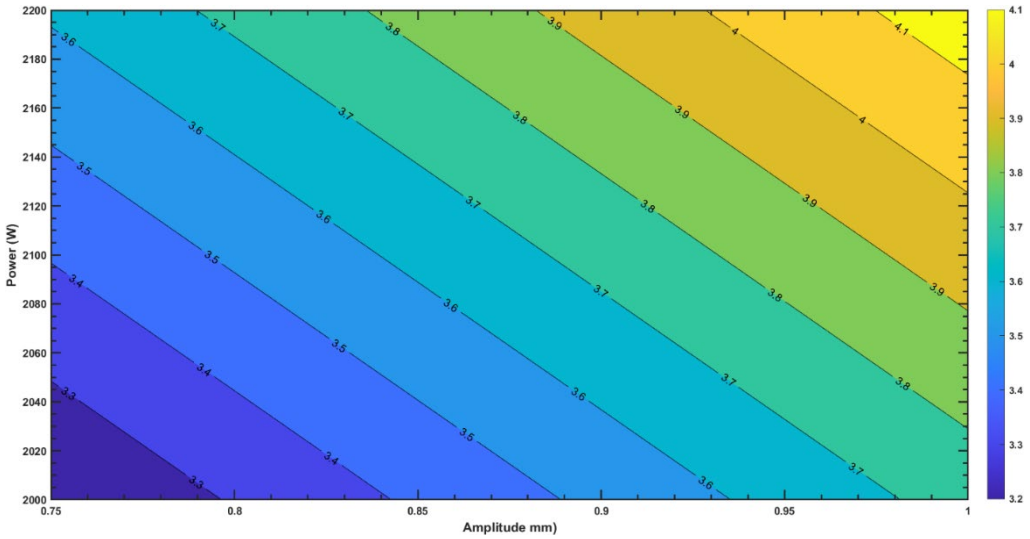


Figure 45. Contour plot of total distortion along welding direction.

$$\text{TDWD} = -2.57 + 0.002074 \text{ x P} - 0.0347 \text{ x V} + 3.55 \text{ x A} \quad (5)$$

The response surface of process factors in Figure 46 presents the contour plot to show the total welding distortion across welding direction as an objective response. The effect of power and speed is presented, and minimum TAWD is obtained in the range between 2.0-2.02 and 30.0-31.1 mm/s. In this range, it is possible to obtain the optimized minimal value for the response. A linear regression model is presented in Equation 6.

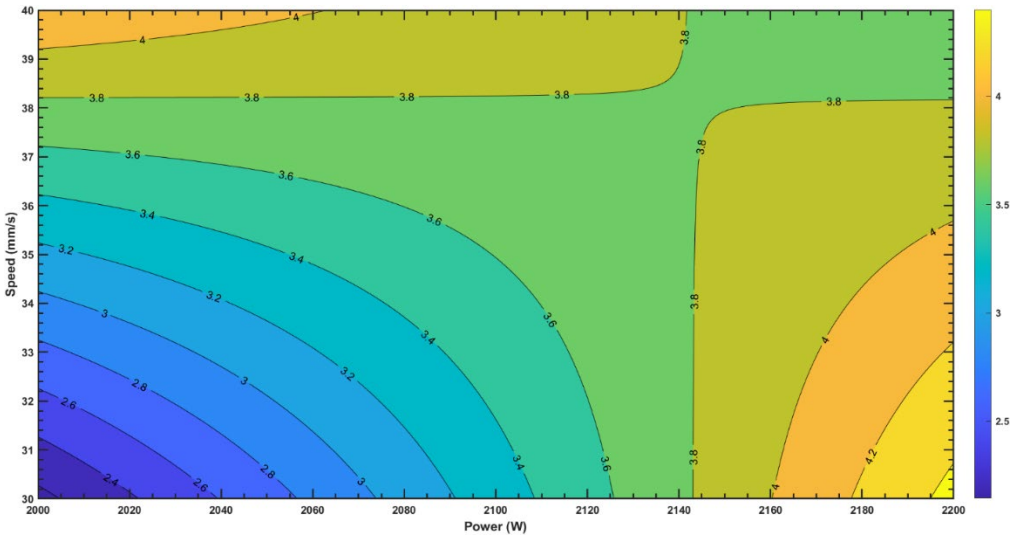


Figure 46. Contour plot of distortion across welding direction.

$$\text{TAWD} = -11.7 + 0.053 \text{ x P } + 2.94 \text{ x V } + 2.98 \text{ x A} - 0.001411 \text{ P x V} \quad (6)$$

### 2.8.4.2 Surface Plots for Geometrical Distortion on Formed Plates

The model equation for calculating the forming distortion across welding direction in function of parameters is presented as Equation 7 and Figure 47 shows the contour plot for FAWD, which has a curved profile due to the interaction (PxV) between statistically significant parameters. In the plot, the yellow region represents the highest FAWD values, and the blue ones represent the lowest. With speed values between 30.0 to 31.8 mm/s, a reduced FAWD amount is reached. At low-speed conditions, the power's increasing condition keeps the FAWD in the lower blue regions.

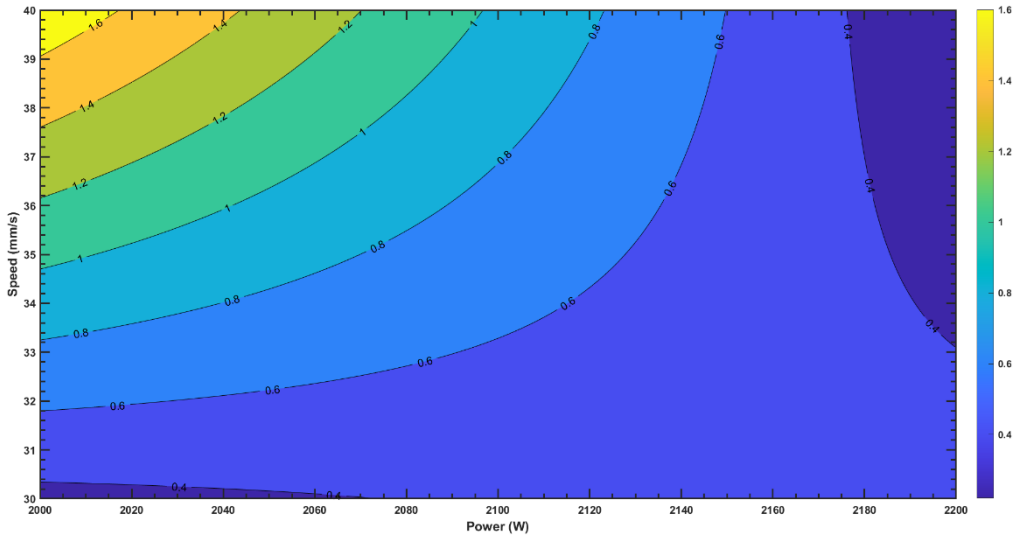


Figure 47. Contour plot forming distortion across welding direction.

$$\text{FAWD} = -54.2 + 0.0252 \text{ x P } + 1.815 \text{ x V} - 1.57 \text{ x A} - 0.000819 \text{ P x V} \quad (7)$$

The contour plot for forming distortion along welding direction is presented in Figure 48. The highest values for FDW are presented in the upper left corner, which corresponds to high-speed values. The lowest values for FDW are presented in the lower left corner corresponding to the lowest speed and power values. The curved profiles presented correspond to the interaction between power and speed, which has a statistical significance in the response. The model equation for the response in function with power, speed and amplitude is presented in Equation 8.

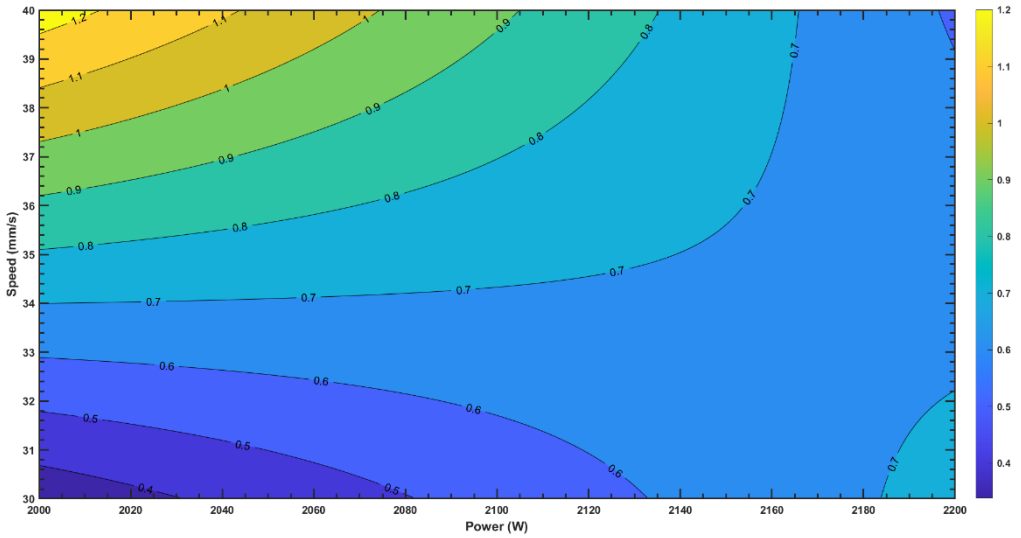


Figure 48. Contour plot forming distortion along welding direction.

$$\text{FDW} = -37.82 + 0.01772 \text{ x P } + 1.144 \text{ x V} - 0.160 \text{ x A} - 0.000525 \text{ P x V} \quad (8)$$

### 2.8.5 Response Optimization

To reduce the effects of welding parameters, the optimal process and operation setup is determined with the response optimization tool in MinitabTM. Table 19, "Optimization of laser-welded blanks for total distortion along welding direction", presents the optimized setup for minimizing the TDWD for laser-welded blanks. The results propose a power value of 2.0 kW, a speed value of 400 mm/s and an amplitude value of 0.75 mm to get the optimal TDWD value of 2.85 mm.

Table 18. Optimization of laser-welded blanks for total distortion along welding direction.

| Response | Goal | Lower Target | Upper | Power (kW) | Amplitude (mm) | Speed (mm/s) | Optimal TDWD (mm) |
|---|---|---|---|---|---|---|---|
| TDWD (mm) | Minimum | 3.02 | 4.78 | 2.0 | 0.75 | 40 | 2.85 |

Table 20 presents the optimized conditions for the TAWD of laser-welded blanks according to the results of the MinitabTM response optimization tool. The results propose a power value of 2.0 kW, a speed value of 30 mm/s and an amplitude value of 0.75 mm to get the optimal TDWD value of 2.15 mm.

Table 19. Optimization of laser-welded blanks for total distortion across welding direction.

| Response | Goal | Lower Target | Upper | Power (kW) | Amplitude (mm) | Speed (mm/s) | Optimal TAWD (mm) |
|---|---|---|---|---|---|---|---|
| TAWD (mm) | Minimum | 2.21 | 5.20 | 2.0 | 0.75 | 30 | 2.15 |

To obtain the optimal process conditions for welding parameters, the response optimization tool is used for TWDW and TAWD in order to reduce the total distortion values along welding direction and across welding direction. Table 21 presents the optimal parameters for reducing the TAWD to 2.21 mm and the TDWD to 3.18 mm, which are power at 2.0 kW, amplitude at 0.75 mm and speed at 30.5 mm/s.

Table 20. Optimization of laser-welded blanks for total distortion along welding direction.

| Response | Goal | Power (kW) | Amplitude (mm) | Speed (mm/s) | Optimal TAWD (mm) | Optimal TDWD (mm) |
|---|---|---|---|---|---|---|
| TAWD + TDWD (mm) | Minimum | 2.0 | 0.75 | 30.5 | 2.21 | 3.18 |

With reference to a maximal TAWD of 5.20 mm and a maximal TDWD of 4.78 mm, we have an optimization value of 57.5% for TAWD and 33.47% for TDWD that is calculated with Equations 9 and 10.

$$\text{Optimization \% TAWD} = \frac{MAX\ \text{TAWD} - \text{Optimal TAWD}}{\text{MAX TAWD}} = \frac{5.20 - 2.21}{5.20} = 57.50\% \quad (9)$$

$$\text{Optimization \% TDWD} = \frac{MAX\ \text{TDWD} - \text{Optimal TDWD}}{\text{MAX TDWD}} = \frac{4.78 - 3.18}{4.78} = 33.47\% \quad (10)$$

The response optimization tool was provided by MinitabTM Software to find the optimal operational conditions for reducing the distortion on formed laser-welded blanks. According to the results, the optimal minimum for experiment conditions in forming distortion across welding direction (FAWD) is 0.31 mm, and for forming distortion in welding direction (FDW) it is of 0.08 mm. The setup that reaches this optimal condition for forming distortion is power at 2.0 kW, amplitude at 1.0 mm and speed at 30 mm/s. Table 22 presents the setup conditions and the resulting distortion values.

Table 21. Optimization of formed laser-welded blanks for forming distortion.

| **Response** | **Goal** | **Power (kW)** | **Amplitude (mm)** | **Speed (mm/s)** | **Optimal FAWD (mm)** | **Optimal FDW (mm)** |
|---|---|---|---|---|---|---|
| FAWD + FDW (mm) | Minimum | 2.0 | 1.0 | 30 | 0.31 | 0.08 |

With reference to a maximal FAWD of 2.30 mm and a maximal FDW of 1.41 mm, an optimization of about 86.52% for FAWD and 94.32% for FDW is obtained with the following equation:

$$\text{Optimization \% FAWD} = \frac{\text{MAX FAWD} - \text{Optimal FAWD}}{\text{MAX FAWD}} = \frac{2.30 - 0.31}{2.30} = 86.52\% \quad (11)$$

$$\text{Optimization \% FDW} = \frac{MAX\ \text{FDW} - \text{Optimal FDW}}{\text{MAX FDW}} = \frac{1.41 - 0.08}{1.41} = 94.32\% \quad (12)$$

## 2.9 CONCLUSIONS:

Aluminum alloy (Al 5052) laser welding, an automatic forming process and an automatic 3D distortion inspection procedure are performed to analyze the impact, relationship and contribution of welding process parameters in the total distortion values for welded blanks and give an approach for automatic distortion control in industrial processes based on cloud manufacturing principles. The finding and conclusions are summarized as follows:

- A process layout and setting for 3D measurements, distortion analysis and optimization is proposed in this paper. This model can be replicated and escalated to industrial applications, with the objective to control and reduce distortion defects on formed laser-welded blanks.

- The amplitude has the highest contribution to the total welding distortion value along welding direction with 66.08%. This is associated with the high impact that this parameter has towards heat input in the laser welding process. It's possible to optimize the distortion effect on laser welding by controlling it.

- The interaction between power and speed has the most statistically significant effect on the total welding distortion value across welding direction with a contribution of 54.18%. An angular distortion is found in the profile results evaluated by the automatic 3D measurement process, and in this direction the heat input is associated with high power values and its combination with the speed parameter.

- The effect of welding speed and power on welding depth and formability can explain the behaviour of distortion in the results. Forming distortion results showed that speed was the parameter with the most statistical significance, with 38.79% for forming distortion across welding direction and 33.7% for distortion in welding direction.

Maximal distortion rates are reached at high-speed values and minimal rates at low speed values. The interaction between power and speed was proposed, and this had the highest statistical significance in welding direction distortion.

- An optimized setup was analyzed according to the results of the response optimization tool in MinitabTM. It found that the optimized minimal value for welding distortion is reached at 2.0 kW for power, 30.5 mm/s for speed and 0.75 mm for amplitude. For forming distortion, the optimized setup is obtained at 2.0 kW for power, 30 mm/s for speed and 1.0 mm for amplitude. The optimization analysis resulted in a distortion reduction of 57.50% for TAWD, 33.47% for TDWD, 86.52% for FAWD and 94.32% for FDW.

## 2.10 REFERENCES:


[1] F. I. Saunders and R. H. Wagoner, "Forming of tailor-welded blanks," *Metallurgical and Materials Transactions A: Physical Metallurgy and Materials Science*, vol. 27, no. 9, pp. 2605–2616, 1996, doi: 10.1007/BF02652354.

[2] "Automotive Steels: Design, Metallurgy, Processing and Applications - Radhakanta Rana, Shiv Brat Singh - Google Livres." https://books.google.ca/books?hl=fr&lr=&id=HrszCwAAQBAJ&oi=fnd&pg=PP1&dq=Automotive+Steels,+Woodhead+Publishing&ots=GE3qxtSHzE&sig=RpEXqfP3Wk5JAt19uzzBmq9BDIY&redir_esc=y#v=onepage&q=Automotive Steels%2C Woodhead Publishing&f=false (accessed Mar. 04, 2021).

[3] H. Huang, S. Tsutsumi, J. Wang, L. Li, and H. Murakawa, "High performance computation of residual stress and distortion in laser welded 301L stainless sheets," *Finite Elements in Analysis and Design*, vol. 135, no. February, pp. 1–10, 2017, doi: 10.1016/j.finel.2017.07.004.

[4] J. Sun, X. Liu, Y. Tong, and D. Deng, “A comparative study on welding temperature fields, residual stress distributions and deformations induced by laser beam welding and CO2 gas arc welding,” *Materials and Design*, vol. 63, pp. 519–530, 2014, doi: 10.1016/j.matdes.2014.06.057.

[5] B. Kinsey, Z. Liu, and J. Cao, “A novel forming technology for tailor-welded blanks.”

[6] S. Han, T. Hwang, I. Oh, M. Choi, and Y. H. Moon, “Manufacturing of tailor-rolled blanks with thickness variations in both the longitudinal and latitudinal directions,” *Journal of Materials Processing Technology*, vol. 256, pp. 172–182, Jun. 2018, doi: 10.1016/j.jmatprotec.2018.02.013.

[7] K. Bandyopadhyay, S. K. Panda, P. Saha, V. H. Baltazar-Hernandez, and Y. N. Zhou, “Microstructures and failure analyses of DP980 laser welded blanks in formability context,” *Materials Science and Engineering A*, vol. 652, pp. 250–263, Jan. 2016, doi: 10.1016/j.msea.2015.11.091.

[8] L. H. Shah, F. Khodabakhshi, and A. Gerlich, “Effect of beam wobbling on laser welding of aluminum and magnesium alloy with nickel interlayer,” *Journal of Manufacturing Processes*, vol. 37, no. December 2018, pp. 212–219, 2019, doi: 10.1016/j.jmapro.2018.11.028.

[9] K. Hao, G. Li, M. Gao, and X. Zeng, “Weld formation mechanism of fiber laser oscillating welding of austenitic stainless steel,” *Journal of Materials Processing Technology*, vol. 225, pp. 77–83, 2015, doi: 10.1016/j.jmatprotec.2015.05.021.

[10] N. Jia, Z. Li, J. Ren, Y. Wang, and L. Yang, “A 3D reconstruction method based on grid laser and gray scale photo for visual inspection of welds,” *Optics and Laser Technology*, vol. 119, Nov. 2019, doi: 10.1016/j.optlastec.2019.105648.

[11] S. Hua, B. Li, L. Shu, P. Jiang, and S. Cheng, “Defect detection method using laser vision with model-based segmentation for laser brazing welds on car body surface,” *Measurement: Journal of the International Measurement Confederation*, vol. 178, Jun. 2021, doi: 10.1016/j.measurement.2021.109370.

[12] A. A. Weckenmann, P. Gall, and A. Gabbia, "3D surface coordinate inspection of formed sheet material parts using optical measurement systems and virtual distortion compensation," in *Eighth International Symposium on Laser Metrology*, Feb. 2005, vol. 5776, p. 640. doi: 10.1117/12.611842.

[13] S. Matthias *et al.*, "Metrological solutions for an adapted inspection of parts and tools of a sheet-bulk metal forming process," *Production Engineering*, vol. 10, no. 1, pp. 51–61, Feb. 2016, doi: 10.1007/s11740-015-0647-2.

[14] A. A. Ghafar and A. B. Abdullah, "Pre-Forming Inspection System to Detect Deep Drawing Defect Due to Punch-Die Misalignment using Image Processing Technique," in *IOP Conference Series: Materials Science and Engineering*, 2019, vol. 530, no. 1. doi: 10.1088/1757-899X/530/1/012015.

[15] J. He, J. Wen, X. Zhou, and Y. Liu, "Hot deformation behavior and processing map of cast 5052 aluminum alloy," *Procedia Manufacturing*, vol. 37, pp. 2–7, 2019, doi: 10.1016/j.promfg.2019.12.003.

[16] Z. Huang, W. Wang, Y. Zhang, and J. Lai, "Low speed impact properties of 5052 aluminum alloy plate," *Procedia Manufacturing*, vol. 50, pp. 668–672, 2020, doi: 10.1016/j.promfg.2020.08.120.

[17] "6 Design of Experiments 6.1 Introduction."

[18] A. Aminzadeh, S. Sattarpanah Karganroudi, N. Barka, and A. el Ouafi, "A real-time 3D scanning of aluminum 5052-H32 laser welded blanks; geometrical and welding characterization," *Materials Letters*, vol. 296, Aug. 2021, doi: 10.1016/j.matlet.2021.129883.

[19] P. K. Kapur, G. Singh, Y. S. Klochkov, and U. Kumar, *Decision Analytics applications in industry*. 2020. doi: 10.1007/978-981-15-3643-4_23.

[20] L. Ren, L. Zhang, L. Wang, F. Tao, and X. Chai, "Cloud manufacturing: key characteristics and applications," *International Journal of Computer Integrated Manufacturing*, vol. 30, no. 6, pp. 501–515, Jun. 2017, doi: 10.1080/0951192X.2014.902105.

[21] K. Ghahremani, M. Safa, J. Yeung, S. Walbridge, C. Haas, and S. Dubois, "Quality assurance for high-frequency mechanical impact (HFMI) treatment of welds using handheld 3D laser scanning technology," *Welding in the World*, vol. 59, no. 3, pp. 391–400, Apr. 2015, doi: 10.1007/s40194-014-0210-3.

[22] J. Günther, P. M. Pilarski, G. Helfrich, H. Shen, and K. Diepold, "Intelligent laser welding through representation, prediction, and control learning: An architecture with deep neural networks and reinforcement learning," *Mechatronics*, vol. 34, no. October 2015, pp. 1–11, 2016, doi: 10.1016/j.mechatronics.2015.09.004.

[23] A. Fernández Villán *et al.*, "Low-cost system for weld tracking based on artificial vision," *IEEE Transactions on Industry Applications*, vol. 47, no. 3, pp. 1159–1167, May 2011, doi: 10.1109/TIA.2011.2124432.

[24] T. J. Cleophas, A. H. Zwinderman, T. J. Cleophas, and A. H. Zwinderman, "Analysis of Variance (Anova)," *Regression Analysis in Medical Research*, vol. 6, pp. 147–155, 2021, doi: 10.1007/978-3-030-61394-5_7.

[25] C. The and M. Oldenburg, *Encyclopedia of Thermal Stresses*. 2014. doi: 10.1007/978-94-007-2739-7.

[26] C. L. Tsai and D. S. Kim, *Understanding residual stress and distortion in welds: An overview*. Woodhead Publishing Limited, 2005. doi: 10.1533/9781845690939.1.3.

[27] J. Ahn, E. He, L. Chen, R. C. Wimpory, J. P. Dear, and C. M. Davies, "Prediction and measurement of residual stresses and distortions in fibre laser welded Ti-6Al-4V considering phase transformation," *Materials and Design*, vol. 115, pp. 441–457, Feb. 2017, doi: 10.1016/j.matdes.2016.11.078.

[28] B. Kumar, S. Bag, and C. P. Paul, "Influence of heat input on welding induced distortion for Yb-fibre laser welded thin sheets," in *Materials Today: Proceedings*, 2019, vol. 26, pp. 2040–2046. doi: 10.1016/j.matpr.2020.02.442.

[29] *Encyclopedia of Thermal Stresses*. Springer Netherlands, 2014. doi: 10.1007/978-94-007-2739-7.

[30] A. Gorkič, M. Jezeršek, J. Možina, and J. Diaci, "Measurement of weldpiece distortion during pulsed laser welding using rapid laser profilometry," *Science and Technology of Welding and Joining*, vol. 11, no. 1, pp. 48–56, Feb. 2006, doi: 10.1179/174329306X77065.

[31] L. Wang, M. Gao, C. Zhang, and X. Zeng, "Effect of beam oscillating pattern on weld characterization of laser welding of AA6061-T6 aluminum alloy," *Materials and Design*, vol. 108, pp. 707–717, Oct. 2016, doi: 10.1016/j.matdes.2016.07.053.

[32] C. L. Tsai and D. S. Kim, "Understanding residual stress and distortion in welds: An overview," in *Processes and Mechanisms of Welding Residual Stress and Distortion*, Elsevier Ltd., 2005, pp. 3–31. doi: 10.1533/9781845690939.1.3.

[33] C. Hagenlocher *et al.*, "The influence of residual stresses on laser beam welding processes of aluminium sheets," in *Procedia CIRP*, 2020, vol. 94, pp. 713–717. doi: 10.1016/j.procir.2020.09.124.

[34] S. Katayama, Y. Kawahito, and M. Mizutani, "Elucidation of laser welding phenomena and factors affecting weld penetration and welding defects," in *Physics Procedia*, 2010, vol. 5, no. PART 2, pp. 9–17. doi: 10.1016/j.phpro.2010.08.024.

[35] S. Katayama, *Introduction: Fundamentals of laser welding*, vol. 9, no. 2012. Woodhead Publishing Limited, 2013. doi: 10.1533/9780857098771.1.3.

[36] H. Yamaoka, M. Yuki, T. Murayama, K. Tsuchiya, and T. Irisawa, "CO2 laser welding of aluminium A6063 alloy," *Welding International*, vol. 6, no. 10, pp. 766–773, Jan. 1992, doi: 10.1080/09507119209548283.

[37] Z. Wang, J. P. Oliveira, Z. Zeng, X. Bu, B. Peng, and X. Shao, "Laser beam oscillating welding of 5A06 aluminum alloys: Microstructure, porosity and mechanical properties," *Optics and Laser*

*Technology*, vol. 111, no. September 2018, pp. 58–65, 2019, doi: 10.1016/j.optlastec.2018.09.036.

[38] S. Il Pak and T. H. Oh, "Correlation and simple linear regression," *Journal of Veterinary Clinics*, vol. 27, no. 4, pp. 427–434, 2010, doi: 10.1007/978-3-319-89993-0_6.

[39] N. J. Gogtay and U. M. Thatte, "Principles of correlation analysis," *Journal of Association of Physicians of India*, vol. 65, no. MARCH, pp. 78–81, 2017.

[40] MathWorks, "Specialization Practical Data sicence with Matlab."

# CHAPITRE 3
# MODELE DE CLASSIFICATION DE LA QUALITE PAR APPRENTISSAGE AUTOMATIQUE POUR LA PREDICTION DE LA POROSITE DANS LES ALLIAGES D'ALUMINIUM SOUDES AU LASER.

Joys S. Rivera[1], Marc-Olivier Gagné[2], Siyu Tu[2], Noureddine Barka[1], François Nadeau[2], Abderrazak El Ouafi[1]
[1] Department of Mathematics, Computer Science and Engineering, Université du Québec à Rimouski, Rimouski, Québec, Canada
[2] National Research Council Canada - Aluminum Technology Centre, QC, Canada

*Corresponding author: joys.silvarivera@uqar.ca

*Cet article a été soumis dans The International Journal of Laser Applications portant le numéro de référence JLA22-AR-ALSTA2021-00292*

## 3.1 RÉSUMÉ

L'utilisation croissante des alliages d'aluminium dans différentes industries a suscité l'intérêt pour l'étude de différents procédés de transformation tels que le soudage au laser. Ce procédé génère différents types de signaux qui peuvent être surveillés et utilisés pour l'évaluation et analyses de la qualité. L'un des défauts les plus critiques dans le procédé de soudage au laser sont les défauts internes qui sont complexes à détecter, dans lesquels la porosité est catégorisée. Ce type de défaut peut entraîner une défaillance critique du produit fabriqué, ce qui est critique pour l'utilisateur final. Dans cette recherche, une méthode de prédiction de la porosité et un flux de travail utilisant un système de surveillance par caméra à haute vitesse et des algorithmes de classification par apprentissage automatique sont proposés et étudiés afin de trouver la méthodologie la plus performante pour résoudre le problème de prédiction. La méthodologie comprend l'extraction de caractéristiques par des vidéos à haute vitesse, l'analyse de radiographies sur des sections de 1 mm, l'ingénierie et la sélection de caractéristiques, le traitement des

déséquilibres, et l'évaluation des algorithmes d'apprentissage automatique par des mesures telles que la précision, l'AUC et le F1. Il en résulte une amélioration de 127 % du score F1 pour l'algorithme des réseaux neuronaux artificiels et une augmentation de 68 % du paramètre AUC, qui indique une amélioration des performances du modèle de classification des porosités pour les algorithmes SVM. En outre, il a été constaté que le meilleur algorithme d'apprentissage automatique pour faire la prédiction de la porosité pour la configuration est Random Forest avec 0,83 AUC, 75% de précision, 0,75 en score F1 pour la classe de non-porosité, et 0,76 en score F1 pour la classe de porosité. Les résultats positifs du modèle et de la méthodologie proposés indiquent qu'ils pourraient être mis en œuvre dans des applications industrielles pour améliorer la qualité du produit final pour les plaques soudées et réduire les déchets et le temps pour l'analyse de la qualité du produit, augmentant ainsi la performance opérationnelle du procédé.

## 3.2 CONTRIBUTIONS

Ce troisième article intitulé « *Quality classification model with Machine Learning for porosity prediction in laser welding aluminum alloys. »* En tant que premier auteur, ma contribution constitue la partie essentielle de la recherche concernant l'état de l'art, la mise en œuvre des méthodes de traitement et sélection de paramètres, la mise en œuvre des algorithmes d'apprentissage automatique, l'analyse et interprétation des résultats, ainsi que la proposition et développement de la méthodologie pour la classification et prédiction de la porosité qui est le cœur du travail. Cet article est aussi le résultat de la collaboration entre l'Université du Québec à Rimouski et le Conseil national de recherches Canada (CNRC). L'équipe du CNRC Marc-Olivier Gagné, Siyu Tu et François Nadeau, a planifié les essais de soudure, les données acquis dans la surveillance et a proposé projet de recherche. Ils ont également contribué à l'amélioration de la rédaction pour la version finale. Le professeur Noureddine Barka et le professeur Abderrazak El Ouafi ont soutenu la définition de la méthodologie et ont donné les recommandations nécessaires pour améliorer le travail grâce à leurs connaissances et leurs expertises.

## 3.3 TITRE TROISIEME ARTICLE

Quality classification model with Machine Learning for porosity prediction in laser welding aluminum alloys.

## 3.4 ABSTRACT

The growing implementation of aluminum alloys in industry has focused the interest in studying transformation processes such as laser welding. This process gets different kinds of signals that can be monitored and used to evaluate it and to make quality analysis. One of the most critical defects in laser welding is the internal defects that are complex to detect, in which porosity is categorized. This kind of defect may result in a critical failure of products, affecting the final user. In this research, a porosity prediction method using a high-speed camera monitoring system and Machine Learning algorithms are proposed and studied to find the most performant methodology to resolve the prediction problem. The methodology includes feature extraction by high-speed, X-ray analysis, feature engineering and selection, Imbalance treatment, and the evaluation of the ML Algorithms by metrics such as Accuracy, AUC, and F1. As result, an improvement of 127% in the F1 score in ANN algorithm was reported, and an increase of 68% in AUC parameter for SVM algorithms was achieved. Additionally, it was found that the best ML Algorithm for porosity prediction in the proposed setup is Random Forest with 0.83 AUC, 75% accuracy, 0.75 in F1 score for No Porosity, and 0.76 in F1 Score for Porosity. The results of the proposed model and methodology indicate that it could be implemented in industrial applications for enhancing the final product quality for welded plates and reducing process waste and product quality analysis time, increasing the operational performance of the process.

***Keywords****: Artificial intelligence, Machine Learning, Laser Welding, Porosity, Product Quality, Advanced Manufacturing.*

## 3.5 NOMENCLATURE

| | |
|---|---|
| **ANN** | Artificial Neural Network |
| **CNN** | Convolutional Neural Network |
| **SVM** | Support Vector Machine |
| **RMSE** | Root mean square error |
| **$R^2$** | R squared, coefficient of determination |
| **ML** | Machine Learning |

| | |
|---|---|
| **MW** | Mean window |
| **SW** | Standard deviation window |
| **VW** | Variance window |
| **RF** | Random Forest |
| **AUC** | Area under the curve |
| **CPU** | Central processing unit |
| **GPU** | Graphics Processing Units |
| **ROC** | Receiver operating characteristic |

## 3.6 INTRODUCTION:

Aluminum alloys have a wide and growing application in transportation, primarily in the automotive industry, aerospace applications, shipbuilding industry, and railway industry, with the goal of lighter weighting and reducing energy consumption, which has a direct relationship to greenhouse gases emission in all of the named industrial productive chains[1]–[3]. Laser welding process is an advanced manufacturing process technology that is widely applied in industry because of its versatility, process efficiency, and adaptability. It is recognized as a high-quality, high-precision, low-distortion, high-performance, high-speed joining process [4]. This process is characterized by a deep, narrow keyhole that is formed in welding with a high-power-density beam of laser, effectively producing a deep, narrow penetration weld [5]. In overlap welding, the parts are joint by the laser beam penetration to the upper part, and the penetration is converted in heat that joint with the lower part [6]. Nevertheless, under inappropriate operational conditions welding defects may happen leading to a fracture or even a failure of manufactured products [4], [7]. In order to manufacture high quality and high reliability products with a laser beam, it is important to apply process parameters monitoring, quality monitoring, quality classification and validation for welding defects. Therefore, it is of crucial importance to understand the welding

physical phenomena as well as defect formation conditions to optimize and improve the process performance [4], [8].

Porosity in laser welding is one of the most critical problems in practical applications. This defect is mainly related to process instability, keyhole collapse, and shrinkage [4], [5]. Lin R. et al reported that keyhole depth is one of the most important predictors [9], but is technically more complex to monitor in industrial applications, for that reason the keyhole behavior is normally used to get more parameters to monitor, control, classify and predict the defects including porosity on the laser welding process. The parameters that can be monitored and used for quality classification in the prediction model are the weld width, keyhole area, keyhole perimeter, and intensity [10], [11]. Deyuan M. et al. used Convolutional Neural Networks (CNN) to detect porosity defects on but-but laser welding on aluminum alloys, based on a 3D cloud map to get the morphological characteristics of keyhole which is obtained by a multi-sensor system and high-speed camera, and a slide window method to characterize the behavior of the monitored signals. Based on just two experiments, the accuracy of the classification process was 93.15% for porosity detection with a procedure that is restricted to high thickness plates (6 to 10 mm), and with a complex monitoring configuration that is not a suitable setup for industrial applications [12].

Dalibor P. studied and proposed a machine learning model based on process parameters to predict the quality of laser welding. Laser power, welding speed, stand-off distance, and clamping pressure were used as input parameters where those were not monitored, to predict the lap-shear strength and weld width, which the author proposed as quality check parameters. This article proposed three models to make the prediction, support vector machine (SVM), artificial neural network (ANN), and Gaussian process (GP), those models were evaluated by $R^2$ and RMSE where the SVM model had the best performance to predict the quality parameters with $R^2$ = 0.9957 and RMSE= 0.7781 and for lap-shear strength, $R^2$ = 0.9999 and RMSE= 0.0042 [13]. Johannes G. et al. suggested an architecture that combines three contemporary machine learning to self-learn in order to control and make a prediction of operational conditions. The laser welding process was monitored by a camera-based system and photodiodes, the reported camera sample rate is 1500Hz. The welding condition was classified by the Support Vector Machine algorithm

(SVM), with five quality conditions based on welding width, with a 0.3 reported error and 0.47 classification error value, and 82% classification accuracy. Where the classification error is almost the 50%, increasing the incertitude of the classification model [10].

Andreas M. et al. proposed a cost-efficient quality monitoring system based on a machine learning architecture in which laser welding quality in the copper alloy is evaluated by four main classes. This study evaluated four different algorithms Support Vector Machine (SVM), Random Forest, AdaBoost, Convolutional Neural Network, and Artificial Neural Networks. Where a feature analysis was implemented to select the best parameter combinations to be implemented for the machine learning model. As result, the best accuracy value obtained is 82%, with a low false-positive rate of 24.7% and a low false negative rate of 7.6%, and with a maximal recall rate near 80% with the AdaBoost algorithm [14]. Adrian R. et al. implemented an Ensemble Data-Driven Fuzzy Network based on Functional Neural Networks to predict laser welding seam quality, based on strategically selected data that restrict the model to specific operational conditions, the data was obtained by a monitoring system that senses the laser beam spectrum and the geometry of the melt pool, a high-speed camera that provided 69 frames per experiment. This method with a prediction performance of about 78% [11]. The study developed by Syed Q. et al. proposes a defect classification method for the gas metal arc welding process for carbon steel. The Machine Learning algorithms proposed by this author were Decision Tree and Support Vector Machine (SVM), the model was taken as input data, the voltage, the wire feed rate, stick out distance, travel speed, and gas flow rate. And according to input parameters classified the weld quality as good, porosity, burn through, and lack of penetration. This model presented a 96.4% accuracy for the Decision tree and 93.75% for SVM [15]. The literature reported studies that are restricted and focused on the laboratory setup with high porosity and defect rates, and which are not easily suitable for industrial applications and are focused to study the machine learning model but not the whole necessary methodology stages that must be applied to make the quality prediction on the laser welding process. In this article, a methodology that studies the quality classification for porosity in laser welding is proposed and developed. Starting from the feature engineering which analyzes different feature selection methods and arrives at the most optimal machine learning model to make porosity predictions on laser welding for aluminum

alloys based on the X-ray analysis results and the keyhole monitoring data obtained with a 10.000 frames/sec high-speed camera. This with the aim to propose a potential procedure for porosity prediction in laser welding aluminum alloys in industrial applications. The methodology is divided in four main stages, 1. Feature extraction and x-ray analysis results, 2. Feature engineering and selection 3. Treatment of the imbalance problem 4. Machine Learning Algorithm for pass/fail prediction.

## 3.7 MATERIAL AND METHODS

The laser welds were provided in overlap joint configuration on AA6061-T6 aluminum alloy using a 1.5mm thick top sheet over a 2.0mm thick bottom sheet. The laser welds were done in continuous mode, without shielding gas, using a Trumpf TRUDISK® 10kW source combined with a Precitec YW52® processing head that allows linear beam wobbling transverse to the weld direction. A Phantom MIRO M310® high-speed camera combined with a 1kW illumination system is also mounted on a fixture directly on a KUKA Quantum® 300kg payload robot arm (Figure 1). A 200µm fiber and a 300mm focal lens were used in combination with the Precitec® wobbling head which dictate a nominal spot size of 0.4mm. A design of experiments (DOE) was conducted providing fourteen different process parameters over a wide range of laser power and weld speed attempting to provide multiple amounts of internal porosities, in Table 22 the welding conditions are stated. Figure 50 presents the procedure and setup implemented in this study for the laser welding online monitoring method and machine learning (ML) prediction model. The stages proposed for porosity prediction consist of principally by 1. Welding process, 2. High-speed camera video monitoring, 3. Feature extraction from the high-speed camera videos, 4. Time series data extraction, 5. Data engineering and treatment, 6. X-ray analysis and pass/fail data extraction, and 7. Machine Learning model for porosity prediction. In the following sections, the methodology for each step will be explained.

Table 22. Table 1: Laser welding parameters DOE.

| Weld ID | Laser power (kW) | Robot speed (m/min) | Focal position (mm) | Oscillation amplitude (mm) | Oscillation frequency (Hz) |
|---|---|---|---|---|---|
| 1 | 5.5 | 5 | 12 | 1 | 500 |
| 2 | 5.5 | 5 | 12 | 0.5 | 500 |
| 3 | 5.5 | 5 | 12 | 0.5 | 200 |
| 4 | 5.5 | 5 | 12 | 0.8 | 200 |
| 5 | 4.5 | 5 | -5 | 0.8 | 500 |
| 6 | 4 | 5 | -5 | 1 | 500 |
| 7 | 6 | 6 | 12 | 1 | 400 |
| 8 | 6 | 6.5 | 12 | 0.5 | 400 |
| 9 | 6 | 6.5 | 12 | 0.2 | 400 |
| 10 | 6.5 | 7 | 12 | 0.2 | 400 |
| 11 | 5.5 | 6 | 6 | 1 | 400 |
| 12 | 3.75 | 5 | 6 | 1 | 500 |
| 13 | 3.9 | 5 | -5 | 1 | 200 |
| 14 | 5 | 6 | 6 | 1 | 400 |

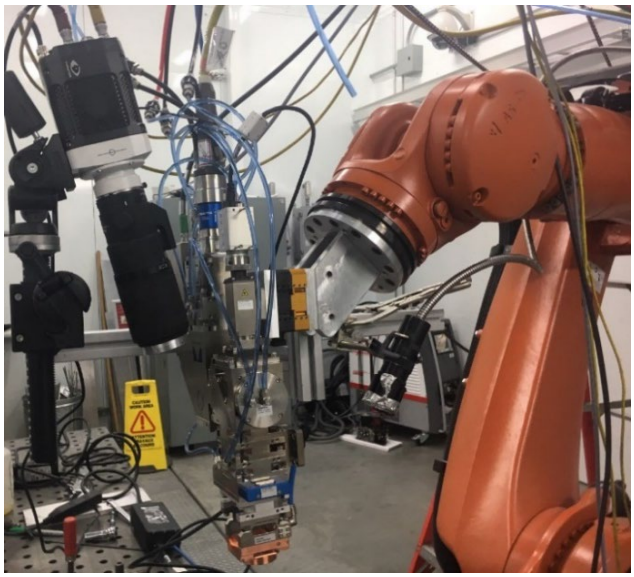

Figure 49. Laser welding cell.

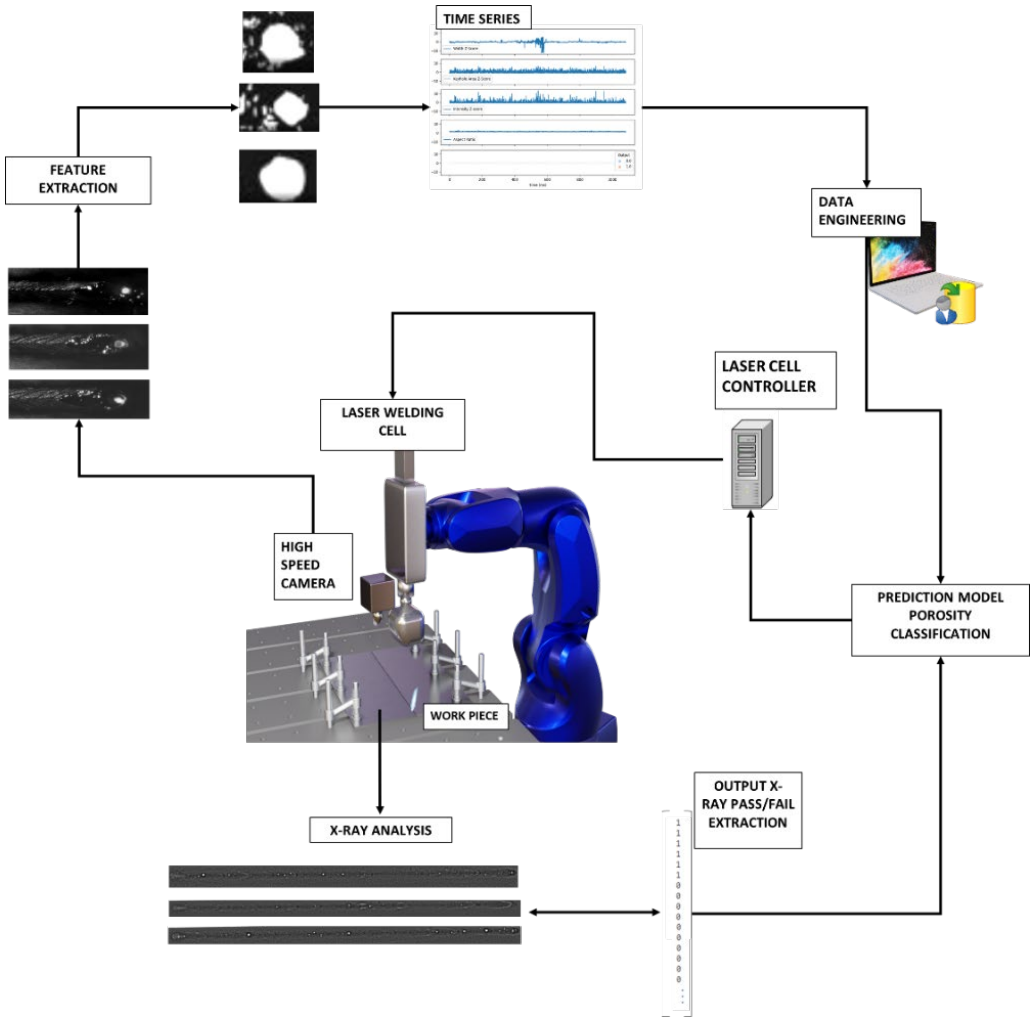


Figure 50. Laser welding experiment setup and prediction workflow.

### 3.7.1 Features definition for laser welding monitoring and prediction model

The laser welding defects, or imperfections have three main classification classes: geometrical or appearance defects, internal or invisible defects, and property or quality defects. Porosity is classified in the internal defect category, and it is associated with process instability (that is one of the characteristics of the laser welding process) that results in bubble formation due to keyhole collapsing [16], Figure 51 presents the main steps in pore formation process were the keyhole collapsing induce the bubble formation in the molten pool [4], [9]. The internal defects as porosities result in deterioration of mechanical properties or may cause catastrophic

failures of the final product. Consequently, monitoring and predicting defect formation is very important to assure the best quality for the product. The detection of internal defects is very difficult [4], for this reason, advanced techniques are implemented for porosity detection [12].

The High-speed camera is one of the most useful and performant methods for laser welding monitoring applied to obtain the data to analyze the process behavior and predict quality defects, based on the geometrical and optical data produced by the process itself [17], [18]. Keyhole depth is reported as one of the most important parameters for the prediction of porosity in laser welding, where the depth variation is related to the keyhole collapsing and is associated with the keyhole-induced pore formation [5], [19]. Width reduction is related to depth increase, Kangda H. et al. reported that Width reduction is related to depth increase and depth variation [20]. It suggests that in the model the width value can be an important predictor. Horník et al. related the reflected intensity in laser welding with depth to width ratio. Consequently, it is suggested that high-intensity pixel values could be related to weld defects [21]. You D. et al. documented that the deepest weld produced the reduction of laser reflection captured by photodiode [22], which suggests that the welding depth is correlated with the variation of the reflected intensity. According to the reported information and the porosity phenomena, the monitoring data chosen for this article are the Weld With, Keyhole pixel Intensity, Keyhole Area, and the Aspect ratio, these parameters are obtained from the high-speed camera.

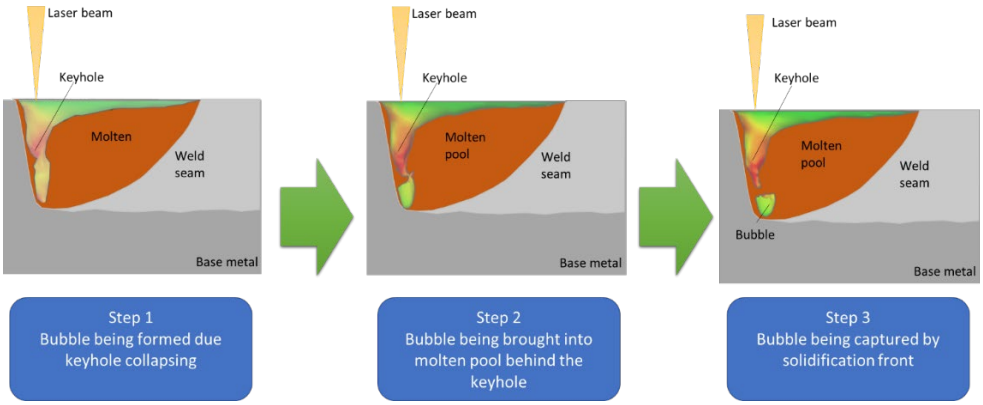


Figure 51. Main steps for keyhole-induced pore formation

### 3.7.2 Features extraction method

After welding the X-ray images are acquired from Yxlon multiplex 5500M with a tension of 185kV, Figure 52 presents the summary of the images obtained in the X-ray analysis procedure. The post-processing of the images was performed with ImageJ 1.53h to obtain the pass/fail output from the 1 mm section along the welds. Since the porosities in the X-ray image appear to be bright spots, a threshold of 220 over 255 on a grayscale was applied to determine the area of the porosities. Within each 1 mm section, the area of porosities over 0.02 mm2 was considered "fail", where 0 was assigned to the section. Otherwise, the section would pass and be assigned 1 in the dataset. Each weld has 90 sections that went through this pass/fail analysis and the array of 90 elements filled with 0 and 1 were then used as dependent variables for further analysis and is defined as the output vector, which is exported as a CSV file. In Figure 53 the image processing workflow is exemplified.

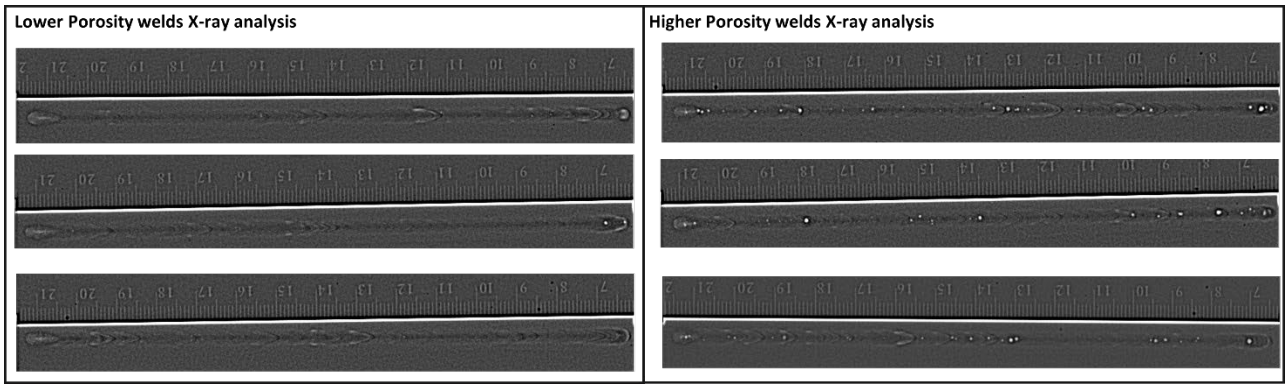


Figure 52. X-ray analysis results.

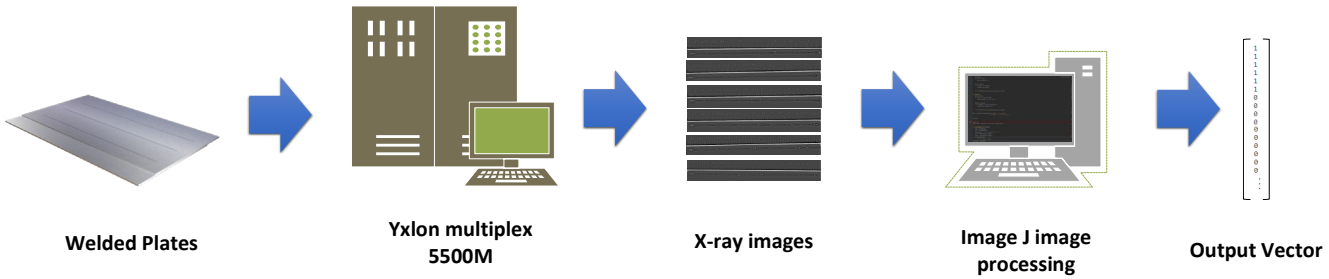


Figure 53. X-ray image processing workflow

High-speed videos were obtained using the High-Speed camera Phantom MIRO M310. Videos were recorded at the speed of 10,000 frames per second with 640 x 480 pixels in each frame. A 93 x 86 pixels region of interest for the keyhole was selected to perform the keyhole analysis, including the intensity, the area, and the aspect ratio. The keyhole intensity was defined as the total pixel gray value in the region of interest. The area and aspect ratio measurements require keyhole segmentation. In fact, since the camera can only acquire the signal from the surface, the keyhole measurements were not from the real keyhole, but from the illuminated vortex produced by the interaction between the laser and fusion zone. Such vortex is the best approximation of the keyhole at the surface, and all the keyhole mentioned in this paper are referred to as the vortex. ImageJ 1.53 and python 3.6 were applied to perform the image analysis for keyhole identification and measurements. Figure 54 shows the feature extraction workflow.

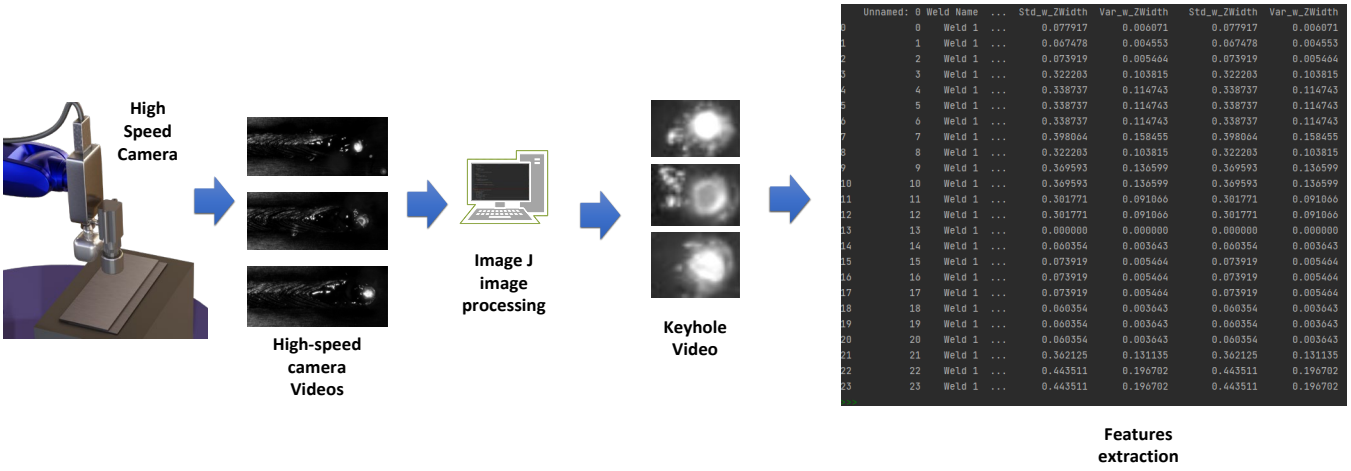


Figure 54. Feature extraction from high-speed camera monitoring.

### 3.7.3 Feature engineering and selection

Feature engineering is considered a fundamental step in the application of machine learning models, it helps to understand the data, define new features to define no-redundant features, and improve the model performance. Feature selection becomes prominent, especially in the data sets with many variables and features that look to reduce the dimensionality of the input data. Feature

selection detects the most important features and rejects the irrelevant ones, intending to obtain a subset of features that describes properly the defined problem with a minimum degradation of performance. It will eliminate unimportant parameters and improve the accuracy as well as the metrics for classification [23]–[25].

In this study, new features were created to improve the performance of the model; a new feature that gets the nominal value of intensity with the multiplication between the Keyhole pixel Intensity and the Keyhole Area is applied because the Keyhole Pixel Intensity is obtained in relations to the Keyhole Are in the feature extraction stage. Two additional sets of parameters based on the application of Z-Score and the mobile window statistics application to single raw data value are created. Weld With, Keyhole pixel Intensity, Keyhole Nominal Intensity, and Keyhole Area were all subjected to the Z-score normalization approach, which is frequently used in the preprocessing step [26]. The formula for the Z-score parameter is given in equation 1. Mobile Window is a technique that detects significant patterns in the dataset. The method can be used to evaluate the stability of a statistical model by back-testing it against historical data [27]. The mobile window method is a crucial strategy documented in numerous research to enhance the quality prediction model and aid in understanding the tendency of the monitored data by creating observable patterns in the dataset [12], [27], [28]. Figure 55 presents the schematic representation of the mobile window method. The mobile window statistics applied to the data set are the Mean (MW), the Standard Deviation (SW), and the Variance (VW). The mobile window range of values utilized for this study was 5 data points, it was selected based on the time that porosity generation takes to appear according to the literature review and the 10.000 frames/sec that is the capacity of the High-Speed camera Phantom MIRO M310 [29], [30]. Table 23 shows the parameters obtained by preprocessing and feature engineering method for this study, in total 30 input parameters are obtained in this stage, and in Figure 56 the results of mobile window calculation for mean, standard deviation, and variance are presented.

$$Z - Score = \frac{x - \mu}{\sigma} \quad (1)$$

Where,

x a single raw data value of the parameter, μ is the population mean, $\sigma$ is the standard deviation.

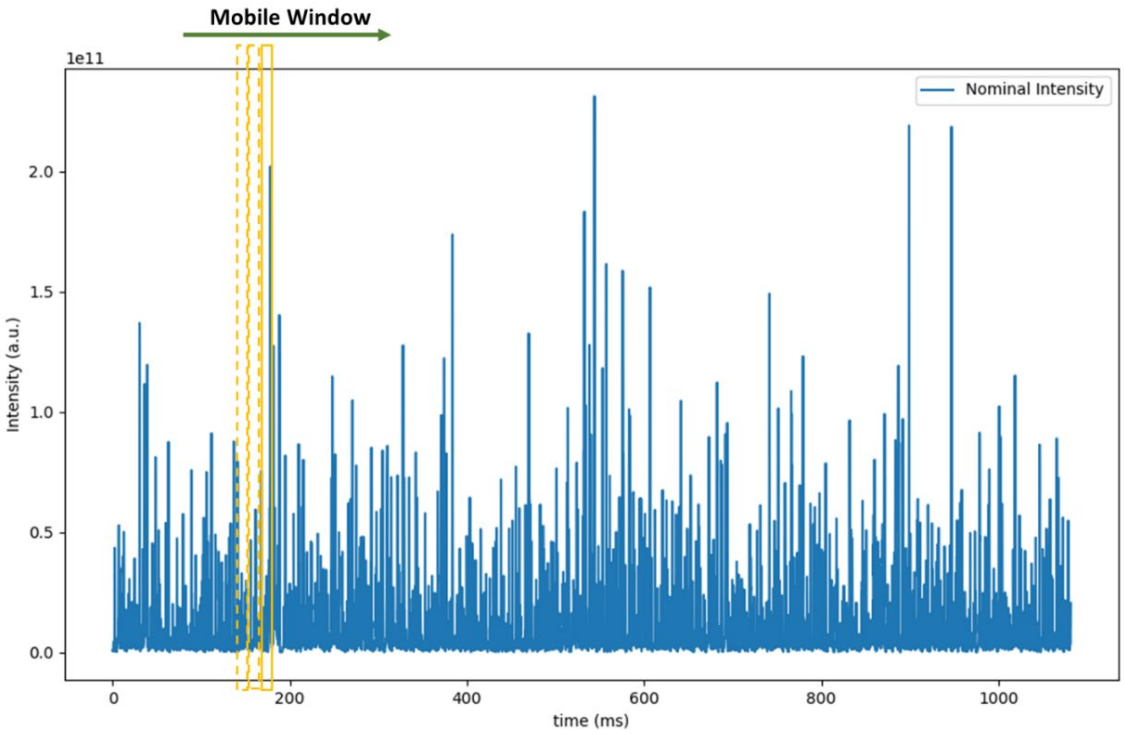


Figure 55. Mobile Window method representation on Nominal Intensity.

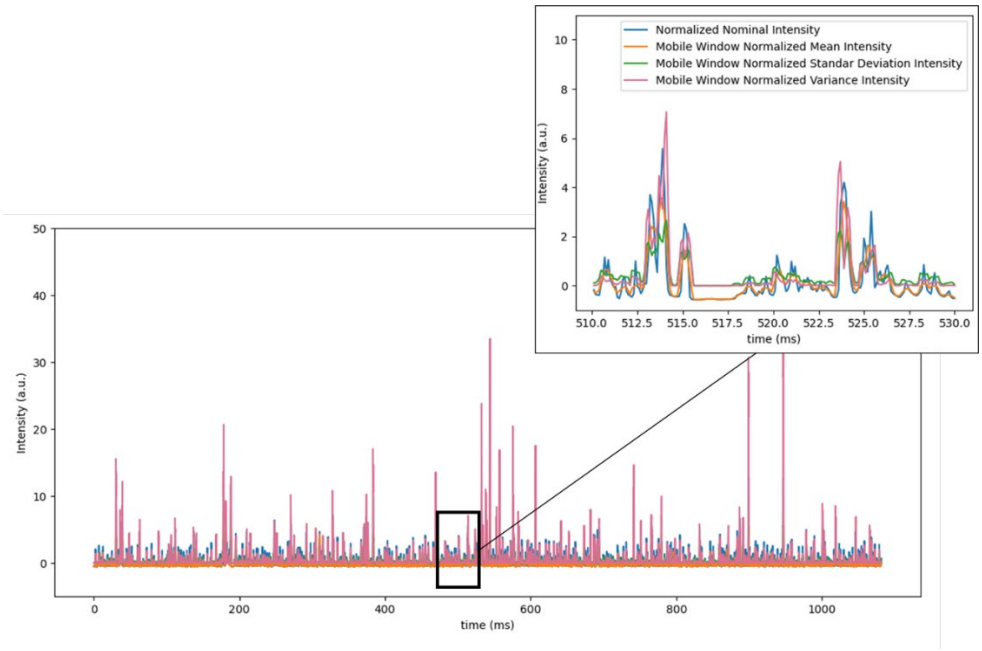


Figure 56. Mobile window results between normalized, mean, standard deviation and variance for Nominal Intensity.

Table 23. Features definition by feature engineering.

| | Keyhole Area | Weld width | Nominal Keyhole Intensity | Keyhole Intensity | Keyhole Aspect ratio |
|---|---|---|---|---|---|
| **Nominal value** | √ | √ | √ | √ | √ |
| **Z-Score normalization** | √ | √ | √ | √ | x |
| **Mean 5 frames Window** | √ | √ | √ | x | x |
| **Mean 5 Frames window to Z-score** | √ | √ | √ | √ | x |
| **Standard deviation 5 frames Window** | √ | √ | √ | x | x |
| **Standard deviation 5 frames Window to Z-score** | √ | √ | √ | √ | x |
| **Variance 5 frames Window** | √ | √ | √ | x | x |
| **Variance 5 frames Window to Z-score** | √ | √ | √ | √ | x |

### 3.7.4 Machine Learning Classification models

The principal focus of Machine Learning (ML) is to predict an output using the existing data. The prediction assignment is called the "Classification problem" when the output presents different classes and is called the "Regression problem when the output represents a numeric measurement. ML algorithms are generally, with some exceptions, able to model complex classes, can accept different input predictor data, and do not make assumptions about data distribution. Multiple studies have largely found that ML methods are higher accuracy compared to parametric classifiers, specifically for complex data with a high dimensional input matrix, with high dimensionality [31]–[33]. In this article, a comparison between machine learning algorithms such as Support Vector Machine (SVM), Artificial Neural Network (ANN), Random Forest (RF),

and Catboost is performed in python 3.8 to choose the suitable classification algorithms for making the quality prediction based on pass/fail approach for laser welding in aluminum alloys.

Support Vector Machine is one of the traditional machine learning techniques that can help to solve big data classification problems. Specifically, it can help the multidomain applications in a big data setting. However, the SVM is mathematically intensive and computationally expensive. SVM provides a classification learning model and a classification algorithm. SVM revolves the classification problem around the concept of a "margin"—either side of a hyperplane that separates two data classes. Maximizing the margin and in that way creating the largest possible distance between the separating hyperplane and the instances on either side of it has been proven to reduce an upper bound on the expected generalization error. Consequently, the model complexity of an SVM is not affected by the number of parameters encountered in the training data. For this reason, SVM can deal with learning tasks where the number of features is large with respect to the number of training instances [31], [32], [34].

Artificial neural networks are defined by Ivan Nunes da Silva et al. as *computational models inspired by the nervous system of living beings* [35]. They can obtain and retain knowledge and can be defined as a set of processing units, represented by artificial neurons, interlinked by a lot of interconnections implemented by vectors and matrices of synaptic weights. Petra P. et al described that a multi-layer neural network consists of a large number of units (neurons) joined together in a pattern of connections [36]. Units in a net are usually classified into three classes: input units, which receive information to be processed; output units, where the results of the processing are found; and units in between known as hidden units. Feed-forward ANNs allow signals to travel one way only, from input to output, where after a forward pass the network compute the loss and then use backpropagation to calculate the partial loss associated to each weight/bias and then update the values before the next forward pass. This is the key to understand how an ANN models the data [31], [35], [37]. In this study 13 inputs with range 0-1 values, that are the normalized data of the features and the Aspect Ratio, one hidden layer with 20 neurons were implemented for the ANN Machine Learning algorithm, the activation method used for the

input units and the hidden layer was the Rectified Linear Unit Activation (RELU), it is defined in equation 2 [38]. Figure 57 presents the ANN architecture implemented in this research.

$$y_i = \begin{cases} x_i \; if \; x_i \geq 0 \\ 0 \; if \; x_i \; < \; 0 \end{cases} \quad (2)$$

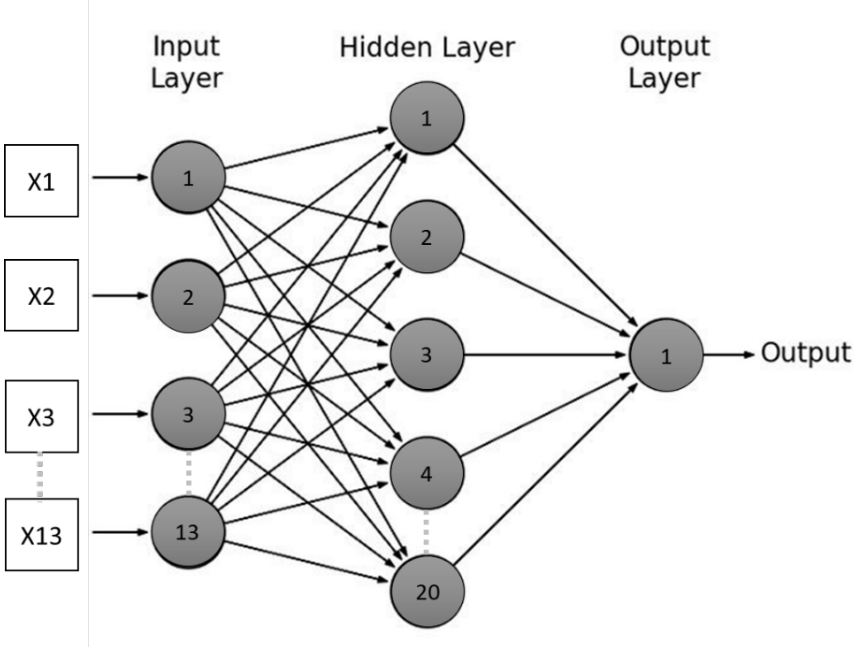


Figure 57. ANN architecture proposed.

Anita P. et al. defined Random Forests as a classifier combining a forest of decision trees grown on random input vectors and splitting nodes on a random subset of features [39]. RF uses the principle of tree classifiers to classify a new feature vector; the input vector is classified with each of the trees in the forest [40]. Each tree provides a classification, and it is specified as a "vote" for that class [41]. The forest chooses the classification that has the most votes over all the trees in the forest. The most significant advantages of RF are unexcelled accuracy among current algorithms, efficient implementation on large data sets, and an easily saved structure for future use of pre-generated trees [39], [41]. A random state value equal to 42 and an n-estimators value of 500 were set for the random forest classifier used for the prediction model. Another algorithm based on the decision trees is the Categorical Boosting algorithm, called CatBoost. CatBoost is a

new supervised open-sourced algorithm that implements a powerful machine-learning method that accomplishes state-of-the-art results in a variety of practical tasks and is used to classify categorical features using gradient boosting on decision trees. It is one of the primary methods for learning problems with heterogeneous features, noisy data, and complex dependencies [42], [43]. CatBoost has both CPU and GPU implementations, where GPU is reported as the much faster training implementation setup [43]. To resolve the classification problem a CatBoost algorithm with a GPU implementation method with an iteration value of 500 was applied in this study.

To evaluate and select the Machine Learning algorithm the metrics to be implemented in this article are accuracy (3), precision (4), recall (5), F1 Score (6), and AUC value. These metrics are widely reported and accepted as the method to evaluate machine learning models for classification [14], [44]. Depending on the application, a high accuracy might not be the primary target to evaluate the model but to minimize one of the two errors, namely false-positive and false-negative. In the quality monitoring setting, identifying a good product as bad would be less critical than letting a bad product go undetected. In this situation, with a bad product being defined as positive, the recall would be the appropriate metric, focusing on a low false-negative rate. For a low false-positive rate, the precision metric is used. For general evaluations, if both errors matter, the F1 score is used as it combines precision and recall [14], [44], [45]. AUC is defined as the Area Under the Curve of the ROC plots that are intended to show the distribution of performance of the model [46]. AUC can be interpreted as a C statistic, which is a measure of goodness of fit for binary outcomes in a model and is reported as a better metric to compare learning algorithms [47]. Where an AUC value below 0.5 indicates a very poor model, a value of 0.5 means that the model is no better at predicting an outcome than random chance. Values over 0.7 indicate a good model, and values over 0.8 indicate a strong model [48].

$$Accuracy = \frac{True\ Positives + True\ Negatives}{Total\ Number\ of\ predictions} \quad (3)$$

$$Precision = \frac{True\ Positives}{True\ Positives+False\ Positives} (4)$$

$$Recall = \frac{True\ Positives}{True\ Positives+False\ Negatives} (5)$$

$$F1\ Score = 2 * \frac{Precision*Recall}{Precision+Recall} (6)$$

## 3.8 RESULTS AND DISCUSSION

### 3.8.1 Feature selection

For the feature selection, two main methods were applied, the Pearson Correlation method, and the feature importance method. The feature importance method applied for this study had two main approaches the first one is the Boruta selection method and the importance value calculation by simulating the ML model that results in the best possible features to optimize the classification metrics.

### 3.8.2 Correlation analysis

The goal of correlation analysis is to measure and understand the strength of a linear or nonlinear relationship between two continuous variables[49], [50], and it is extensively employed as a filter method in statistical data processing [51]. The Pearson correlation approach was used in this investigation with Pandas in python, and the findings are shown in Figure 58. To evaluate if the relationship between parameters and response is strong (|Corr| > 0.7), moderate (0.4 |Corr| 0.7), or weak (|Corr| 0.4) in a range of values from -1 to 1, one standard and statistical range of values and thresholds is created and used [49], [52]. The Pearson Correlation analysis was performed to find possible relationships between predictors and discard the redundant features in the model. According to the findings of the correlation analysis, the possible predictors that

should be excluded in the training model based on the high correlation values between predictors are Keyhole Intensity, Nominal Intensity, Keyhole Area Z-Score, MW Z-Score Keyhole Intensity, SW Z-Score Nominal Intensity, SW Z-Score Keyhole Intensity, VW Z-Score Keyhole Intensity, VW Z-Score Keyhole Area.

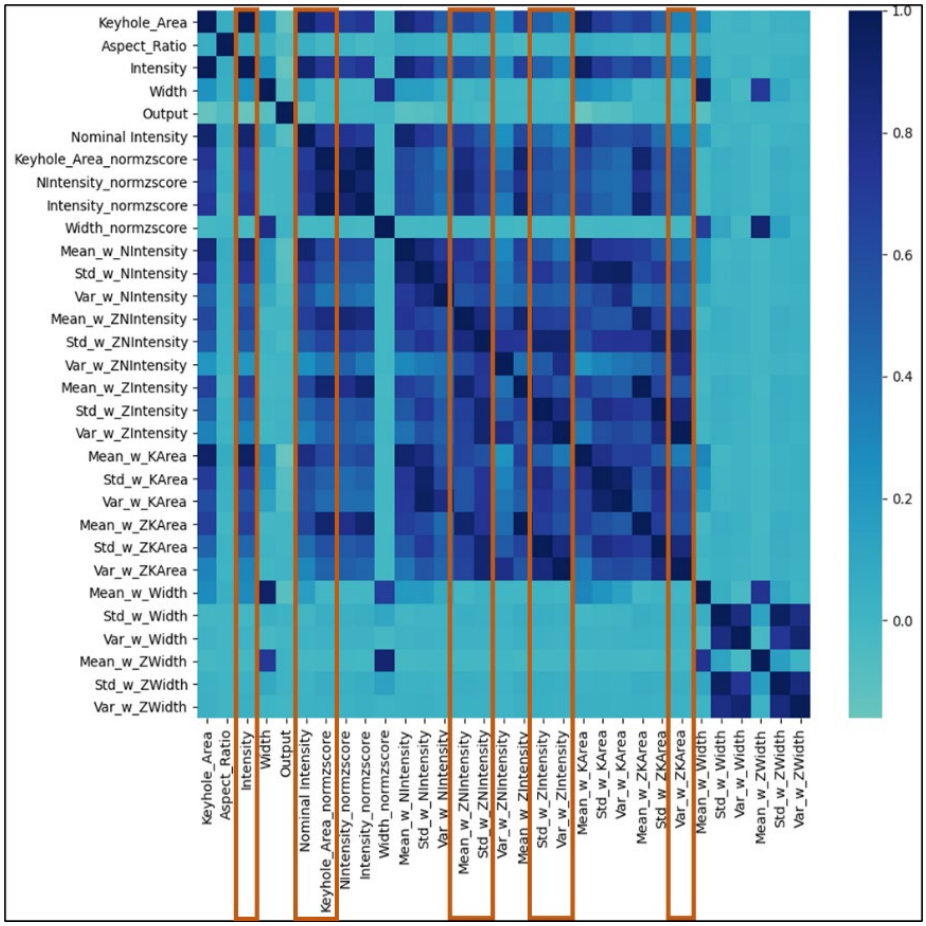


Figure 58. Heat Map for Pearson Correlation Results

### 3.8.3 Boruta method results

The Boruta algorithm is based on the same idea as the random forest classifier. It considers the fluctuations in the average precision loss of trees in the forest and uses the average drop accuracy to measure the feature's importance[53]. Principally based on the complete feature set,

to eliminate the correlation between the feature and the predicted value a mixed shadow feature set before is created before selection, which is a stronger solution for data with feature correlation, this process is repeated until the algorithm iteration limits [54], [55]. To do the Boruta analysis the Python Boruta package was imported and implemented, with 100 iterations which is the maximal number of iterations in the Python package. Table 24 shows the results of the Boruta algorithm method, where 21 features are recommended to be used, and 9 are rejected.

Table 24. Boruta Algorithm feature selection results.

| Feature | Rank | Keep |
|---|---|---|
| Keyhole Area | 1 | True |
| Mean Window Z-Score Width | 1 | True |
| Mean Window Width | 1 | True |
| Mean Window Z-Score Keyhole Area | 1 | True |
| Variance Window Keyhole Area | 1 | True |
| Standard Deviation Window Keyhole Area | 1 | True |
| Mean Window Keyhole Area | 1 | True |
| Mean Window Z-Score Keyhole Intensity | 1 | True |
| Standard Deviation Window Z-Score Width | 1 | True |
| Standard Deviation Window Z-Score Nominal Intensity | 1 | True |
| Mean Window Z-Score Nominal Intensity | 1 | True |
| Variance Window Z-Score Nominal Intensity | 1 | True |
| Standard Deviation Window Nominal Intensity | 1 | True |
| Keyhole Intensity | 1 | True |
| Variance Window Nominal Intensity | 1 | True |
| Nominal Intensity Z-Score | 1 | True |
| Nominal Intensity | 1 | True |
| Keyhole Intensity Z-Score | 1 | True |
| Width Z-Score | 1 | True |
| Mean Window Nominal Intensity | 1 | True |
| Variance Window Z-Score Width | 1 | True |
| Keyhole Area Z-Score | 2 | False |
| Variance Window Z-Score Keyhole Area | 3 | False |
| Standard Deviation Window Z-Score Keyhole Area | 4 | False |
| Variance Window Z-Score Keyhole Intensity | 5 | False |

| | | |
|---|---|---|
| Standard Deviation Window Z-Score Keyhole Intensity | 6 | False |
| Width | 7 | False |
| Aspect Ratio | 8 | False |
| Standard Deviation Window Width | 9 | False |
| Variance Window Width | 10 | False |

### 3.8.4 Features importance analysis method

Defining the features' importance to optimize the results in the machine learning model is a widely studied and implemented approach[56], [57]. Current methodologies for the identification of important features can be classified according to the restrictions of the learning machines. Based on the principle of finding feature weightings that have few non-zero components, this is to quantify the importance of any given feature. The advantage of using a model-based approach is that results will be closely tied to the model performance[56]. It may be able to incorporate the correlation structure between the predictors into the importance calculation. To find the feature's importance, the expected output of the score function under the condition that the feature attains a certain value should be defined. Then the importance is calculated, and each predictor will have a separate value of importance for each class. Next, all the important results are scaled to have a maximum value of 100. This method offers an accurate way to define the prominent variables before we input them into a machine learning algorithm [57]. For this study, the feature importance threshold was defined in 95/100, which means that just the features that give an importance value until 95% will be retained, and the remaining 5% features importance will be rejected.

Random Forest and CatBoost algorithms were chosen to evaluate the feature importance, those ML algorithms have this function available in Python and are widely used for feature importance calculation [58]. The feature that obtained the remaining 5% of feature importance for the model according to RF analysis are Width, SW Width, and VW Width. It means that the named features will be rejected for the ML classification model. In Figure 59, the graph with the results obtained for the feature importance by RF are presented. CatBoost feature important analysis rejected more features, placing the Keyhole Intensity, Aspect Ratio, VW Nominal Intensity, SW Z-Score Keyhole Area, Variance Window Keyhole Area, Nominal Intensity,

Variance Window Z-Score Keyhole Intensity, Keyhole Area Z-Score, SW Z-Score Keyhole Intensity, VW Z-Score Keyhole Area as the 5% remaining in accumulative importance, that was defined as the rejection threshold. Figure 60 presents the results of the feature importance analysis and the rejection threshold is represented.

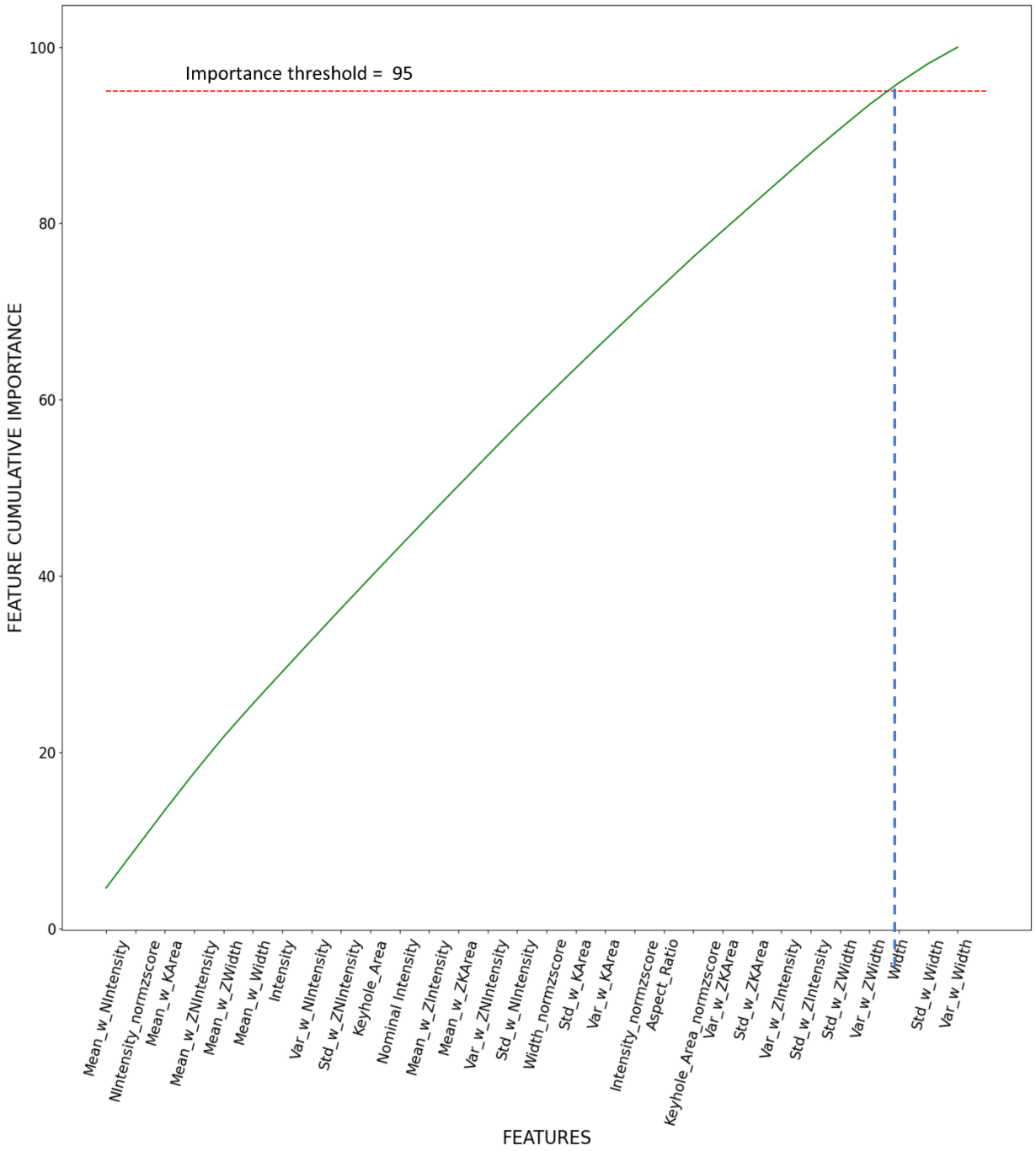


Figure 59. Random Forest feature importance analysis method with feature cumulative importance plot.

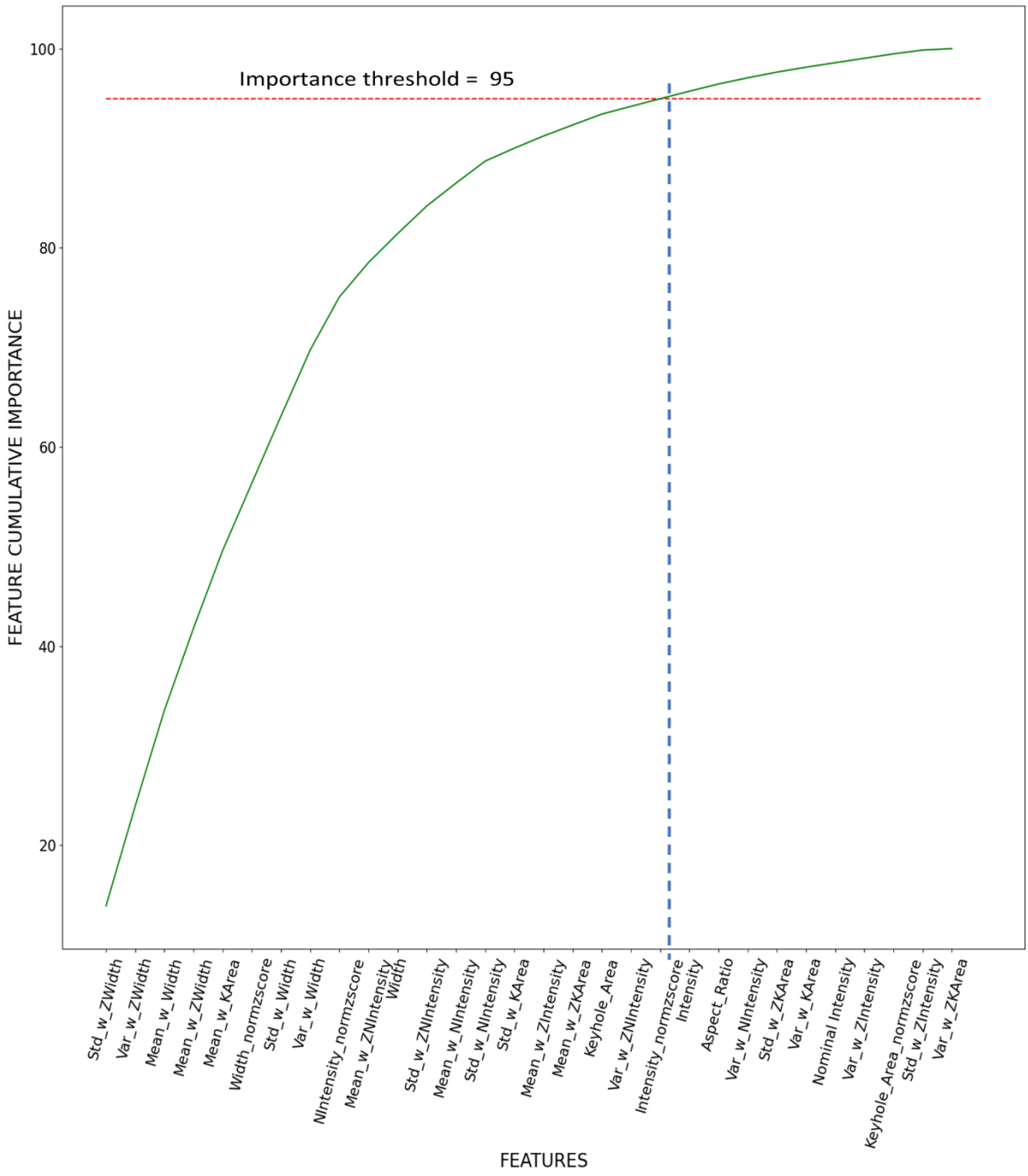


Figure 60. CatBoost feature importance analysis method with feature cumulative importance plot.

### 3.8.5 Machine Learning and Feature selection methods

Based on the Pearson Correlation, Boruta, and importance analysis a preliminary execution of the prediction model was executed and analyzed based on the classification metrics (Accuracy, F1 Score, and AUC) to select the best feature combination to optimize the accuracy of the model in the prediction task. Each combination was tested in SVM, RF, CatBoost, and ANN. In Table 25 the metrics to evaluate the Feature Selection Method for the ML model are presented, according to results the best combination of features are the proposed by the Feature Importance method with CatBoost, with the higher metrics values for Random Forest (Accuracy = 0.82, AUC = 0.83) , Catboost (Accuracy = 0.81, AUC = 0.82) and SVM (Accuracy = 0.75, AUC = 0.45), and with no changes for ANN. According to the results, an imbalance problem in the data may be presented based on the low F1 Score of Negative Class (Fail), even for SVM an F1 Score equal to 0 is reported for all the Feature Selection methods proposed in this study. Literature reports that a low F1 Score behavior is an indicator of an imbalance problem in the data set [59]–[61]. According to reported in section 2.4 of this article based on the literature, the AUC will be implemented as the main metric to analyze the performance for every Feature Selection method. The proposed techniques improved the performance of the machine learning models to do prediction compared with the initial condition of the dataset it means with no Feature Selection method applied on it. According to results presented in Table 26, the feature selection method with the lowest impact on performance was the Pearson Correlation method, follow by the Feature Selection method by RF. The best method performance was obtained by CatBoost Feature Selection method with an improvement in AUC from 6% to 18%, and the second-best method is Boruta with an improvement in AUC from 5% to 11%.

Table 25. Results of Feature selection method evaluation.

| ML Model | Metrics | No feature Selection | Pearson Correlation | Boruta Method | Feature selection RF | Feature Selection CatBoost |
|---|---|---|---|---|---|---|
| **Random Forest** | Accuracy | 0.81 | 0.82 | 0.81 | 0.81 | 0.82 |
| | AUC | 0.74 | 0.74 | 0.82 | 0.81 | 0.83 |
| | F1 Pass | 0.88 | 0.88 | 0.88 | 0.88 | 0.89 |
| | F1 Fail | 0.52 | 0.54 | 0.53 | 0.51 | 0.56 |
| **CatBoost** | Accuracy | 0.8 | 0.81 | 0.8 | 0.79 | 0.81 |
| | AUC | 0.77 | 0.78 | 0.81 | 0.81 | 0.82 |
| | F1 Pass | 0.87 | 0.88 | 0.87 | 0.87 | 0.88 |
| | F1 Fail | 0.55 | 0.55 | 0.52 | 0.51 | 0.56 |
| **SVM** | Accuracy | 0.75 | 0.75 | 0.75 | 0.75 | 0.75 |
| | AUC | 0.38 | 0.4 | 0.4 | 0.4 | 0.45 |
| | F1 Pass | 0.86 | 0.86 | 0.86 | 0.86 | 0.86 |
| | F1 Fail | 0 | 0 | 0 | 0 | 0 |
| **ANN** | Accuracy | 0.76 | 0.75 | 0.75 | 0.75 | 0.75 |
| | AUC | 0.56 | 0.54 | 0.54 | 0.55 | 0.56 |
| | F1 Pass | 0.85 | 0.85 | 0.85 | 0.85 | 0.85 |
| | F1 Fail | 0.26 | 0.18 | 0.17 | 0.24 | 0.25 |

Table 26. Prediction optimization percentage of Feature Selection method

| ML Model | Metrics | % Optimization with Pearson Correlation | % Optimization with Boruta Method | % Optimization with Feature selection RF | % Optimization with Feature Selection CatBoost |
|---|---|---|---|---|---|
| **Random Forest** | Accuracy | 1% | 0% | 0% | 1% |
| | AUC | 0% | 11% | 9% | 12% |
| | F1 Pass | 0% | 0% | 0% | 1% |
| | F1 Fail | 4% | 2% | -2% | 8% |
| **CatBoost** | Accuracy | 1% | 0% | -1% | 1% |
| | AUC | 1% | 5% | 5% | 6% |
| | F1 Pass | 1% | 0% | 0% | 1% |
| | F1 Fail | 0% | -5% | -7% | 2% |
| **SVM** | Accuracy | 0% | 0% | 0% | 0% |
| | AUC | 5% | 5% | 5% | 18% |
| | F1 Pass | 0% | 0% | 0% | 0% |

| | | | | | |
|---|---|---|---|---|---|
| | F1 Fail | 0% | 0% | 0% | 0% |
| **ANN** | Accuracy | -1% | -1% | -1% | -1% |
| | AUC | -4% | -4% | -2% | 0% |
| | F1 Pass | 0% | 0% | 0% | 0% |
| | F1 Fail | -31% | -35% | -8% | -4% |

## 3.9 MACHINE LEARNING MODEL FOR POROSITY CLASSIFICATION

### 3.9.1 Imbalance problem

The results in Table 25 suggested an imbalance problem in the data set. That is defined as any dataset with an unequal distribution is technically imbalanced. It means the class imbalance happens when the number of examples in one class is lower than for the other classes. In addition, the proposed case of study presents overlapping or class separability, which means that the decision boundary is not clearly established [59]. Figure 61 shows the bar plot and the scatter plot that support the imbalance problem hypotheses for the dataset. To resolve this common problem, multiple techniques have been proposed, the most studied and common is the Undersampling Method. Random Undersampling is a non-heuristic method for balancing class distribution by removing majority class examples randomly to produce a balanced instance collection [62]. This method will be applied in this article to handle the imbalance problem of the dataset. Figure 62 presents the results of the Undersampling method in the dataset, according to the results a balanced dataset for the ML model is obtained by this method, the scatterplot suggests that this method increases the overlapping, therefore, further analysis should be done in future studies to reduce the overlapping problem for porosity classification.

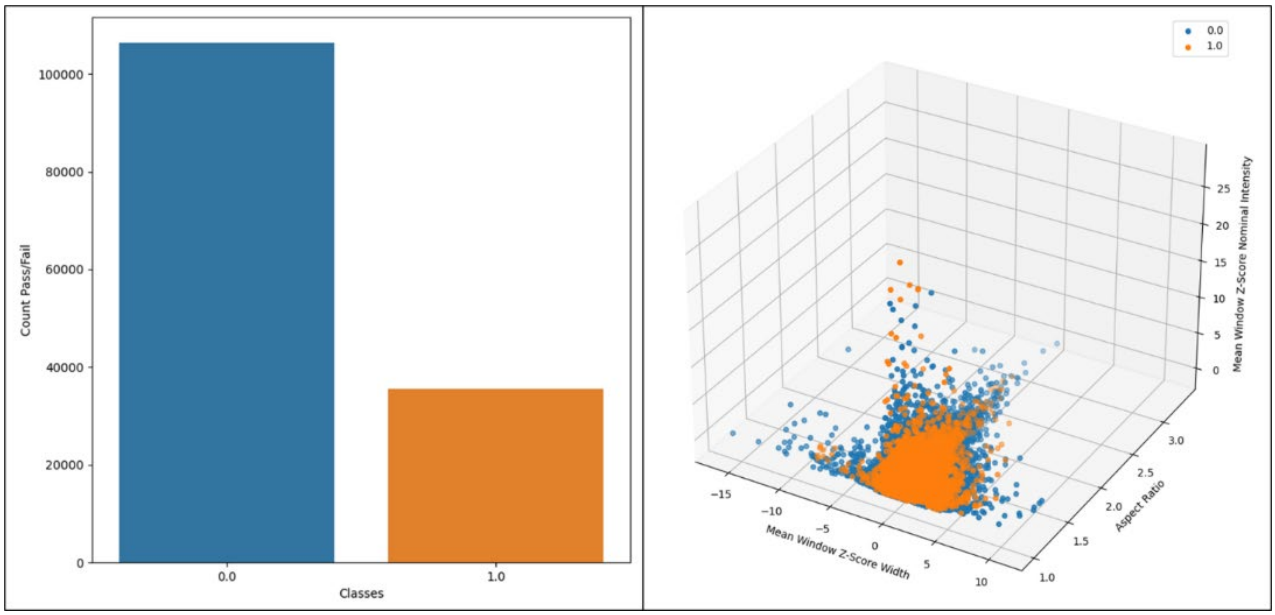


Figure 61. Imbalance problem in Dataset representation. Left, Bar plot. Right, 3D Scatterplot.

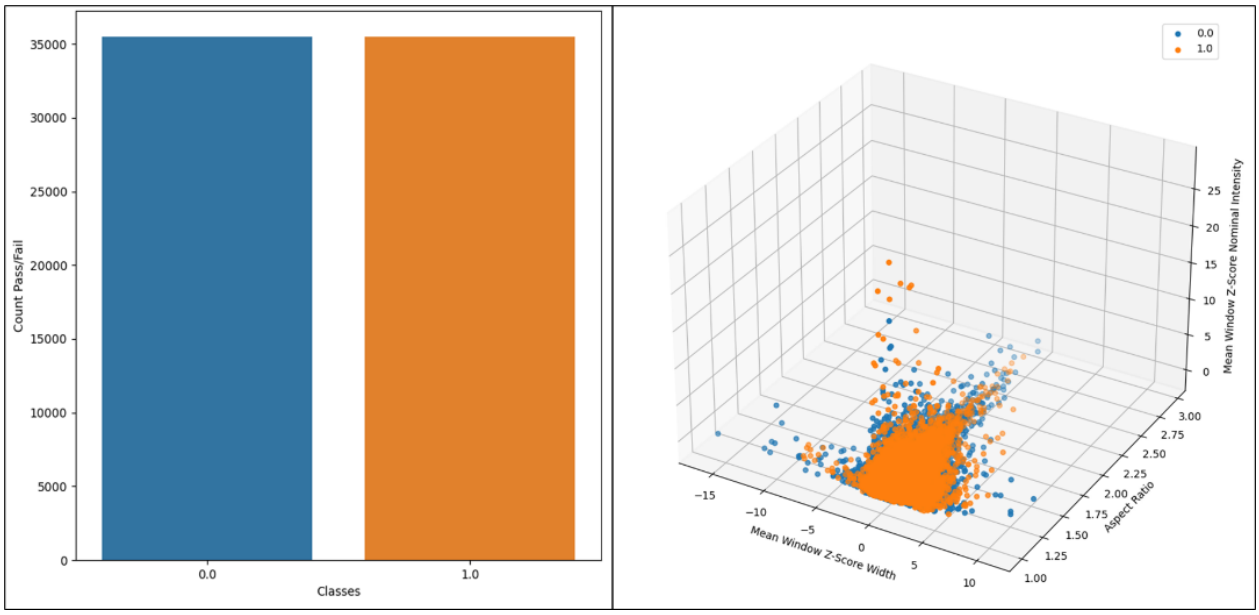


Figure 62. Balanced Dataset by Undersampling method representation. Left, Bar plot. Right, 3D Scatterplot.

### 3.9.2 Machine Learning classification model results

The Machine Learning algorithms for classification were performed based on the Imbalanced, Balanced dataset (see Figure 62) and previous results presented in Table 25 where the feature combination proposed by the CatBoost Feature importance model got the best results for all the proposed ML models. In Table 27 the metrics suggested by the literature and proposed in this research are calculated and analyzed to evaluate the best model to resolve the prediction of porosity problem based on the high-speed camera monitoring and features extraction results. Three scenarios are proposed to validate the method implemented in this study and make suggestions for future studies and research, the first scenario is defined without the application of the Undersampling method to resolve the imbalance problem, and the second one takes into consideration the Undersampling method but no feature selection, and the third scenario that gets the balanced dataset by the Undersampling method and the feature selection suggested by the results in Table 25 and Table 26, and an optimization percentage was calculated comparing thescenario with FS and Undersampling method applied, it with the aim to define the best ML to make classification for this research. According to the results for all the proposed models obtained an improvement in AUC value that indicates how strong is the prediction model to make future classification and is reported as the best metric to analyze a classification ML model. The highest AUC value was reported for RF with 0.83, with an accuracy of 75%, it represented a reduction in this metric of around 7% but made the model 12% stronger to predict (AUC) and with an increase in the F1 score for fail class (porosity) about 46%, that indicates that for RF the application of the proposed methodology in this research had an important improvement on the capacity of the extracted data by the monitoring process to make porosity predictions.

The CatBoost algorithm show an increase in an AUC value of 5% with a maximal result of 0.81 classified as a strong model for prediction, therefore is 5% stronger to predict porosities, with an accuracy of 74% that means a reduction of 8% and an increase of F1 score of 35%. Going from 0.55 to 0.74 means that the model improved by a 35% the capacity to predict the porosity in the welding setup. The SVM algorithm reported the lowest accuracy with 62% representing a reduction of 17% in this metric, for AUC the model gets strongest at around a 68%, going from

an AUC value of 0.38 to 0.64 passing from being a very poor performance closer to be a strong model to predict close to the 0.7 suggested threshold and with better performance to classify porosities going from an F1 score of 0 in fail to 0.65, this results and the improvement of AUC support the improvement in the performance of the model [48]. The ANN algorithm got the biggest evolution in F1 score for the Fail class (porosity) at 127%, with an increase of 14% in AUC and a reduction of 16% in accuracy going from 76% to 64%. According to the results, the best ML algorithm to make the porosity prediction using high-speed camera monitoring was Random Forest with a 75% accuracy, 0.83 in AUC, 0.75 in F1 score for pass (no porosity), and a 0.76 in F1 score for fail (porosity). To improve the accuracy of the model further methods to resolve the imbalance might be explored and optimization methods for the ML algorithms should be studied for future research.

Table 27. Metrics results of Machine Learning models for porosity prediction.

| ML Model | Metrics | Imbalanced Dataset No Feature Selection | Balanced Data Set No Feature Selection | Balanced Data Set with Feature Selection | % Optimization ML and FS techniques |
|---|---|---|---|---|---|
| **Random Forest** | Accuracy | 0.81 | 0.74 | 0.75 | -7% |
| | AUC | 0.74 | 0.81 | 0.83 | 12% |
| | F1 Pass | 0.88 | 0.73 | 0.75 | -15% |
| | F1 Fail | 0.52 | 0.74 | 0.76 | 46% |
| **CatBoost** | Accuracy | 0.8 | 0.73 | 0.74 | -8% |
| | AUC | 0.77 | 0.8 | 0.81 | 5% |
| | F1 Pass | 0.87 | 0.73 | 0.73 | -16% |
| | F1 Fail | 0.55 | 0.74 | 0.74 | 35% |
| **SVM** | Accuracy | 0.75 | 0.54 | 0.62 | -17% |
| | AUC | 0.38 | 0.6 | 0.64 | 68% |
| | F1 Pass | 0.86 | 0.3 | 0.58 | -33% |
| | F1 Fail | 0 | 0.66 | 0.65 | N/A |
| **ANN** | Accuracy | 0.76 | 0.63 | 0.64 | -16% |
| | AUC | 0.56 | 0.63 | 0.64 | 14% |
| | F1 Pass | 0.85 | 0.64 | 0.68 | -20% |
| | F1 Fail | 0.26 | 0.62 | 0.59 | 127% |

## 3.10 CONCLUSIONS

Machine Learning Classification model for Porosity prediction in Laser welding with a high-speed camera at 10.000 frames/sec and a 1 mm section X-ray analysis is performed to analyze the impact of the features in prediction and get one approach about the features selection method, feature combination and ML model that may be applied in industrial applications to make the quality control for porosity in Aluminum alloys to make the quality control for porosity in aluminum alloys. The findings and conclusions are summarized as follows:

- The proposed methodology gives a closer approach to industrial applications where low quantities of defects are expected and real-time monitoring can help to make on-time decisions to improve the quality of the final product. The application of the suggested workflow and methods improved the metric results for all the ML algorithms implemented in this research, getting a maximal improvement of 127% for the F1 score for Fail class (porosity) in ANN, a maximal increase of AUC parameter for SVM of 68% and increasing the F1 score for Fail class from 0 to 0.65.

- The results of this study shown and suggest that monitoring the geometrical and optical welding parameters get features that are good predictors for porosity with Machine Learning Models.

- The implementation of feature selection improves the metrics results of the proposed Machine Learning algorithms, finding that the most performant method was the feature importance evaluation by CatBoost.

- The dataset was imbalanced, it reduced the capacity of the algorithms to predict the class with lower presence in the dataset affecting the classification implementation in real applications, solving this problem was an important stage to assure the best performance possible for the Machine Learning model.

- According to the calculated metrics suggested by the literature and evaluated in this work, the best Machine Learning algorithm to resolve the prediction of porosity problems based

on high-speed camera monitoring is the Random Forest with an accuracy of 75%, AUC 0.83, an F1 score for Pass (no porosity) of 0.75 and F1 score for Fail class of 0.76.

- To improve the Accuracy of the model, ML algorithm performance should be optimized, and different imbalance problem resolution techniques should be explored and analyzed in future research.

## 3.11 REFERENCES


[1] X. Wang, X. Zhou, Z. Xia, and X. Gu, "A survey of welding robot intelligent path optimization," *Journal of Manufacturing Processes*, no. December 2019, pp. 0–1, 2020, doi: 10.1016/j.jmapro.2020.04.085.

[2] J. Klæstrup Kristensen, "Applications of laser welding in the shipbuilding industry," *Handbook of Laser Welding Technologies*, pp. 596–612, 2013, doi: 10.1533/9780857098771.4.596.

[3] M. Graudenz and M. Baur, "Applications of laser welding in the automotive industry," *Handbook of Laser Welding Technologies*, pp. 555–574, 2013, doi: 10.1533/9780857098771.4.555.

[4] S. Katayama, *Defect formation mechanisms and preventive procedures in laser welding*. 2013. doi: 10.1533/9780857098771.2.332.

[5] S. Katayama, *Introduction: Fundamentals of laser welding*, vol. 9, no. 2012. Woodhead Publishing Limited, 2013. doi: 10.1533/9780857098771.1.3.

[6] X. Gao, Y. Sun, D. You, Z. Xiao, and X. Chen, "Multi-sensor information fusion for monitoring disk laser welding," *International Journal of Advanced Manufacturing Technology*, vol. 85, no. 5–8, pp. 1167–1175, Jul. 2016, doi: 10.1007/s00170-015-8032-z.

[7] S. J. Na and W. I. Cho, *Developments in modelling and simulation of laser and hybrid laser welding*. 2013. doi: 10.1533/9780857098771.3.522.

[8] J. Günther, P. M. Pilarski, G. Helfrich, H. Shen, and K. Diepold, “Intelligent laser welding through representation, prediction, and control learning: An architecture with deep neural networks and reinforcement learning,” *Mechatronics*, vol. 34, pp. 1–11, Mar. 2016, doi: 10.1016/j.mechatronics.2015.09.004.

[9] R. Lin, H. ping Wang, F. Lu, J. Solomon, and B. E. Carlson, “Numerical study of keyhole dynamics and keyhole-induced porosity formation in remote laser welding of Al alloys,” *International Journal of Heat and Mass Transfer*, vol. 108, pp. 244–256, May 2017, doi: 10.1016/j.ijheatmasstransfer.2016.12.019.

[10] J. Günther, P. M. Pilarski, G. Helfrich, H. Shen, and K. Diepold, “Intelligent laser welding through representation, prediction, and control learning: An architecture with deep neural networks and reinforcement learning,” *Mechatronics*, vol. 34, pp. 1–11, Mar. 2016, doi: 10.1016/j.mechatronics.2015.09.004.

[11] BMS College of Engineering. Department of Information Science and Engineering, BMS College of Engineering. Department of Computer Science and Engineering, BMS College of Engineering. Department of Computer Applications, and Institute of Electrical and Electronics Engineers., *Souvenir of the 2015 IEEE International Advance Computing Conference (IACC) : June 12-13, 2015 : B.M.S. College of Engineering, Bangalore, India*.

[12] D. Ma, P. Jiang, L. Shu, and S. Geng, “Multi-sensing signals diagnosis and CNN-based detection of porosity defect during Al alloys laser welding,” *Journal of Manufacturing Systems*, vol. 62, pp. 334–346, Jan. 2022, doi: 10.1016/j.jmsy.2021.12.004.

[13] D. Petković, “Prediction of laser welding quality by computational intelligence approaches,” *Optik (Stuttg)*, vol. 140, pp. 597–600, Jul. 2017, doi: 10.1016/j.ijleo.2017.04.088.

[14] Institute of Electrical and Electronics Engineers, Friedrich-Alexander-Universität Erlangen-Nürnberg, IEEE Power Engineering Society, IEEE Industry Applications Society, and Süddeutscher Verlag Veranstaltungen GmbH*8 2018*, *th International Electric Drives Production Conference (EDPC) : proceedings : 4 and 5 December 2018, Schweinfurt, Germany*.

[15] S. Q. Moinuddin, S. S. Hameed, A. K. Dewangan, K. Ramesh Kumar, and A. Shanta Kumari, "A study on weld defects classification in gas metal arc welding process using machine learning techniques," in *Materials Today: Proceedings*, 2020, vol. 43, pp. 623–628. doi: 10.1016/j.matpr.2020.12.159.

[16] C. P. Bergmann and S. Katayama, "Topics in Mining, Metallurgy and Materials Engineering Series Editor: Fundamentals and Details of Laser Welding." [Online]. Available: http://www.springer.com/series/11054

[17] Z. Zhang, B. Li, W. Zhang, R. Lu, S. Wada, and Y. Zhang, "Real-time penetration state monitoring using convolutional neural network for laser welding of tailor rolled blanks," *Journal of Manufacturing Systems*, vol. 54, no. January, pp. 348–360, 2020, doi: 10.1016/j.jmsy.2020.01.006.

[18] J. Chen, T. Wang, X. Gao, and L. Wei, "Real-time monitoring of high-power disk laser welding based on support vector machine," *Computers in Industry*, vol. 94, pp. 75–81, 2018, doi: 10.1016/j.compind.2017.10.003.

[19] Z. Wang, J. P. Oliveira, Z. Zeng, X. Bu, B. Peng, and X. Shao, "Laser beam oscillating welding of 5A06 aluminum alloys: Microstructure, porosity and mechanical properties," *Optics and Laser Technology*, vol. 111, no. September 2018, pp. 58–65, 2019, doi: 10.1016/j.optlastec.2018.09.036.

[20] K. Hao, G. Li, M. Gao, and X. Zeng, "Weld formation mechanism of fiber laser oscillating welding of austenitic stainless steel," *Journal of Materials Processing Technology*, vol. 225, pp. 77–83, 2015, doi: 10.1016/j.jmatprotec.2015.05.021.

[21] P. Horník, H. Šebestová, J. Novotný, and L. Mrňa, "Visualization of laser back-reflection distribution during laser welding," *IOP Conference Series: Materials Science and Engineering*, vol. 1135, no. 1, p. 012015, Nov. 2021, doi: 10.1088/1757-899x/1135/1/012015.

[22] D. You, X. Gao, and S. Katayama, "Multiple-optics sensing of high-brightness disk laser welding process," *NDT and E International*, vol. 60, pp. 32–39, 2013, doi: 10.1016/j.ndteint.2013.07.005.

[23] S. Scott and S. Matwin, “Feature Engineering for Text Classification.” [Online]. Available: http://ai.iit.nrc.ca/II_public/Classification/resources.html.

[24] V. Bolón-Canedo, N. Sánchez-Maroño, and A. Alonso-Betanzos, “Feature selection and classification in multiple class datasets: An application to KDD Cup 99 dataset,” *Expert Systems with Applications*, vol. 38, no. 5, pp. 5947–5957, May 2011, doi: 10.1016/j.eswa.2010.11.028.

[25] R. C. Chen, C. Dewi, S. W. Huang, and R. E. Caraka, “Selecting critical features for data classification based on machine learning methods,” *Journal of Big Data*, vol. 7, no. 1, Dec. 2020, doi: 10.1186/s40537-020-00327-4.

[26] S. Gopal, K. Patro, and K. Kumar Sahu, “Normalization: A Preprocessing Stage.” [Online]. Available: www.kiplinger.com,

[27] IEEE Electron Devices Society, Institute of Electrical and Electronics Engineers, and Vaigai College of Engineering, *Proceeding of the 2018 International Conference on Intelligent Computing and Control Systems (ICICCS) : June 14-15, 2018*.

[28] D. Ma, L. Shu, Q. Zhou, S. Cao, and P. Jiang, “Online porosity defect detection based on convolutional neural network for Al alloy laser welding,” in *Journal of Physics: Conference Series*, Apr. 2021, vol. 1884, no. 1. doi: 10.1088/1742-6596/1884/1/012008.

[29] S. Pang, W. Chen, and W. Wang, “A quantitative model of keyhole instability induced porosity in laser welding of titanium alloy,” *Metallurgical and Materials Transactions A: Physical Metallurgy and Materials Science*, vol. 45, no. 6, pp. 2808–2818, 2014, doi: 10.1007/s11661-014-2231-3.

[30] N. Seto, S. Katayama, and A. Matsunawa, “High-speed simultaneous observation of plasma and keyhole behavior during high power CO2 laser welding: Effect of shielding gas on porosity formation,” *Journal of Laser Applications*, vol. 12, no. 6, pp. 245–250, Dec. 2000, doi: 10.2351/1.1324717.

[31] S. B. Kotsiantis, I. D. Zaharakis, and P. E. Pintelas, “Machine learning: A review of classification and combining techniques,” *Artificial Intelligence Review*, vol. 26, no. 3, pp. 159–190, Nov. 2006, doi: 10.1007/s10462-007-9052-3.

[32] M. Grandini, E. Bagli, and G. Visani, “Metrics for Multi-Class Classification: an Overview,” Aug. 2020, [Online]. Available: http://arxiv.org/abs/2008.05756

[33] A. E. Maxwell, T. A. Warner, and F. Fang, “Implementation of machine-learning classification in remote sensing: An applied review,” *International Journal of Remote Sensing*, vol. 39, no. 9. Taylor and Francis Ltd., pp. 2784–2817, May 03, 2018. doi: 10.1080/01431161.2018.1433343.

[34] R. Sharda, S. Voß, and S. Suthaharan, “Integrated Series in Information Systems 36 Machine Learning Models and Algorithms for Big Data Classifi cation Thinking with Examples for Eff ective Learning.” [Online]. Available: http://www.springer.com/series/6157

[35] I. Nunes *et al.*, “Artificial Neural Networks A Practical Course.”

[36] “Lecture Notes in Artificial Intelligence.”

[37] R. Sharda, S. Voß, and S. Suthaharan, “Integrated Series in Information Systems 36 Machine Learning Models and Algorithms for Big Data Classifi cation Thinking with Examples for Eff ective Learning.” [Online]. Available: http://www.springer.com/series/6157

[38] B. Xu, N. Wang, T. Chen, and M. Li, “Empirical Evaluation of Rectified Activations in Convolutional Network,” May 2015, [Online]. Available: http://arxiv.org/abs/1505.00853

[39] A. Prinzie and D. van den Poel, “Random Forests for multiclass classification: Random MultiNomial Logit,” *Expert Systems with Applications*, vol. 34, no. 3, pp. 1721–1732, Apr. 2008, doi: 10.1016/j.eswa.2007.01.029.

[40] Institute of Electrical and Electronics Engineers, IEEE International Conference on Computer Vision 11 2007.10.14-21 Rio de Janeiro, and ICCV 11 2007.10.14-21 Rio de Janeiro, *IEEE 11th International Conference on Computer Vision, 2007 ICCV 2007 ; 14-21 Oct. 2007, Rio de Janeiro, Brazil*.

[41] A. D. Kulkarni and B. Lowe, “Random Forest Algorithm for Land Cover Classification International Journal on Recent and Innovation Trends in Computing and Communication Random Forest Algorithm for Land Cover Classification,” 2016, [Online]. Available: http://hdl.handle.net/10950/341http://www.ijritcc.org

[42] S. ben Jabeur, C. Gharib, S. Mefteh-Wali, and W. ben Arfi, “CatBoost model and artificial intelligence techniques for corporate failure prediction,” *Technological Forecasting and Social Change*, vol. 166, May 2021, doi: 10.1016/j.techfore.2021.120658.

[43] A. V. Dorogush, V. Ershov, and A. G. Yandex, “CatBoost: gradient boosting with categorical features support.” [Online]. Available: https://github.com/Microsoft/LightGBM

[44] M. Ikonomakis, S. Kotsiantis, and V. Tampakas, “Text Classification Using Machine Learning Techniques.”

[45] J. Li *et al.*, “Machine Learning for Patient-Specific Quality Assurance of VMAT: Prediction and Classification Accuracy,” *International Journal of Radiation Oncology Biology Physics*, vol. 105, no. 4, pp. 893–902, Nov. 2019, doi: 10.1016/j.ijrobp.2019.07.049.

[46] A. M. Carrington *et al.*, “Deep ROC Analysis and AUC as Balanced Average Accuracy to Improve Model Selection, Understanding and Interpretation,” Mar. 2021, doi: 10.1109/TPAMI.2022.3145392.

[47] “Lecture Notes in Artificial Intelligence Subseries of Lecture Notes in Computer Science.”

[48] D. W. , L. S. , & S. R. X. Hosmer Jr, “Applied logistic regression,” vol. 398, 2013.

[49] S. il Pak and T. H. Oh, “Correlation and simple linear regression,” *Journal of Veterinary Clinics*, vol. 27, no. 4, pp. 427–434, 2010, doi: 10.1007/978-3-319-89993-0_6.

[50] N. J. Gogtay and U. M. Thatte, “Principles of correlation analysis,” *Journal of Association of Physicians of India*, vol. 65, no. MARCH, pp. 78–81, 2017.

[51] MathWorks, “Specialization Practical Data sicence with Matlab.”

[52] L. Wang, M. Gao, C. Zhang, and X. Zeng, “Effect of beam oscillating pattern on weld characterization of laser welding of AA6061-T6 aluminum alloy,” *Materials and Design*, vol. 108, pp. 707–717, Oct. 2016, doi: 10.1016/j.matdes.2016.07.053.

[53] M. B. Kursa and W. R. Rudnicki, “Feature Selection with the Boruta Package,” 2010. [Online]. Available: http://www.jstatsoft.org/

[54] M. B. Kursa, A. Jankowski, and W. R. Rudnicki, “Boruta - A system for feature selection,” *Fundamenta Informaticae*, vol. 101, no. 4, pp. 271–285, 2010, doi: 10.3233/FI-2010-288.

[55] R. Tang and X. Zhang, “CART Decision Tree Combined with Boruta Feature Selection for Medical Data Classification,” in *2020 5th IEEE International Conference on Big Data Analytics, ICBDA 2020*, May 2020, pp. 80–84. doi: 10.1109/ICBDA49040.2020.9101199.

[56] R. C. Chen, C. Dewi, S. W. Huang, and R. E. Caraka, “Selecting critical features for data classification based on machine learning methods,” *Journal of Big Data*, vol. 7, no. 1, Dec. 2020, doi: 10.1186/s40537-020-00327-4.

[57] A. Zien, N. Krämer, S. Sonnenburg, and G. Rätsch, “LNAI 5782 - The Feature Importance Ranking Measure.”

[58] R. Goebel, W. Wahlster, and J. Siekmann, “Lecture Notes in Artificial Intelligence 9851 Subseries of Lecture Notes in Computer Science LNAI Series Editors LNAI Founding Series Editor.” [Online]. Available: http://www.springer.com/series/1244

[59] A. Salvadorrgarcíaa, M. R. Pratii, and B. Franciscooherrera, “Learning from Imbalanced Data Sets.”

[60] C. Huang, Y. Li, C. C. Loy, and X. Tang, “Learning deep representation for imbalanced classification,” in *Proceedings of the IEEE Computer Society Conference on Computer Vision and Pattern Recognition*, Dec. 2016, vol. 2016-December, pp. 5375–5384. doi: 10.1109/CVPR.2016.580.

[61] M. Tripathi, “Understanding Imbalanced Datasets and techniques for handling them,” 2015.

[62] A. Salvadorrgarcíaa, M. R. Pratii, and B. Franciscooherrera, “Learning from Imbalanced Data Sets.”

# CONCLUSION GÉNÉRALE

L'application du procédé de soudage au laser est un domaine en pleine expansion dans les industries. Les systèmes de surveillance constituent un défi lorsqu'il s'agit de la mise en œuvre, de l'optimisation des paramètres du procédé et du contrôle de la qualité du produit final. Le procédé de soudage au laser offre des avantages importants pour les industries, notamment une petite zone affectée par la chaleur qui réduit la distorsion géométrique, une grande efficacité énergétique et une vitesse de soudage plus élevée par rapport aux méthodes de soudage conventionnelles, mais c'est néanmoins un procédé complexe en raison des phénomènes physiques impliqués et des difficultés de surveillance et de contrôle. Pour cette raison, l'étude et la définition des méthodes et des technologies de surveillance est un sujet très important pour le développement de solutions fiables et robustes. L'évolution technologique récente de l'industrie 4.0 propose des outils pertinents pour résoudre les problèmes que pose la surveillance et le contrôle des paramètres du procédé. La mise en œuvre d'algorithmes d'apprentissage automatique et de solutions d'intelligence artificielle peut garantir la meilleure qualité de produit et une utilisation plus efficace des matières premières et des ressources dans des applications réelles. Dans le cadre de ce projet, une revue de la littérature sur les configurations de détection, les techniques et technologies de surveillance, la surveillance intelligente et les algorithmes appliqués au procédé de soudage laser a été réalisée, étudiée et présentée pour une approche de l'industrie 4.0. Ce projet propose des orientations technologiques susceptibles d’apporter des réponses pratiques pour l’industrie et présente les méthodes les plus efficaces pour la surveillance en ligne dans les applications de soudage au laser. En outre, un flux de travail de surveillance est décrit et présenté en détail, qui peut être appliqué comme un guide pratique aux applications réelles pour la recherche et le développement industriel.

Le soudage au laser d'un alliage d'aluminium (Al 5052), un procédé de formage automatique et une procédure d'inspection automatique de la distorsion en 3D ont été réalisés pour analyser les effets des paramètres du procédé de soudage sur les valeurs de distorsion totale des flans soudés et proposer une approche pour le contrôle automatique de la distorsion basée sur les principes du *Cloud Manufacturing*. Ce modèle peut être reproduit et étendu à d'autres applications industrielles, dans le but de contrôler et de réduire les défauts de distorsion sur les flancs formés par soudage au laser. Les résultats suggèrent que l'amplitude au soudage a la plus grande contribution à la valeur totale de la distorsion dans la direction de soudage. Ceci est associé à l'impact élevé que ce paramètre a sur l'apport de chaleur dans le procédé de soudage au laser. L'interaction entre la puissance et la vitesse présente l'effet le plus significatif statistiquement sur la valeur totale de la distorsion dans la direction de soudage. Une distorsion angulaire est constatée également dans les résultats du profil évalué par le processus de mesure automatique 3D, et dans cette direction, l'apport de chaleur est associé à des valeurs de puissance élevées et à sa combinaison avec la vitesse. Les résultats de la distorsion de formage ont montré que la vitesse est le paramètre ayant la plus grande signification statistique pour la distorsion dans la direction de soudage. Les taux de distorsion maximaux sont atteints à des valeurs de vitesse élevées et les taux minimaux à des valeurs de vitesse faibles. L'interaction entre la puissance et la vitesse a aussi l'effet le plus élevé sur la distorsion géométrique de la pièce formée dans la direction de soudage. Cette analyse a permis d'identifier une configuration optimisée. La valeur minimale pour la distorsion géométrique des plaques soudées est atteinte à une puissance de 2,0 kW, une vitesse de 30,5 mm/s et une amplitude de 0,75 mm pour l'amplitude. Pour les plaques embouties dans la distorsion de formage, la configuration optimisée est obtenue à 2,0 kW pour la puissance, 30 mm/s pour la vitesse et 1,0 mm pour l'amplitude.

Un modèle de classification par apprentissage automatique pour la prédiction de la porosité dans le soudage au laser avec une caméra à haute vitesse à 10 000 images/seconde et une analyse aux rayons X d'une section de 1 mm est réalisé pour évaluer l'impact des paramètres sur la qualité de la prédiction et développer une méthode pour les sélectionner. Cela a permis d'identifier la combinaison la plus performante et le modèle ML qui peut être

appliqué dans l'industrie pour faire le contrôle de qualité de la porosité dans les alliages d'aluminium. La méthode la plus performante est l'évaluation de l'importance par l'algorithme *CatBoost*. Pour résoudre le problème d'*Imblance* qui réduit la capacité des algorithmes à prédire la classe avec une présence plus faible dans l'ensemble de données, la méthode d'*Undersampling* a été appliquée et le *Random Forest* est le algorithme ML le plus performant pour faire la classification de la porosité avec une précision de 75 %, une AUC de 0,83, un score F1 pour la classe Pass (pas de porosité) de 0,75 et un score F1 pour la classe Fail (porosité) de 0,76. L'application du modèle proposé a amélioré la capacité de prédire la porosité avec Random Forest à 12 % pour le AUC et à 46 % pour le F1 de cette classe.

## RECOMMANDATIONS POUR LES TRAVAUX FUTURS

- La transition numérique a accéléré l'utilisation de techniques et de méthodes de surveillance, de contrôle, de prédiction et d'optimisation intelligentes. En conséquence, étudier la mise en œuvre de *Cloud Manufacturing* et de possibles technologies qui puissent être appliquées au soudage laser gagne en importance pour l'avenir.

- Pour améliorer la performance de l'utilisation de la méthode de surveillance et de contrôle de la distorsion géométrique, il faudrait adapter les systèmes robotisés pour le processus de scanning 3D.

- L'analyse ANOVA de la distorsion géométrique ouvre la fenêtre pour l'utilisation de systèmes d'apprentissage automatique et d'intelligence artificielle pour faire la classification et la prédiction de la qualité.

- Pour améliorer la précision du modèle de classification et la prédiction de la porosité, la performance de l'algorithme ML devrait être optimisée et différentes techniques de résolution des problèmes de déséquilibre devraient être explorées et analysées dans les recherches futures.

## RÉFÉRENCES BIBLIOGRAPHIQUES


A. A. Ghafar and A. B. Abdullah, “Pre-Forming Inspection System to Detect Deep Drawing Defect Due to Punch-Die Misalignment using Image Processing Technique,” in *IOP Conference Series: Materials Science and Engineering*, 2019, vol. 530, no. 1. doi: 10.1088/1757-899X/530/1/012015.

A. A. Weckenmann, P. Gall, and A. Gabbia, “3D surface coordinate inspection of formed sheet material parts using optical measurement systems and virtual distortion compensation,” in *Eighth International Symposium on Laser Metrology*, Feb. 2005, vol. 5776, p. 640. doi: 10.1117/12.611842.

A. Aminzadeh, S. Sattarpanah Karganroudi, N. Barka, and A. el Ouafi, “A real-time 3D scanning of aluminum 5052-H32 laser welded blanks; geometrical and welding characterization,” *Materials Letters*, vol. 296, Aug. 2021, doi: 10.1016/j.matlet.2021.129883.

A. C. Popescu, C. Delval, and M. Leparoux, “Control of porosity and spatter in laser welding of thick AlMg5 parts using high-speed imaging and optical microscopy,” *Metals (Basel)*, vol. 7, no. 11, Nov. 2017, doi: 10.3390/met7110452.

A. D. Kulkarni and B. Lowe, “Random Forest Algorithm for Land Cover Classification International Journal on Recent and Innovation Trends in Computing and Communication Random Forest Algorithm for Land Cover Classification,” 2016, [Online]. Available: http://hdl.handle.net/10950/341http://www.ijritcc.org

A. E. Maxwell, T. A. Warner, and F. Fang, “Implementation of machine-learning classification in remote sensing: An applied review,” *International Journal of Remote Sensing*, vol. 39, no. 9. Taylor and Francis Ltd., pp. 2784–2817, May 03, 2018. doi: 10.1080/01431161.2018.1433343.

A. Fernández Villán *et al.*, “Low-cost system for weld tracking based on artificial vision,” *IEEE Transactions on Industry Applications*, vol. 47, no. 3, pp. 1159–1167, May 2011, doi: 10.1109/TIA.2011.2124432.

A. Giampieri, J. Ling-Chin, Z. Ma, A. Smallbone, and A. P. Roskilly, “A review of the current automotive manufacturing practice from an energy perspective,” *Applied Energy*, vol. 261. Elsevier Ltd, Mar. 01, 2020. doi: 10.1016/j.apenergy.2019.114074.

A. Giampieri, J. Ling-Chin, Z. Ma, A. Smallbone, and A. P. Roskilly, “A review of the current automotive manufacturing practice from an energy perspective,” *Applied Energy*, vol. 261. Elsevier Ltd, Mar. 01, 2020. doi: 10.1016/j.apenergy.2019.114074.

A. Gorkič, M. Jezeršek, J. Možina, and J. Diaci, “Measurement of weldpiece distortion during pulsed laser welding using rapid laser profilometry,” *Science and Technology of Welding and Joining*, vol. 11, no. 1, pp. 48–56, Feb. 2006, doi: 10.1179/174329306X77065.

A. Lisiecki, “Diode laser welding of high yield steel,” in *Laser Technology 2012: Applications of Lasers*, Jan. 2013, vol. 8703, p. 87030S. doi: 10.1117/12.2013429.

A. M. Carrington *et al.*, “Deep ROC Analysis and AUC as Balanced Average Accuracy to Improve Model Selection, Understanding and Interpretation,” Mar. 2021, doi: 10.1109/TPAMI.2022.3145392.

A. Magalhães, J. de Backer, and G. Bolmsjö, “Thermal dissipation effect on temperature-controlled friction stir welding,” *Soldagem e Inspecao*, vol. 24, 2019, doi: 10.1590/0104-9224/SI24.28.

A. N. Bakhtiyari, Z. Wang, L. Wang, and H. Zheng, “A review on applications of artificial intelligence in modeling and optimization of laser beam machining,” *Optics and Laser Technology*, vol. 135. Elsevier Ltd, Mar. 01, 2021. doi: 10.1016/j.optlastec.2020.106721.

A. Prinzie and D. van den Poel, “Random Forests for multiclass classification: Random MultiNomial Logit,” *Expert Systems with Applications*, vol. 34, no. 3, pp. 1721–1732, Apr. 2008, doi: 10.1016/j.eswa.2007.01.029.

A. Salvadorrgarcíaa, M. R. Pratii, and B. Franciscooherrera, “Learning from Imbalanced Data Sets.”

A. Salvadorrgarcíaa, M. R. Pratii, and B. Franciscooherrera, “Learning from Imbalanced Data Sets.”

A. V. Dorogush, V. Ershov, and A. G. Yandex, “CatBoost: gradient boosting with categorical features support.” [Online]. Available: https://github.com/Microsoft/LightGBM

A. Zien, N. Krämer, S. Sonnenburg, and G. Rätsch, “LNAI 5782 - The Feature Importance Ranking Measure.”

B. J. Simonds, B. Tran, and P. A. Williams, “In situ monitoring of Cu/Al laser welding using Laser Induced Fluorescence,” *Procedia CIRP*, vol. 94, pp. 605–609, 2020, doi: 10.1016/j.procir.2020.09.088.

B. J. Simonds, B. Tran, and P. A. Williams, “In situ monitoring of Cu/Al laser welding using Laser Induced Fluorescence,” *Procedia CIRP*, vol. 94, pp. 605–609, 2020, doi: 10.1016/j.procir.2020.09.088.

B. Kinsey, Z. Liu, and J. Cao, “A novel forming technology for tailor-welded blanks.”

B. Kumar, S. Bag, and C. P. Paul, “Influence of heat input on welding induced distortion for Yb-fibre laser welded thin sheets,” in *Materials Today: Proceedings*, 2019, vol. 26, pp. 2040–2046. doi: 10.1016/j.matpr.2020.02.442.

B. Wang, S. J. Hu, L. Sun, and T. Freiheit, “Intelligent welding system technologies: State-of-the-art review and perspectives,” *Journal of Manufacturing Systems*, vol. 56, no. July, pp. 373–391, 2020, doi: 10.1016/j.jmsy.2020.06.020.

B. Xu, N. Wang, T. Chen, and M. Li, “Empirical Evaluation of Rectified Activations in Convolutional Network,” May 2015, [Online]. Available: http://arxiv.org/abs/1505.00853

BMS College of Engineering. Department of Information Science and Engineering, BMS College of Engineering. Department of Computer Science and Engineering, BMS College of Engineering. Department of Computer Applications, and Institute of Electrical and Electronics Engineers., *Souvenir of the 2015 IEEE International Advance Computing Conference (IACC) : June 12-13, 2015 : B.M.S. College of Engineering, Bangalore, India*.

C. Hagenlocher *et al.*, "The influence of residual stresses on laser beam welding processes of aluminium sheets," in *Procedia CIRP*, 2020, vol. 94, pp. 713–717. doi: 10.1016/j.procir.2020.09.124.

C. Huang, Y. Li, C. C. Loy, and X. Tang, "Learning deep representation for imbalanced classification," in *Proceedings of the IEEE Computer Society Conference on Computer Vision and Pattern Recognition*, Dec. 2016, vol. 2016-December, pp. 5375–5384. doi: 10.1109/CVPR.2016.580.

C. Knaak, U. Thombansen, P. Abels, and M. Kröger, "Machine learning as a comparative tool to determine the relevance of signal features in laser welding," *Procedia CIRP*, vol. 74, pp. 623–627, 2018, doi: 10.1016/j.procir.2018.08.073.

C. L. Tsai and D. S. Kim, "Understanding residual stress and distortion in welds: An overview," in *Processes and Mechanisms of Welding Residual Stress and Distortion*, Elsevier Ltd., 2005, pp. 3–31. doi: 10.1533/9781845690939.1.3.

C. L. Tsai and D. S. Kim, *Understanding residual stress and distortion in welds: An overview*. Woodhead Publishing Limited, 2005. doi: 10.1533/9781845690939.1.3.

C. P. Bergmann and S. Katayama, "Topics in Mining, Metallurgy and Materials Engineering Series Editor: Fundamentals and Details of Laser Welding." [Online]. Available: http://www.springer.com/series/11054

C. The and M. Oldenburg, *Encyclopedia of Thermal Stresses*. 2014. doi: 10.1007/978-94-007-2739-7.

D. Chen *et al.*, “Research on in situ monitoring of selective laser melting: a state of the art review”, doi: 10.1007/s00170-020-06432-1/Published.

D. Colombo, B. M. Colosimo, and B. Previtali, “Comparison of methods for data analysis in the remote monitoring of remote laser welding,” *Optics and Lasers in Engineering*, vol. 51, no. 1, pp. 34–46, Jan. 2013, doi: 10.1016/j.optlaseng.2012.07.022.

D. F. Farson, K. S. Fang, and J. Kern, “Intelligent laser welding control,” in *LIA (Laser Institute of America)*, 1992, vol. 74, pp. 104–112. doi: 10.2351/1.5058430.

D. K. Koli, G. Agnihotri, and R. Purohit, “Advanced Aluminium Matrix Composites: The Critical Need of Automotive and Aerospace Engineering Fields,” in *Materials Today: Proceedings*, 2015, vol. 2, no. 4–5, pp. 3032–3041. doi: 10.1016/j.matpr.2015.07.290.

D. Ma, L. Shu, Q. Zhou, S. Cao, and P. Jiang, “Online porosity defect detection based on convolutional neural network for Al alloy laser welding,” in *Journal of Physics: Conference Series*, Apr. 2021, vol. 1884, no. 1. doi: 10.1088/1742-6596/1884/1/012008.

D. Ma, P. Jiang, L. Shu, and S. Geng, “Multi-sensing signals diagnosis and CNN-based detection of porosity defect during Al alloys laser welding,” *Journal of Manufacturing Systems*, vol. 62, pp. 334–346, Jan. 2022, doi: 10.1016/j.jmsy.2021.12.004.

D. Petković, “Prediction of laser welding quality by computational intelligence approaches,” *Optik (Stuttg)*, vol. 140, pp. 597–600, Jul. 2017, doi: 10.1016/j.ijleo.2017.04.088.

D. W. , L. S. , & S. R. X. Hosmer Jr, “Applied logistic regression,” vol. 398, 2013.

D. Y. You, X. D. Gao, and S. Katayama, “Review of laser welding monitoring,” *Science and Technology of Welding and Joining*, vol. 19, no. 3, pp. 181–201, 2014, doi: 10.1179/1362171813Y.0000000180.

D. You, X. Gao, and S. Katayama, “Multiple-optics sensing of high-brightness disk laser welding process,” *NDT and E International*, vol. 60, pp. 32–39, 2013, doi: 10.1016/j.ndteint.2013.07.005.

E. A. Starke, “Alloys: Aluminum.”

E. Georgantzia, M. Gkantou, and G. S. Kamaris, “Aluminium alloys as structural material: A review of research,” *Engineering Structures*, vol. 227. Elsevier Ltd, Jan. 15, 2021. doi: 10.1016/j.engstruct.2020.111372.

E. Rodriguez *et al.*, “Integration of a thermal imaging feedback control system in electron beam melting,” *WM Keck Center for 3D Innovation, University of Texas at El Paso*, pp. 945–961, 2012.

*Encyclopedia of Thermal Stresses*. Springer Netherlands, 2014. doi: 10.1007/978-94-007-2739-7.

F. I. Saunders and R. H. Wagoner, “Forming of tailor-welded blanks,” *Metallurgical and Materials Transactions A: Physical Metallurgy and Materials Science*, vol. 27, no. 9, pp. 2605–2616, 1996, doi: 10.1007/BF02652354.

G. Casalino, “Computational intelligence for smart laser materials processing,” *Optics and Laser Technology*, vol. 100, pp. 165–175, 2018, doi: 10.1016/j.optlastec.2017.10.011.

G. Meschut, V. Janzen, and T. Olfermann, “Innovative and highly productive joining technologies for multi-material lightweight car body structures,” in *Journal of Materials Engineering and Performance*, 2014, vol. 23, no. 5, pp. 1515–1523. doi: 10.1007/s11665-014-0962-3.

H. Huang, S. Tsutsumi, J. Wang, L. Li, and H. Murakawa, “High performance computation of residual stress and distortion in laser welded 301L stainless sheets,” *Finite Elements in Analysis and Design*, vol. 135, no. February, pp. 1–10, 2017, doi: 10.1016/j.finel.2017.07.004.

H. M. M. A. Rashed, “Control of Distortion in Aluminium Heat Treatment,” in *Fundamentals of Aluminium Metallurgy*, Elsevier, 2018, pp. 495–524. doi: 10.1016/b978-0-08-102063-0.00013-8.

H. Murakawa, “Residual stress and distortion in laser welding,” *Handbook of Laser Welding Technologies*, vol. 2, pp. 374–398, 2013, doi: 10.1533/9780857098771.2.374.

H. Wang, “Applications of laser welding in the railway industry,” *Handbook of Laser Welding Technologies*, pp. 575–595, 2013, doi: 10.1533/9780857098771.4.575.

H. Yamaoka, M. Yuki, T. Murayama, K. Tsuchiya, and T. Irisawa, “CO2 laser welding of aluminium A6063 alloy,” *Welding International*, vol. 6, no. 10, pp. 766–773, Jan. 1992, doi: 10.1080/09507119209548283.

I. Nunes *et al.*, “Artificial Neural Networks A Practical Course.”

IEEE Electron Devices Society, Institute of Electrical and Electronics Engineers, and Vaigai College of Engineering, *Proceeding of the 2018 International Conference on Intelligent Computing and Control Systems (ICICCS) : June 14-15, 2018*.

Institute of Electrical and Electronics Engineers, Friedrich-Alexander-Universität Erlangen-Nürnberg, IEEE Power Engineering Society, IEEE Industry Applications Society, and Süddeutscher Verlag Veranstaltungen GmbH*8 2018*, *th International Electric Drives Production Conference (EDPC) : proceedings : 4 and 5 December 2018, Schweinfurt, Germany*.

Institute of Electrical and Electronics Engineers, IEEE International Conference on Computer Vision 11 2007.10.14-21 Rio de Janeiro, and ICCV 11 2007.10.14-21 Rio de Janeiro, *IEEE 11th International Conference on Computer Vision, 2007 ICCV 2007 ; 14-21 Oct. 2007, Rio de Janeiro, Brazil*.

J. Ahn, E. He, L. Chen, R. C. Wimpory, J. P. Dear, and C. M. Davies, “Prediction and measurement of residual stresses and distortions in fibre laser welded Ti-6Al-4V

considering phase transformation," *Materials and Design*, vol. 115, pp. 441–457, Feb. 2017, doi: 10.1016/j.matdes.2016.11.078.

J. Chen, T. Wang, X. Gao, and L. Wei, "Real-time monitoring of high-power disk laser welding based on support vector machine," *Computers in Industry*, vol. 94, pp. 75–81, 2018, doi: 10.1016/j.compind.2017.10.003.

J. Chen, T. Wang, X. Gao, and L. Wei, "Real-time monitoring of high-power disk laser welding based on support vector machine," *Computers in Industry*, vol. 94, pp. 75–81, 2018, doi: 10.1016/j.compind.2017.10.003.

J. Fathi, P. Ebrahimzadeh, R. Farasati, and R. Teimouri, "Friction stir welding of aluminum 6061-T6 in presence of watercooling: Analyzing mechanical properties and residual stress distribution," *International Journal of Lightweight Materials and Manufacture*, vol. 2, no. 2, pp. 107–115, 2019, doi: 10.1016/j.ijlmm.2019.04.007.

J. G. (John G. Kaufman, E. L. Rooy, and American Foundry Society., *Aluminum alloy castings : properties, processes, and applications*. ASM International, 2004.

J. Günther, P. M. Pilarski, G. Helfrich, H. Shen, and K. Diepold, "Intelligent laser welding through representation, prediction, and control learning: An architecture with deep neural networks and reinforcement learning," *Mechatronics*, vol. 34, pp. 1–11, 2016, doi: 10.1016/j.mechatronics.2015.09.004.

J. Günther, P. M. Pilarski, G. Helfrich, H. Shen, and K. Diepold, "Intelligent laser welding through representation, prediction, and control learning: An architecture with deep neural networks and reinforcement learning," *Mechatronics*, vol. 34, no. October 2015, pp. 1–11, 2016, doi: 10.1016/j.mechatronics.2015.09.004.

J. Günther, P. M. Pilarski, G. Helfrich, H. Shen, and K. Diepold, "Intelligent laser welding through representation, prediction, and control learning: An architecture with deep neural networks and reinforcement learning," *Mechatronics*, vol. 34, pp. 1–11, Mar. 2016, doi: 10.1016/j.mechatronics.2015.09.004.

J. Günther, P. M. Pilarski, G. Helfrich, H. Shen, and K. Diepold, “Intelligent laser welding through representation, prediction, and control learning: An architecture with deep neural networks and reinforcement learning,” *Mechatronics*, vol. 34, pp. 1–11, Mar. 2016, doi: 10.1016/j.mechatronics.2015.09.004.

J. He, J. Wen, X. Zhou, and Y. Liu, “Hot deformation behavior and processing map of cast 5052 aluminum alloy,” *Procedia Manufacturing*, vol. 37, pp. 2–7, 2019, doi: 10.1016/j.promfg.2019.12.003.

J. Klæstrup Kristensen, “Applications of laser welding in the shipbuilding industry,” *Handbook of Laser Welding Technologies*, pp. 596–612, 2013, doi: 10.1533/9780857098771.4.596.

J. Li *et al.*, “Machine Learning for Patient-Specific Quality Assurance of VMAT: Prediction and Classification Accuracy,” *International Journal of Radiation Oncology Biology Physics*, vol. 105, no. 4, pp. 893–902, Nov. 2019, doi: 10.1016/j.ijrobp.2019.07.049.

J. M. Sánchez Amaya, M. R. Amaya-Vázquez, and F. J. Botana, *Laser welding of light metal alloys: Aluminium and titanium alloys*. 2013. doi: 10.1533/9780857098771.2.215.

J. Ryan and C. Heavey, “Process modeling for simulation,” *Computers in Industry*, vol. 57, no. 5, pp. 437–450, Jun. 2006, doi: 10.1016/j.compind.2006.02.002.

J. Stavridis, A. Papacharalampopoulos, and P. Stavropoulos, “Quality assessment in laser welding: a critical review,” *International Journal of Advanced Manufacturing Technology*, vol. 94, no. 5–8, pp. 1825–1847, 2018, doi: 10.1007/s00170-017-0461-4.

J. Stephen Leon, G. Bharathiraja, and V. Jayakumar, “A review on Friction Stir Welding in Aluminium Alloys,” in *IOP Conference Series: Materials Science and Engineering*, Oct. 2020, vol. 954, no. 1. doi: 10.1088/1757-899X/954/1/012007.

J. Sun, X. Liu, Y. Tong, and D. Deng, “A comparative study on welding temperature fields, residual stress distributions and deformations induced by laser beam welding and CO2

gas arc welding," *Materials and Design*, vol. 63, pp. 519–530, 2014, doi: 10.1016/j.matdes.2014.06.057.

J. Wang, P. Fu, and R. X. Gao, "Machine vision intelligence for product defect inspection based on deep learning and Hough transform," *Journal of Manufacturing Systems*, vol. 51, pp. 52–60, Apr. 2019, doi: 10.1016/j.jmsy.2019.03.002.

J. Xu, Y. Rong, Y. Huang, P. Wang, and C. Wang, "Keyhole-induced porosity formation during laser welding," *Journal of Materials Processing Technology*, vol. 252, pp. 720–727, Feb. 2018, doi: 10.1016/j.jmatprotec.2017.10.038.

J. Zhou, Y. Zhou, B. Wang, and J. Zang, "Human–Cyber–Physical Systems (HCPSs) in the Context of New-Generation Intelligent Manufacturing," *Engineering*, vol. 5, no. 4, pp. 624–636, 2019, doi: 10.1016/j.eng.2019.07.015.

K. Bandyopadhyay, S. K. Panda, P. Saha, V. H. Baltazar-Hernandez, and Y. N. Zhou, "Microstructures and failure analyses of DP980 laser welded blanks in formability context," *Materials Science and Engineering A*, vol. 652, pp. 250–263, Jan. 2016, doi: 10.1016/j.msea.2015.11.091.

K. Ghahremani, M. Safa, J. Yeung, S. Walbridge, C. Haas, and S. Dubois, "Quality assurance for high-frequency mechanical impact (HFMI) treatment of welds using handheld 3D laser scanning technology," *Welding in the World*, vol. 59, no. 3, pp. 391–400, Apr. 2015, doi: 10.1007/s40194-014-0210-3.

K. Hao, G. Li, M. Gao, and X. Zeng, "Weld formation mechanism of fiber laser oscillating welding of austenitic stainless steel," *Journal of Materials Processing Technology*, vol. 225, pp. 77–83, 2015, doi: 10.1016/j.jmatprotec.2015.05.021.

K. Li, F. G. Lu, S. T. Guo, H. C. Cui, and X. H. Tang, "Porosity sensitivity of A356 Al alloy during fiber laser welding," *Transactions of Nonferrous Metals Society of China (English Edition)*, vol. 25, no. 8, pp. 2516–2523, 2015, doi: 10.1016/S1003-6326(15)63870-5.

L. H. Shah, F. Khodabakhshi, and A. Gerlich, “Effect of beam wobbling on laser welding of aluminum and magnesium alloy with nickel interlayer,” *Journal of Manufacturing Processes*, vol. 37, no. December 2018, pp. 212–219, 2019, doi: 10.1016/j.jmapro.2018.11.028.

L. Ren, L. Zhang, L. Wang, F. Tao, and X. Chai, “Cloud manufacturing: key characteristics and applications,” *International Journal of Computer Integrated Manufacturing*, vol. 30, no. 6, pp. 501–515, Jun. 2017, doi: 10.1080/0951192X.2014.902105.

L. Schmidt *et al.*, “Acoustic process monitoring in laser beam welding,” *Procedia CIRP*, vol. 94, pp. 763–768, 2020, doi: 10.1016/j.procir.2020.09.139.

L. Wang, M. Gao, C. Zhang, and X. Zeng, “Effect of beam oscillating pattern on weld characterization of laser welding of AA6061-T6 aluminum alloy,” *Materials and Design*, vol. 108, pp. 707–717, Oct. 2016, doi: 10.1016/j.matdes.2016.07.053.

L. Zhang, A. C. Basantes-Defaz, D. Ozevin, and E. Indacochea, “Real-time monitoring of welding process using air-coupled ultrasonics and acoustic emission,” *International Journal of Advanced Manufacturing Technology*, vol. 101, no. 5–8, pp. 1623–1634, 2019, doi: 10.1007/s00170-018-3042-2.

L. Zhang, L. Zhou, L. Ren, and Y. Laili, “Modeling and simulation in intelligent manufacturing,” *Computers in Industry*, vol. 112. Elsevier B.V., Nov. 01, 2019. doi: 10.1016/j.compind.2019.08.004.

M. B. Kursa and W. R. Rudnicki, “Feature Selection with the Boruta Package,” 2010. [Online]. Available: http://www.jstatsoft.org/

M. B. Kursa, A. Jankowski, and W. R. Rudnicki, “Boruta - A system for feature selection,” *Fundamenta Informaticae*, vol. 101, no. 4, pp. 271–285, 2010, doi: 10.3233/FI-2010-288.

M. de Graaf and R. Aarts, “Applications of robotics in laser welding,” *Handbook of Laser Welding Technologies*, pp. 401–421, 2013, doi: 10.1533/9780857098771.3.401.

M. Doubenskaia, Ph. Bertrand, H. Pinon, and I.Smurov, “On-line optical monitoring of Nd: YAG laser lap welding of Zn-coated steel sheets ,” *IV International WLT-Conference on Lasers in Manufacturing*, no. January 2015, pp. 543–547, 2007.

M. Grandini, E. Bagli, and G. Visani, “Metrics for Multi-Class Classification: an Overview,” Aug. 2020, [Online]. Available: http://arxiv.org/abs/2008.05756

M. Graudenz and M. Baur, “Applications of laser welding in the automotive industry,” *Handbook of Laser Welding Technologies*, pp. 555–574, 2013, doi: 10.1533/9780857098771.4.555.

M. Heber, M. Lenz, M. Rüther, H. Bischof, H. Fronthaler, and G. Croonen, “Weld seam tracking and panorama image generation for on-line quality assurance,” *International Journal of Advanced Manufacturing Technology*, vol. 65, no. 9–12, pp. 1371–1382, 2013, doi: 10.1007/s00170-012-4263-4.

M. Ikonomakis, S. Kotsiantis, and V. Tampakas, “Text Classification Using Machine Learning Techniques.”

M. Nilsen, F. Sikström, A. K. Christiansson, and A. Ancona, “In-process Monitoring and Control of Robotized Laser Beam Welding of Closed Square Butt Joints,” *Procedia Manufacturing*, vol. 25, pp. 511–516, 2018, doi: 10.1016/j.promfg.2018.06.123.

M. Nilsen, F. Sikström, A. K. Christiansson, and A. Ancona, “In-process Monitoring and Control of Robotized Laser Beam Welding of Closed Square Butt Joints,” *Procedia Manufacturing*, vol. 25, pp. 511–516, 2018, doi: 10.1016/j.promfg.2018.06.123.

M. R. Maina, Y. Okamoto, A. Okada, M. Närhi, J. Kangastupa, and J. Vihinen, “High surface quality welding of aluminum using adjustable ring-mode fiber laser,” *Journal of Materials Processing Technology*, vol. 258, no. April, pp. 180–188, 2018, doi: 10.1016/j.jmatprotec.2018.03.030.

M. Rossini, P. R. Spena, L. Cortese, P. Matteis, and D. Firrao, "Investigation on dissimilar laser welding of advanced high strength steel sheets for the automotive industry," *Materials Science and Engineering A*, vol. 628, pp. 288–296, Mar. 2015, doi: 10.1016/j.msea.2015.01.037.

M. Tripathi, "Understanding Imbalanced Datasets and techniques for handling them," 2015.

MathWorks, "Specialization Practical Data sicence with Matlab." Matlab R2020a

N. J. Gogtay and U. M. Thatte, "Principles of correlation analysis," *Journal of Association of Physicians of India*, vol. 65, no. MARCH, pp. 78–81, 2017.

N. Jia, Z. Li, J. Ren, Y. Wang, and L. Yang, "A 3D reconstruction method based on grid laser and gray scale photo for visual inspection of welds," *Optics and Laser Technology*, vol. 119, Nov. 2019, doi: 10.1016/j.optlastec.2019.105648.

N. Seto, S. Katayama, and A. Matsunawa, "High-speed simultaneous observation of plasma and keyhole behavior during high power CO2 laser welding: Effect of shielding gas on porosity formation," *Journal of Laser Applications*, vol. 12, no. 6, pp. 245–250, Dec. 2000, doi: 10.2351/1.1324717.

O. O. Oladimeji and E. Taban, "Trend and innovations in laser beam welding of wrought aluminum alloys," *Welding in the World*, vol. 60, no. 3, pp. 415–457, 2016, doi: 10.1007/s40194-016-0317-9.

P. Briskham, N. Blundell, L. Han, R. Hewitt, K. Young, and D. Boomer, "Comparison of Self-Pierce Riveting, Resistance Spot Welding and Spot Friction Joining for aluminium automotive sheet," 2006. doi: 10.4271/2006-01-0774.

P. de Bono, C. Allen, G. D'Angelo, and A. Cisi, "Investigation of optical sensor approaches for real-time monitoring during fibre laser welding," *Journal of Laser Applications*, vol. 29, no. 2, p. 022417, May 2017, doi: 10.2351/1.4983253.

P. Horník, H. Šebestová, J. Novotný, and L. Mrňa, “Visualization of laser back-reflection distribution during laser welding,” *IOP Conference Series: Materials Science and Engineering*, vol. 1135, no. 1, p. 012015, Nov. 2021, doi: 10.1088/1757-899x/1135/1/012015.

P. K. Kapur, G. Singh, Y. S. Klochkov, and U. Kumar, *Decision Analytics applications in industry*. 2020. doi: 10.1007/978-981-15-3643-4_23.

R. C. Chen, C. Dewi, S. W. Huang, and R. E. Caraka, “Selecting critical features for data classification based on machine learning methods,” *Journal of Big Data*, vol. 7, no. 1, Dec. 2020, doi: 10.1186/s40537-020-00327-4.

R. C. Chen, C. Dewi, S. W. Huang, and R. E. Caraka, “Selecting critical features for data classification based on machine learning methods,” *Journal of Big Data*, vol. 7, no. 1, Dec. 2020, doi: 10.1186/s40537-020-00327-4.

R. Goebel, W. Wahlster, and J. Siekmann, “Lecture Notes in Artificial Intelligence 9851 Subseries of Lecture Notes in Computer Science LNAI Series Editors LNAI Founding Series Editor.” [Online]. Available: http://www.springer.com/series/1244

R. Lin, H. ping Wang, F. Lu, J. Solomon, and B. E. Carlson, “Numerical study of keyhole dynamics and keyhole-induced porosity formation in remote laser welding of Al alloys,” *International Journal of Heat and Mass Transfer*, vol. 108, pp. 244–256, May 2017, doi: 10.1016/j.ijheatmasstransfer.2016.12.019.

R. Sharda, S. Voß, and S. Suthaharan, “Integrated Series in Information Systems 36 Machine Learning Models and Algorithms for Big Data Classifi cation Thinking with Examples for Eff ective Learning.” [Online]. Available: http://www.springer.com/series/6157

R. Sharda, S. Voß, and S. Suthaharan, “Integrated Series in Information Systems 36 Machine Learning Models and Algorithms for Big Data Classifi cation Thinking with Examples for Eff ective Learning.” [Online]. Available: http://www.springer.com/series/6157

R. Tang and X. Zhang, “CART Decision Tree Combined with Boruta Feature Selection for Medical Data Classification,” in *2020 5th IEEE International Conference on Big Data Analytics, ICBDA 2020*, May 2020, pp. 80–84. doi: 10.1109/ICBDA49040.2020.9101199.

S. B. Kotsiantis, I. D. Zaharakis, and P. E. Pintelas, “Machine learning: A review of classification and combining techniques,” *Artificial Intelligence Review*, vol. 26, no. 3, pp. 159–190, Nov. 2006, doi: 10.1007/s10462-007-9052-3.

S. ben Jabeur, C. Gharib, S. Mefteh-Wali, and W. ben Arfi, “CatBoost model and artificial intelligence techniques for corporate failure prediction,” *Technological Forecasting and Social Change*, vol. 166, May 2021, doi: 10.1016/j.techfore.2021.120658.

Ben-David, S., Case, J., & Maruoka, A. (2004). Lecture Notes in Artificial Intelligence (Subseries of Lecture Notes in Computer Science): Preface. Lecture Notes in Artificial Intelligence (Subseries of Lecture Notes in Computer Science), 3244, vi-vii.

S. Ferretti, D. Caputo, M. Penza, and D. M. D’Addona, “Monitoring systems for zero defect manufacturing,” in *Procedia CIRP*, 2013, vol. 12, pp. 258–263. doi: 10.1016/j.procir.2013.09.045.

S. Gopal, K. Patro, and K. Kumar Sahu, “Normalization: A Preprocessing Stage.” [Online]. Available: www.kiplinger.com,

S. Han, T. Hwang, I. Oh, M. Choi, and Y. H. Moon, “Manufacturing of tailor-rolled blanks with thickness variations in both the longitudinal and latitudinal directions,” *Journal of Materials Processing Technology*, vol. 256, pp. 172–182, Jun. 2018, doi: 10.1016/j.jmatprotec.2018.02.013.

S. Hofstetter, (1993). Process improvement through designed experiments (Doctoral dissertation, Massachusetts Institute of Technology).

S. Hua, B. Li, L. Shu, P. Jiang, and S. Cheng, “Defect detection method using laser vision with model-based segmentation for laser brazing welds on car body surface,” *Measurement: Journal of the International Measurement Confederation*, vol. 178, Jun. 2021, doi: 10.1016/j.measurement.2021.109370.

S. il Pak and T. H. Oh, “Correlation and simple linear regression,” *Journal of Veterinary Clinics*, vol. 27, no. 4, pp. 427–434, 2010, doi: 10.1007/978-3-319-89993-0_6.

S. J. Na and W. I. Cho, *Developments in modelling and simulation of laser and hybrid laser welding*. 2013. doi: 10.1533/9780857098771.3.522.

S. Katayama, *Defect formation mechanisms and preventive procedures in laser welding*. 2013. doi: 10.1533/9780857098771.2.332.

S. Katayama, *Introduction: Fundamentals of laser welding*, vol. 9, no. 2012. Woodhead Publishing Limited, 2013. doi: 10.1533/9780857098771.1.3.

S. Katayama, Y. Kawahito, and M. Mizutani, “Elucidation of laser welding phenomena and factors affecting weld penetration and welding defects,” in *Physics Procedia*, 2010, vol. 5, no. PART 2, pp. 9–17. doi: 10.1016/j.phpro.2010.08.024.

S. M. Manladan, F. Yusof, S. Ramesh, M. Fadzil, Z. Luo, and S. Ao, “A review on resistance spot welding of aluminum alloys,” *International Journal of Advanced Manufacturing Technology*, vol. 90, no. 1–4. Springer London, pp. 605–634, Apr. 01, 2017. doi: 10.1007/s00170-016-9225-9.

S. Matthias *et al.*, “Metrological solutions for an adapted inspection of parts and tools of a sheet-bulk metal forming process,” *Production Engineering*, vol. 10, no. 1, pp. 51–61, Feb. 2016, doi: 10.1007/s11740-015-0647-2.

S. Pang, W. Chen, and W. Wang, “A quantitative model of keyhole instability induced porosity in laser welding of titanium alloy,” *Metallurgical and Materials Transactions A: Physical*

*Metallurgy and Materials Science*, vol. 45, no. 6, pp. 2808–2818, 2014, doi: 10.1007/s11661-014-2231-3.

S. Q. Moinuddin, S. S. Hameed, A. K. Dewangan, K. Ramesh Kumar, and A. Shanta Kumari, "A study on weld defects classification in gas metal arc welding process using machine learning techniques," in *Materials Today: Proceedings*, 2020, vol. 43, pp. 623–628. doi: 10.1016/j.matpr.2020.12.159.

S. Scott and S. Matwin, "Feature Engineering for Text Classification." [Online]. Available: http://ai.iit.nrc.ca/II_public/Classification/resources.html.

S. Shevchik *et al.*, "Supervised deep learning for real-time quality monitoring of laser welding with X-ray radiographic guidance," *Sci Rep*, vol. 10, no. 1, pp. 1–12, 2020.

T. A. Barnes and I. R. Pashby, "Joining techniques for aluminium spaceframes used in automobiles Part II Ð adhesive bonding and mechanical fasteners."

T. A. Barnes and I. R. Pashby, "Joining techniques for aluminium spaceframes used in automobiles Part I Ð solid and liquid phase welding."

T. J. Cleophas, A. H. Zwinderman, T. J. Cleophas, and A. H. Zwinderman, "Analysis of Variance (Anova)," *Regression Analysis in Medical Research*, vol. 6, pp. 147–155, 2021, doi: 10.1007/978-3-030-61394-5_7.

T. Purtonen, A. Kalliosaari, and A. Salminen, "Monitoring and adaptive control of laser processes," *Physics Procedia*, vol. 56, no. C, pp. 1218–1231, 2014, doi: 10.1016/j.phpro.2014.08.038.

T. Sibalija, *Metaheuristic Algorithms in Industrial Process Optimisation: Performance, Comparison and Recommendations*, vol. 1198. Springer Singapore, 2020. doi: 10.1007/978-981-15-5232-8_24.

T. Sibillano, A. Ancona, V. Berardi, and P. M. Lugarà, “A real-time spectroscopic sensor for monitoring laser welding processes,” *Sensors*, vol. 9, no. 5. pp. 3376–3385, Apr. 27, 2009. doi: 10.3390/s90503376.

Thomas, W.M., Staines, D.G., Norris, I.M. et al. Friction Stir Welding Tools and Developments. Weld World 47, 10–17 (2003). https://doi.org/10.1007/BF03266403

V. Bolón-Canedo, N. Sánchez-Maroño, and A. Alonso-Betanzos, “Feature selection and classification in multiple class datasets: An application to KDD Cup 99 dataset,” *Expert Systems with Applications*, vol. 38, no. 5, pp. 5947–5957, May 2011, doi: 10.1016/j.eswa.2010.11.028.

W. Cai, J. Z. Wang, P. Jiang, L. C. Cao, G. Y. Mi, and Q. Zhou, “Application of sensing techniques and artificial intelligence-based methods to laser welding real-time monitoring: A critical review of recent literature,” *Journal of Manufacturing Systems*, vol. 57. Elsevier B.V., pp. 1–18, Oct. 01, 2020. doi: 10.1016/j.jmsy.2020.07.021.

W. Cai, J. Z. Wang, P. Jiang, L. C. Cao, G. Y. Mi, and Q. Zhou, “Application of sensing techniques and artificial intelligence-based methods to laser welding real-time monitoring: A critical review of recent literature,” *Journal of Manufacturing Systems*, vol. 57, no. July, pp. 1–18, 2020, doi: 10.1016/j.jmsy.2020.07.021.

W. Cassada, J. Liu, and J. Staley, “Aluminum alloys for aircraft structures,” *Advanced Materials and Processes*, vol. 160, no. 12. ASM International, pp. 27–29, 2002. doi: 10.1533/9780857095152.173.

X. Gao, Y. Sun, D. You, Z. Xiao, and X. Chen, “Multi-sensor information fusion for monitoring disk laser welding,” *International Journal of Advanced Manufacturing Technology*, vol. 85, no. 5–8, pp. 1167–1175, Jul. 2016, doi: 10.1007/s00170-015-8032-z.

X. Wang, X. Zhou, Z. Xia, and X. Gu, “A survey of welding robot intelligent path optimization,” *Journal of Manufacturing Processes*, no. December 2019, pp. 0–1, 2020, doi: 10.1016/j.jmapro.2020.04.085.

X. Xiao, X. Liu, M. Cheng, and L. Song, “Towards monitoring laser welding process via a coaxial pyrometer,” *Journal of Materials Processing Technology*, vol. 277, no. August 2019, p. 116409, 2020, doi: 10.1016/j.jmatprotec.2019.116409.

Y. Ai, X. Shao, P. Jiang, P. Li, Y. Liu, and C. Yue, “Process modeling and parameter optimization using radial basis function neural network and genetic algorithm for laser welding of dissimilar materials,” *Applied Physics A: Materials Science and Processing*, vol. 121, no. 2, pp. 555–569, 2015, doi: 10.1007/s00339-015-9408-5.

Y. Huang, Y. Yuan, L. Yang, D. Wu, and S. Chen, “Real-time monitoring and control of porosity defects during arc welding of aluminum alloys,” *Journal of Materials Processing Technology*, vol. 286, no. July, 2020, doi: 10.1016/j.jmatprotec.2020.116832.

Y. Luo, L. Zhu, J. Han, X. Xie, R. Wan, and Y. Zhu, “Study on the acoustic emission effect of plasma plume in pulsed laser welding,” *Mechanical Systems and Signal Processing*, vol. 124, pp. 715–723, Jun. 2019, doi: 10.1016/j.ymssp.2019.01.045.

Y. Mao, G. Kinsman, and W. W. Duley, “ Real-Time Fast Fourier Transform Analysis of Acoustic Emission during CO 2 Laser Welding of Materials ,” *Journal of Laser Applications*, vol. 5, no. 2, pp. 17–22, Oct. 1993, doi: 10.2351/1.4745326.

Y. Zhang, D. You, X. Gao, N. Zhang, and P. P. Gao, “Welding defects detection based on deep learning with multiple optical sensors during disk laser welding of thick plates,” *Journal of Manufacturing Systems*, vol. 51, pp. 87–94, Apr. 2019, doi: 10.1016/j.jmsy.2019.02.004.

Z. Chen, Y. Song, J. Zhang, W. Zhang, L. Jiang, and X. Xia, “Laser vision sensing based on adaptive welding for aluminum alloy,” *Frontiers of Mechanical Engineering in China*, vol. 2, no. 2, pp. 218–223, 2007, doi: 10.1007/s11465-007-0038-2.

Z. Huang, W. Wang, Y. Zhang, and J. Lai, “Low speed impact properties of 5052 aluminum alloy plate,” *Procedia Manufacturing*, vol. 50, pp. 668–672, 2020, doi: 10.1016/j.promfg.2020.08.120.

Z. jue Tang, W. wei Liu, N. Zhang, Y. wen Wang, and H. chao Zhang, “Real–time prediction of penetration depths of laser surface melting based on coaxial visual monitoring,” *Optics and Lasers in Engineering*, vol. 128, May 2020, doi: 10.1016/j.optlaseng.2020.106034.

Z. Luo, W. Liu, Z. Wang, and S. Ao, “Monitoring of laser welding using source localization and tracking processing by microphone array,” *International Journal of Advanced Manufacturing Technology*, vol. 86, no. 1–4, pp. 21–28, Sep. 2016, doi: 10.1007/s00170-015-8095-x.

Z. M. Liu, S. L. Cui, Z. Luo, C. Z. Zhang, Z. M. Wang, and Y. C. Zhang, “Plasma arc welding: Process variants and its recent developments of sensing, controlling and modeling,” *Journal of Manufacturing Processes*, vol. 23. Elsevier Ltd, pp. 315–327, Aug. 01, 2016. doi: 10.1016/j.jmapro.2016.04.004.

Z. Wang, J. P. Oliveira, Z. Zeng, X. Bu, B. Peng, and X. Shao, “Laser beam oscillating welding of 5A06 aluminum alloys: Microstructure, porosity and mechanical properties,” *Optics and Laser Technology*, vol. 111, no. September 2018, pp. 58–65, 2019, doi: 10.1016/j.optlastec.2018.09.036.

Z. Zhang, B. Li, W. Zhang, R. Lu, S. Wada, and Y. Zhang, “Real-time penetration state monitoring using convolutional neural network for laser welding of tailor rolled blanks,” *Journal of Manufacturing Systems*, vol. 54, no. January, pp. 348–360, 2020, doi: 10.1016/j.jmsy.2020.01.006.

“Automotive Steels: Design, Metallurgy, Processing and Applications - Radhakanta Rana, Shiv Brat Singh - Google Livres.” https://books.google.ca/books?hl=fr&lr=&id=HrszCwAAQBAJ&oi=fnd&pg=PP1&dq=Automotive+Steels,+Woodhead+Publishing&ots=GE3qxtSHzE&sig=RpEXqfP3Wk5JAt19uz

zBmq9BDIY&redir_esc=y#v=onepage&q=Automotive Steels%2C Woodhead Publishing&f=false (accessed Mar. 04, 2021).